Pannexin-1 channels promote CD8$^+$ T cell effector and memory responses through distinct intracellular pathways

Authors: Trupti Vardam-Kaur[1,3,6], Alma Banuelos[1,6], Maria Gabaldon-Parish[1,6], Kelsey Marie Wanhainen[2], Maggie Hanqi Zhou[1], Sarah van Dijk[1,4], Bruna Gois Macedo[1], Caio Loureiro Salgado[1], Igor Santiago-Carvalho[1], Changwei Peng[2,5], Stephen C. Jameson[2], Henrique Borges da Silva[1,*]

Affiliations:

1 – Department of Immunology, Mayo Clinic Arizona, Scottsdale, AZ

2 – Center for Immunology, University of Minnesota, Minneapolis, MN

3 – Present address: Omeros Corporation, Seattle, WA

4 – Present address: School of Life Sciences, Arizona State University, Tempe, AZ

5 – Present address: Department of Immunology & HMS Center for Immune Imaging, Harvard Medical School, Boston, MA

6 – These authors contributed equally to this manuscript.

* - Correspondence should be sent to Henrique Borges da Silva, Mayo Clinic, Scottsdale, AZ. E-mail address: borgesdasilva.henrique@mayo.edu

Abstract

Sensing of extracellular metabolites controls $CD8^+$ T cell function. Their accumulation can occur through export by specialized molecules, such as the release channel Pannexin-1 (Panx1). Whether Panx1 controls $CD8^+$ T cell immune responses to antigen, however, has not been previously addressed. Here, we report that T cell-specific Panx1 is needed for $CD8^+$ T cell responses to viral infections and cancer. We found that CD8-specific Panx1 favors memory $CD8^+$ T cell survival primarily through ATP export and induction of mitochondrial metabolism. CD8-specific Panx1 is also crucial for the effector expansion of $CD8^+$ T cells, however this regulation occurs independently of eATP. Instead, our results suggest a connection between Panx1-induced extracellular lactate accumulation and the complete activation of effector $CD8^+$ T cells. In summary, Panx1 regulates effector and memory $CD8^+$ T cells through export of distinct metabolites and by engaging different metabolic and signaling pathways.

Cytotoxic CD8$^+$ T cells control viral infections and solid tumors [1, 2]. These cells, upon antigen priming, quickly activate intracellular signaling pathways that lead to effector function and clonal expansion [2]. Effector CD8$^+$ T cells differentiate into either memory precursors (MP) cells or terminal effectors (TE), which perform distinct functions and have different fates during T cell contraction. While MP cells become long-lived memory CD8$^+$ T cell subsets, TE cells display heightened effector function and mostly die during contraction [2], except for long-lived effector cells (LLECs) [3, 4]. Effector CD8$^+$ T cells expansion and differentiation are controlled by a network of supporting cells, and extracellular signals [2, 5, 6, 7]. Many components of this network have been described, such as interactions with innate immune cells [8, 9], and cytokine sensing [10, 11, 12, 13]. Extracellular accumulation of metabolites, however, may also play an important role. Metabolites are often released as a byproduct of dead cells [14]. However, they can sometimes be actively released via transmembrane channels [15, 16, 17].

One of the most well-described metabolite transporters is the homo-heptameric release channel Pannexin-1 (Panx1) [18, 19]. Through release of “find-me” signals such as the nucleotide ATP, Panx1 plays a critical role in the triggering of apoptotic cell clearance [19, 20, 21, 22]. Panx1 can also promote ATP export in healthy cells [20, 23, 24, 25, 26, 27]. Panx1 is expressed by many immune and non-immune cells, including T cells [28, 29]. Panx-1-mediated ATP export promotes the anti-allergic function of regulatory CD4$^+$ T cells (Tregs) [30]. Conventional CD4$^+$ T cells or CD8$^+$ T cells can also export ATP via Panx1, influencing their function [28, 31, 32]. Panx1 also promote the export of many other metabolites smaller than 1 kDa [19 20 21]. Metabolite export via Panx1, therefore, can regulate T cell function and its downstream physiological consequences. However, no comprehensive studies on the *in vivo* role of Panx1 in CD8$^+$ T cells have been done.

Extracellular ATP (eATP) is sensed by immune cells via purinergic receptors, like the low-affinity ion channel P2RX7 [33]. We and others have previously shown that P2RX7 is expressed by

antigen-specific CD8$^+$ T cells [34, 35, 36] and is crucial for the generation and survival of memory CD8$^+$ T cells [32, 34, 37]. In addition to Panx1 export, eATP can accumulate through infection-induced tissue damage [38]. The role of P2RX7 for memory CD8$^+$ T cell survival raises an interesting conundrum: these cells rely on consistent eATP signaling, yet tissue damage release of ATP is likely absent after pathogen is gone. In this work, we investigated the role of Panx1 in the development of antigen-specific CD8$^+$ T cell responses to viral infection. We found that Panx1 favors both the expansion of effector CD8$^+$ T cells and the survival of memory CD8$^+$ T cells. Our data suggests that, while memory CD8$^+$ T cells require Panx1 for survival via induction of mitochondrial function, Panx1 promotes both mitochondrial and glycolytic pathways in effector CD8$^+$ T cells. Panx1 promotes memory CD8$^+$ T cell survival through ATP export. In contrast, our results indicate that Panx1 promotes effector CD8$^+$ T cells through accumulation of extracellular lactate and its subsequent recycling into saturated phosphatidylinositol biosynthesis. The overarching role of Panx1 for CD8$^+$ T cells is evidenced by its importance in promoting optimal control of melanoma tumors by CD8$^+$ T cells.

Results

T-cell specific Panx1 induces both effector CD8$^+$ T cell expansion and memory CD8$^+$ T cell survival

Panx1 channels are constitutively expressed in antigen-specific CD8$^+$ T cells (**Fig. 1a, Extended Data Fig. 1a**). These channels are functional in CD8$^+$ T cells since ATP export was significantly decreased – and intracellular ATP levels are concomitantly increased – when Panx1 is inhibited by Trovafloxacin [22] (**Extended Data Fig. 1b**). Global or T cell-specific knockout of Panx1 does not affect CD8$^+$ T cell thymic development (**data not shown**). Panx1 can promote, upon triggering by Caspase 3, nucleotide export in apoptotic cells [22]. However, we did not find increased To-Pro3 uptake in WT CD8$^+$ T cells in comparison to CD8$^+$ T cells

deficient for Panx1 (Panx1-KO) (**Extended Data Fig. 1c**), suggesting that Panx1 primarily drives metabolite export from healthy $CD8^+$ T cells.

Given its Panx1 inhibitory role, we used Trovafloxacin treatment of Lymphocytic Choriomeningitis Virus (LCMV)-infected mice (previously transferred with LCMV gp33-TCR transgenic $CD8^+$ P14 T cells) to test how Panx1 blockade affects the formation of antigen-specific $CD8^+$ T cell responses. At one-week post-infection, we encountered significantly decreased numbers of splenic P14 cells (**Extended Data Fig. 2a**). However, this numerical defect was not found at the memory phase (**Extended Data Fig. 2b**). Likewise, LCMV-infected global Panx1-KO mice did not display significant differences in antigen-specific $CD8^+$ T cell numbers, except for the accumulation of CD103-expressing salivary gland (SG) tissue-resident memory (Trm) $CD8^+$ T cells (**Extended Data Figs. 2c-e**).

Because Panx1 is expressed by $CD8^+$ T cells and many other immune cells (**Extended Data Fig. 1d**), we used T cell-specific KO systems to test the $CD8^+$ T cell-specific role of Panx1 expression. LCMV-infected T cell-specific Panx1-KO (CD4-Cre *Panx1*$^{fl/fl}$) mice had significantly decreased numbers of spleen gp33-specific $CD8^+$ T cells, both at the effector stage of the immune response (**Fig. 1b, left**) and at memory (**Fig. 1b, right**). These mice also had decreased numbers of small intestine intraepithelial (SI IEL) Trm cells (**Extended Data Fig. 3a**). To ensure the observed defects are $CD8^+$ T cell-specific, we generated 1:1 WT:CD4-Cre *Panx1*$^{fl/fl}$ mixed bone marrow (BM) chimeras and infected them with LCMV (**Fig. 1c**). As shown in **Fig. 1d-e** and **Extended Data Fig. 3b** (red dotted lines), Panx1-KO $CD8^+$ T cells had lower levels of homeostatic expansion in irradiated mice compared to WT cells. In these experiments, we considered the pre-infection (after two months reconstitution) ratios as our comparison points. After LCMV infection, there is significantly decreased Panx1-KO:WT ratios of spleen gp33-specific $CD8^+$ T cells. This defect was already evident one week after infection (**Fig. 1d**)

and carried over the memory phase among multiple memory CD8$^+$ T cell subsets (**Fig. 1e**). We also found decreased representation of Panx1-KO Trm cells in multiple non-lymphoid tissues (**Extended Data Fig. 3b**).

We found decreased numbers of memory CD8$^+$ T cells in Panx1-KO. Our BM chimera data also showed a specific loss of central memory (Tcm) CD8$^+$ T cells in Panx1-KO at the memory phase of the immune response. To test whether memory CD8$^+$ T cell survival is specifically regulated by Panx1, we used a tamoxifen-inducible KO system (**Fig. 1f**). Tamoxifen-induced Panx1 ablation during the effector stage affected both the accumulation of effector CD8$^+$ T cells and the establishment of memory CD8$^+$ T cells (**Fig. 1g, 1i and 1j, left panels**). Panx1 ablation after memory establishment resulted in a steady decline of CD8$^+$ T cell numbers (**Fig. 1g, right panel**). The decrease in memory CD8$^+$ T cell numbers in late Panx1 ablation was true for all subsets of circulating memory, although the most pronounced decline was in Tcm cells (**Fig. 1h, Fig. 1i – right panel**). Late Panx1 ablation also led to a decrease in Trm cells, except for the SI IEL compartment (**Fig. 1j, right panel**). These results showed a crucial role for Panx1 in both the establishment of effector CD8$^+$ T cells and the survival of memory CD8$^+$ T cells.

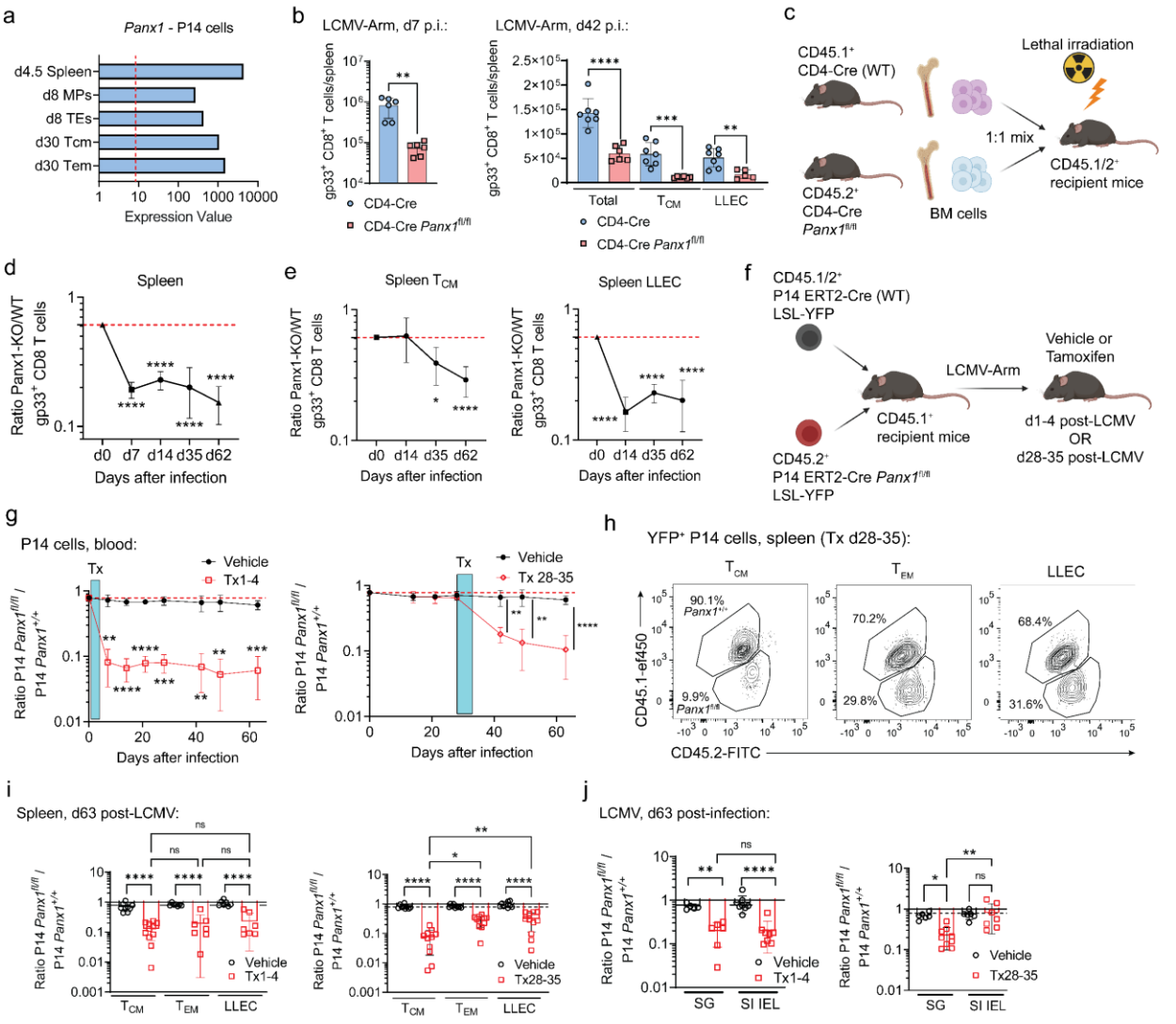

Fig. 1. CD8⁺ T cell-specific Panx1 is required for the accumulation of effector CD8⁺ T cells and the survival of memory CD8⁺ T cells. (**a**) *Panx1* mRNA expression from RNA-seq samples in the indicated subsets of LCMV-gp33 transgenic P14 CD8⁺ T cells. (**b**) WT (CD4-Cre) or CD4-Cre *Panx1*$^{fl/fl}$ mice were infected with LCMV-Arm and gp33⁺ CD8⁺ T cells were tracked over time. Numbers of total spleen gp33⁺ CD8⁺ T cells at day 7 (left) and of total, T_{CM} and LLEC spleen gp33⁺ CD8⁺ T cells at day 42 (right) post-infection are shown. (**c-e**) A 1:1 mix of bone marrow cells from CD4-Cre (WT; CD45.1⁺) and CD4-Cre *Panx1*$^{fl/fl}$ (Panx1-KO; CD45.2⁺) mice was transferred into lethally irradiated C57BL/6 mice (CD45.1/2⁺). After two months, BM chimeric mice were infected with LCMV-Arm. The red dotted lines show the Panx1-KO:WT ratios after two months of reconstitution. (**c**) Graphical scheme. (**d**) Panx1-KO/WT ratios of total spleen gp33⁺ CD8⁺ T cells over time post-infection. (**e**) Panx1-KO/WT ratios of T_{CM} and LLEC gp33⁺ spleen CD8⁺ T cells over time post-infection. (**f-j**) Recipient C57BL/6 mice (CD45.1⁺)

were adoptively transferred with a 1:1 mix of P14 ERT2-Cre LSL-YFP *Panx1*$^{+/+}$ (WT; CD45.1/2^{+}) and P14 ERT2-Cre LSL-YFP *Panx1*$^{fl/fl}$ (CD45.2^{+}) cells, then infected with LCMV-Arm. Infected mice were treated with vehicle or tamoxifen (Tx) at the indicated time intervals. (**f**) Graphical scheme. (**g**) *Panx1*$^{fl/fl}$/*Panx1*$^{+/+}$ P14 cell ratios in the blood over time post-infection, in mice treated with vehicle or with Tx between days 1-4 (d1-4; left) or 28-35 (d28-35; right) post-infection. Treatment periods is indicated by the blue shaded box. (**h**) Representative flow cytometry plots showing the distribution of spleen T_{CM}, T_{EM} and LLEC *Panx1*$^{+/+}$ and *Panx1*$^{fl/fl}$ P14 cells from mice treated with Tx d28-35 at 63d post-infection. (**i**) *Panx1*$^{fl/fl}$/*Panx1*$^{+/+}$ ratios of spleen T_{CM}, T_{EM} and LLEC P14 cells from mice treated with vehicle or Tx d1-4 (left) or d28-35 (right), at 63d post-infection. (**j**) *Panx1*$^{fl/fl}$/*Panx1*$^{+/+}$ P14 cell ratios in SG and SI IEL at day 63 post-infection, in mice treated with Tx between days 1-4 (left) or 28-35 (right). (**b, d, g-j**) Data from three independent experiments, n=6-12 per time point. (**b, i-j**) * $p<0.05$, ** $p<0.01$, *** $p<0.001$, **** $p<0.0001$, One-way ANOVA with Tukey's post-test. (**d-e, g**) * $p<0.05$, ** $p<0.01$, *** $p<0.001$, **** $p<0.0001$, Two-way ANOVA with Bonferroni post-test. (**b**) ** $p<0.01$, Unpaired t-test.

CD8^{+} T cell-specific Panx1 promotes the differentiation of both terminal effector and memory precursor subsets

After defining the importance of Panx1 for effector and memory CD8^{+} T cells, we next asked if these concomitant phenotypes arise at the effector-versus-memory fate decision stage. Using multiple experimental models to track gp33-specific CD8^{+} T cell responses to LCMV, Panx1-KO CD8^{+} T cells had decreased numbers of both KLRG1^{+}CD127^{-} terminal effectors (TE) and CD127^{+}KLRG1^{-} memory precursors (MP) (**Fig. 2a-g**). These results evidence that expression of Panx1 in CD8^{+} T cells themselves is required for the accumulation of both TE and MP cells. We also found decreased numbers of TE and MP cells in spleen CD8^{+} T cells specific for the Nucleoprotein (NP^{+}) of the Influenza virus, in CD4-Cre *Panx1*$^{fl/fl}$ mice infected with Influenza (**Fig. 2h**). These results showed that T cell-specific Panx1 induces simultaneous formation of TEs and MPs in response to multiple viral infections. Initial establishment of lung-resident NP^{+}

CD8⁺ T cells, however, was normal in CD4-Cre *Panx1*$^{fl/fl}$ mice (**Fig. 2i**), suggesting a tissue- and context-dependent role of Panx1 for Trm cells.

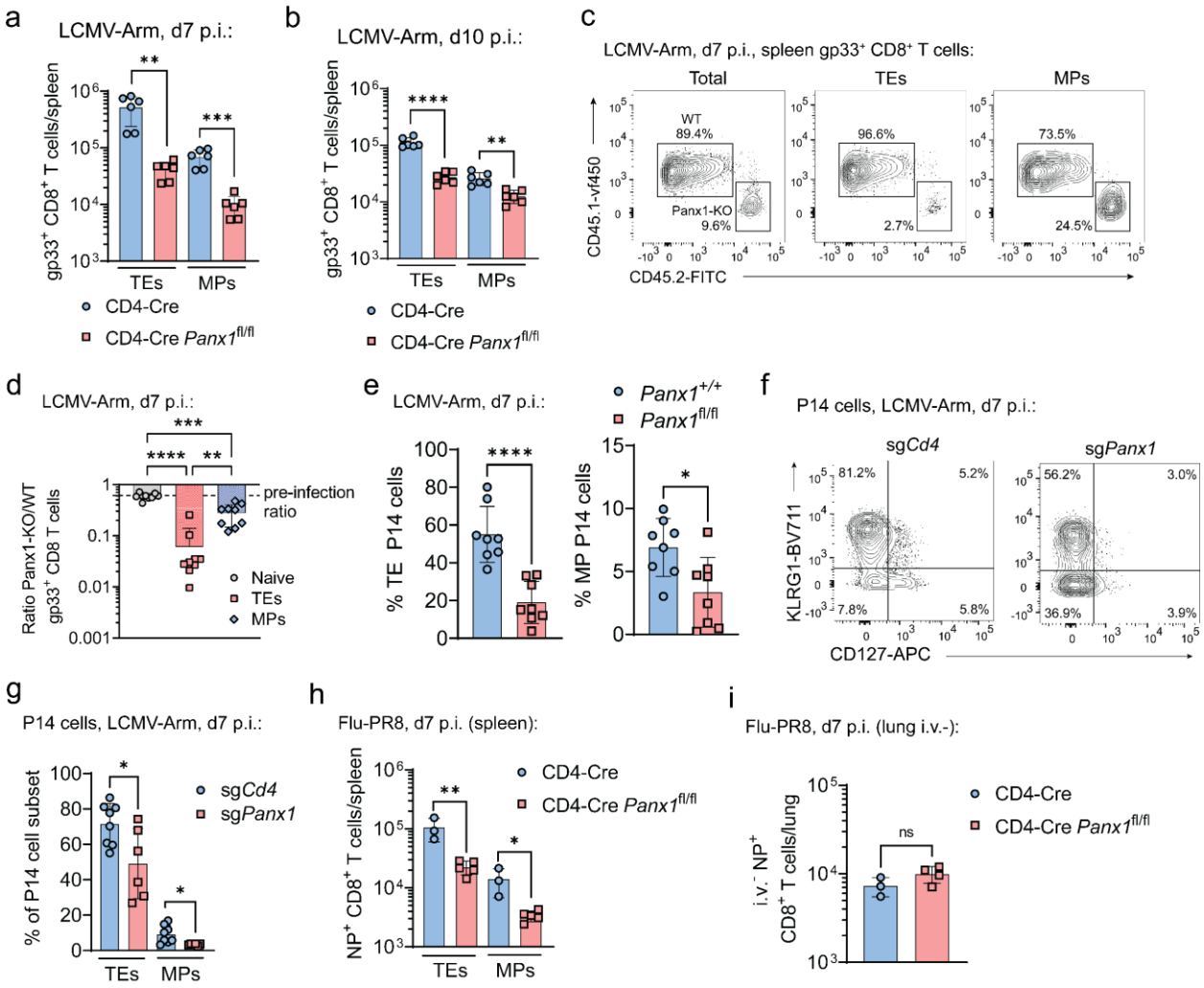

Fig. 2. CD8⁺ T cell-specific Panx1 promotes the differentiation of both terminal effector and memory precursor CD8⁺ T cells. (**a-b**) WT (CD4-Cre) or CD4-Cre *Panx1*$^{fl/fl}$ mice were infected with LCMV-Arm and gp33⁺ CD8⁺ T cells were tracked over time. (**a**) Numbers of TE and MP spleen gp33⁺ CD8⁺ T cells at day 7 post-infection. (**b**) Numbers of total TE and MP spleen gp33⁺ CD8⁺ T cells at day 10 post-infection. (**c-d**) A 1:1 mix of bone marrow cells from CD4-Cre (WT; CD45.1⁺) and CD4-Cre *Panx1*$^{fl/fl}$ (Panx1-KO; CD45.2⁺) mice was transferred into lethally irradiated C57BL/6 mice (CD45.1/2⁺). After two months, BM chimeric mice were infected with LCMV-Arm. (**c**) Representative flow cytometry plots showing WT and Panx1-KO total, TE and MP spleen gp33⁺ CD8⁺ T cells at day 7 post-infection. (**d**) Panx1-KO/WT ratios of spleen naïve,

TE and MP gp33$^+$ CD8$^+$ T cells at day 7 post-infection. (**e**) Average percentages of WT (*Panx1*$^{+/+}$) and tamoxifen-induced (ERT2-Cre) Panx1-KO (*Panx1*$^{fl/fl}$) TE and MP P14 cells at day 7 post-infection with LCMV-Arm, in mice treated with tamoxifen between days 1-4 post-infection as described in Fig.1. (**f-g**) P14 cells (CD45.2$^+$) were in vitro activated and transduced via electroporation with a mix of Cas9 and either single-guide RNAs for *Cd4* (sg*Cd4*) or *Panx1* (sg*Panx1*). After a 48h rest period, cells were adoptively transferred into CD45.1$^+$ recipient mice, which were infected with LCMV-Arm. (**f**) Representative flow cytometry plots showing expression of KLRG1 and CD127 in spleen sg*Cd4* and sg*Panx1*-P14 cells, at day 7 post-infection. (**g**) Percentages of TE and MP WT P14 cells (right) at day 7 post-infection. (**h-i**) In other experiments, WT or CD4-Cre *Panx1*$^{fl/fl}$ mice were infected with Influenza virus (PR8 strain). At 7 days p.i., the spleens and lung parenchyma (lung i.v.$^-$) were assessed. (**h**) Average numbers of NP-tetramer$^+$ CD8$^+$ TE and MP cells per spleen. (**i**) Average numbers of NP-tetramer$^+$ CD8$^+$ T cells per lung. (**a-b, d-e, g**) Data from three independent experiments, n=6-9 per time point. (**h-i**) Data from two independent experiments, n=3-5 per group. (**a-b, d-e, g-i**) * $p<0.05$, ** $p<0.01$, *** $p<0.001$, **** $p<0.0001$, One-way ANOVA with Tukey's post-test.

Panx1 expression is needed for the expansion and effector differentiation of CD8$^+$ T cells

We next measured which aspects of CD8$^+$ T cell function rely on Panx1 expression. Panx1, although expressed constitutively in CD8$^+$ T cells (**Extended Data Fig. 1**), is recruited to the immunological synapse after T cell priming [28]. Therefore, Panx1 may specifically promote the activation of CD8$^+$ T cells. RNA-seq analysis of WT versus Panx1-KO CD8$^+$ T cells activated *in vitro* (**Extended Data Fig. 4a**) showed decreased expression of many genes associated with the T cell receptor (TCR) signaling pathway in Panx1-KO CD8$^+$ T cells (**Fig. 3a**). We then compared the *in vitro* activation of WT versus Panx1-KO CD8$^+$ T cells. At 24h after activation, Panx1-KO CD8$^+$ T cells displayed significant defects in the expression of activation markers such as CD69, CD25 and CD44. Most of these defects were sustained or expanded at 48h and 72h after activation (**Fig. 3b-c**). Together with these defects, the proliferation of Panx1-KO CD8$^+$ T cells was significantly decreased (**Fig. 3b-c**), as well as their ability to produce IFN-γ (**Fig.**

3d). The defects in proliferation of Panx1-KO CD8$^+$ T cells were also observed *in vivo* (**Fig. 3e**), and cell cycle genes are decreased in Panx1-KO sorted TE cells (**Fig. 3f**). Thus, Panx1 is needed for the full activation, proliferation, and effector differentiation of CD8$^+$ T cells.

Our transcriptional data also showed that activated Panx1-KO CD8$^+$ T cells had increased expression of cell death-related genes (**Fig. 3g, Extended Data Fig. 4b**). This was also observed in IL-15-treated memory-like Panx1-KO CD8$^+$ T cells (**Extended Data Fig. 4c**) and in cell-sorted Panx1-KO MP cells (**Extended Data Fig. 4d**). Therefore, we quantified the cell death of WT versus Panx1-KO gp33-specific CD8$^+$ T cells after LCMV infection. At day 7 post-infection, Panx1-KO CD8$^+$ T cells displayed increased percentages of cell death (**Fig. 3h**). This is observed both in total gp33$^+$ CD8$^+$ T cells, and within TE cells (**Fig. 3h-i**). Despite a non-significant trend in cell death increase in Panx1-KO MP cells (**Fig. 3j, left**), we observed increased cell death of Panx1-KO CD62L$^+$ Tcm precursors (**Fig. 3j, right**). Altogether, these results suggest that Panx1, beyond its role in activation and proliferation, is also required for antigen-primed CD8$^+$ T cells to resist cell death.

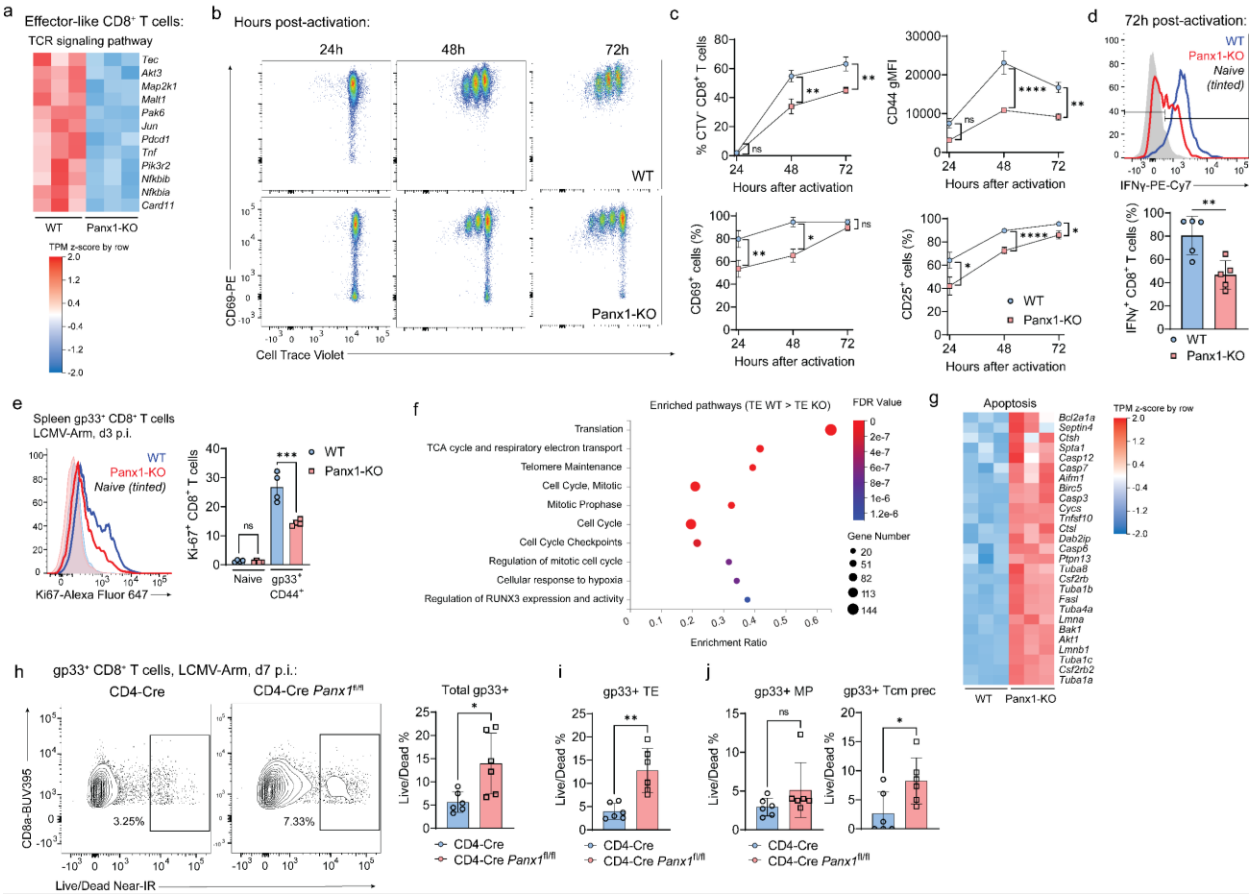

Fig. 3. Panx1 regulates the proliferation, activation, and cell survival of effector CD8⁺ T cells. (**a-d**) WT (CD4-Cre) or Panx1-KO (CD4-Cre *Panx1*$^{fl/fl}$) CD8⁺ T cells were activated *in vitro* (α-CD3 + α-CD28 + IL-2) for 72h (effector-like CD8⁺ T cells). (**a**) Heatmaps showing the expression of TCR signaling pathway genes from RNA-seq data of effector-like WT and Panx1-KO CD8⁺ T cells. (**b-d**) In some experiments, *in vitro*-activated WT and Panx1-KO CD8⁺ T cells were tracked every 24h for activation markers. (**b**) Representative flow cytometry plots showing expression of CD69 and dilution of Cell Trace Violet at 24h, 48h and 72h after activation. (**c**) Percentages of Cell Trace Violet (CTV) divided cells (top left), average gMFI values for CD44 (top right), and percentages of CD69⁺ (bottom left) and CD25⁺ (bottom right) cells at 24h, 48h and 72h after activation. (**d**) Representative histograms showing expression of IFNγ (top) and average percentages of IFNγ⁺ CD8⁺ T cells (bottom) at 72h after activation. (**e-f**) WT or Panx1-KO mice were infected with LCMV-Arm and evaluated at 3 or 7 days after infection. (**e**) Representative histograms (left) and average percentages (right) of Ki-67⁺ gp33⁺ CD8⁺ T cells are shown. (**f**) Gene expression pathways enriched in gp33⁺ WT TE cells (KLRG1⁺CD127⁻) compared to Panx1-KO TE cells. (**g**) Heatmap showing the expression of Apoptosis pathway genes from RNA-seq data from effector-like WT and Panx1-KO CD8⁺ T cells is shown. (**h-j**) WT

or Panx1-KO mice were infected with LCMV-Arm and evaluated at 7 days after infection. (**h**) Representative flow cytometry plots showing, in gp33$^+$ CD8$^+$ T cells, the staining with the viability dye Live/Dead (left); in the right, average percentages of Live/Dead$^+$ spleen gp33$^+$ CD8$^+$ T cells. (**i**) Average percentages of Live/Dead$^+$ spleen gp33$^+$ TE cells. (**j**) Average percentages of Live/Dead$^+$ spleen gp33$^+$ MP and Tcm precursor cells. (**a, g**) Each replicate is a pool of activated CD8$^+$ T cells from three mice; n=3 replicates per experimental group. (**f**) Each replicate is a pool of gp33$^+$ TE or MP cells from three mice; n=3 replicates per experimental group. (**b-d**) Data from four independent experiments, n=7-11 per experimental group per time point. (**e, h-j**) Data from three independent experiments n=4-6 per experimental group. (**d**) * $p<0.05$, ** $p<0.01$, **** $p<0.0001$, multiple t-tests. (**g, i-j**) * $p<0.05$, ** $p<0.01$, *** $p<0.001$, Unpaired t-test.

Panx1 promotes Tcm cell survival through the eATP receptor P2RX7

Panx1 is usually described as an ATP exporter [20, 23, 24, 25, 26, 27], and has been linked with activation of the eATP sensor P2RX7 [32, 39]. However, we found an important role for Panx1 in both effector and memory CD8$^+$ T cell establishment. This is at odds with our previous studies on P2RX7, which reported a crucial role for memory CD8$^+$ T cell homeostasis but not for effector CD8$^+$ T cell expansion [32]. To test if Panx1 regulates effector or memory CD8$^+$ T cells through P2RX7, we used CRISPR-Cas9 [40] to induce Panx1-KO in WT and P2RX7-KO P14 cells, thus generating double-knockout (DKO) CD8$^+$ T cells (**Fig. 4a**). Upon adoptive transfer and LCMV infection, spleen DKO P14 cells were significantly underrepresented at the effector phase of the immune response, when compared to either WT or P2RX7-KO P14 cells (**Fig. 4b**). DKO P14 cell numbers were equal to single Panx1-KO P14 cells (**Fig. 4b**). These results suggest that Panx1 promotes the expansion of effector CD8$^+$ T cells independently of P2RX7. At the memory phase, we observed similar P14 Tcm cell numbers between Panx1-KO, P2RX7-KO and DKO groups – all lower than WT P14 Tcm cells (**Fig. 4c**). Therefore, in contrast with effector CD8$^+$ T cells, Panx1 may regulate Tcm cell establishment through P2RX7. The

numbers of LLEC P14 cells follow the pattern observed for effector $CD8^+$ T cells, with no redundancy between Panx1-KO and DKO cells (**Fig. 4d**).

We have previously established that P2RX7 promotes memory $CD8^+$ T cells partly through activation of the AMPK pathway [32]. AMPK activation can be triggered, among other signals, by increased AMP-to-ATP ratios [41, 42]. Since Panx1 blockade promoted increased intracellular ATP (**Extended Data Fig. 1**), we monitored activation of the AMPK pathway in Panx1-KO memory $CD8^+$ T cells. Panx1-KO led to decreased phosphorylation of the downstream AMPK target Acetyl-CoA-Carboxylase (pACC) in memory $CD8^+$ T cells, especially Tcm cells (**Fig. 4e**). This suggests a connection between Panx1 promotion of memory $CD8^+$ T cells and activation of the AMPK pathway.

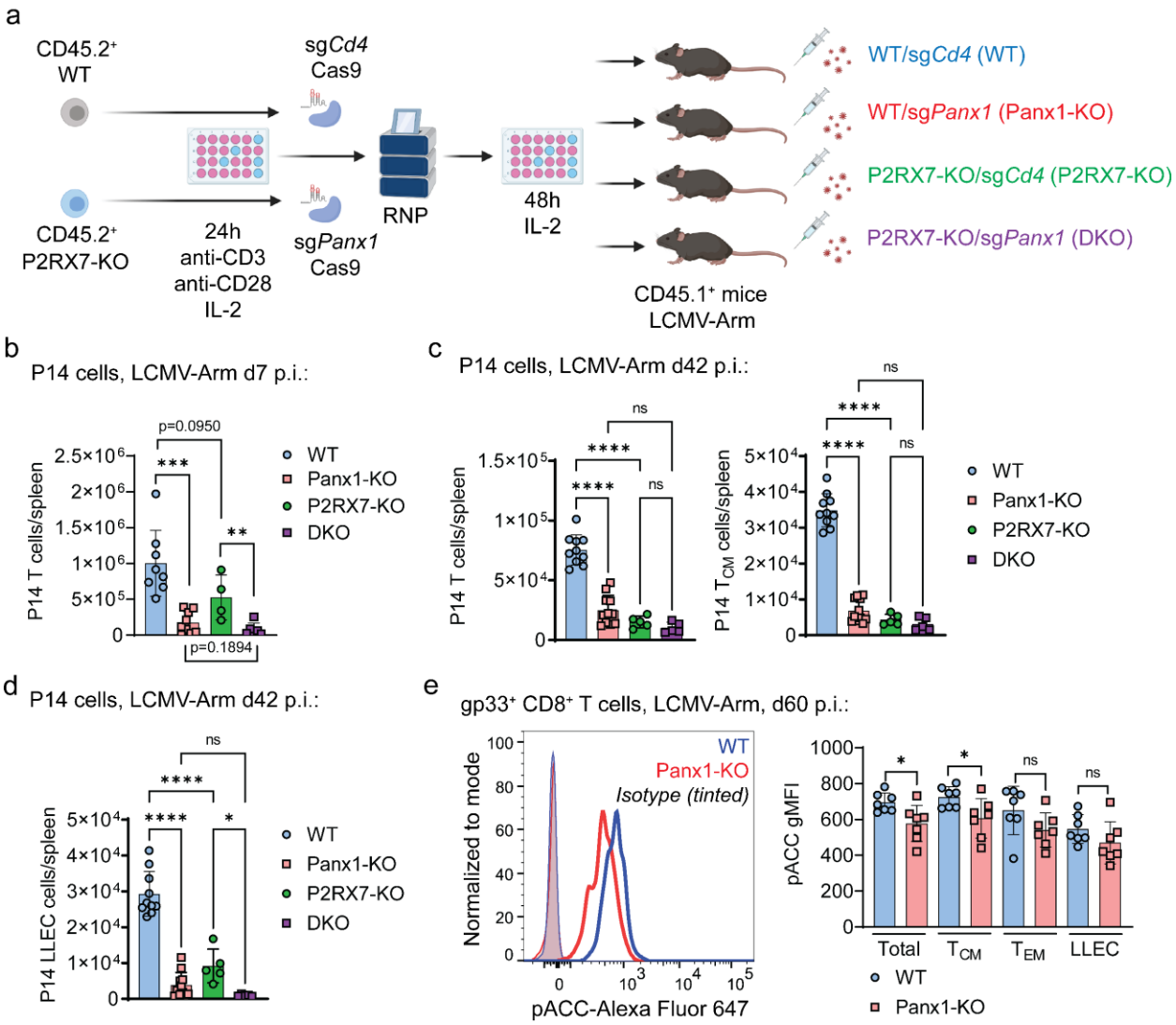

Fig. 4. Panx1 promotes Tcm establishment of CD8⁺ T cells through P2RX7 and activation of AMPK. (**a-d**) WT (CD4-Cre) or P2RX7-KO (CD4-Cre *P2rx7*$^{fl/fl}$) P14 cells (CD45.2⁺) were *in vitro* activated for 24h, then were electroporated with the Cas9 protein combined with sgRNAs for *Cd4* (sg*Cd4*; control) or *Panx1* (sg*Panx1*; Panx1-KO). After 48h of resting with IL-2, P14 cells were transferred into recipient mice (CD45.1⁺) infected with LCMV-Arm. (**a**) Experimental design. (**b**) Numbers of spleen P14 cells at day 7 post-infection. (**c**) Numbers of total spleen P14 cells (left) and spleen Tcm P14 cells (right) at day 42 post-infection. (**d**) Numbers of spleen LLEC P14 cells at day 42 post-infection. (**e**) WT (CD4-Cre) and Panx1-KO (CD4-Cre *Panx1*$^{fl/fl}$) were infected with LCMV-Arm. In the left, representative histograms showing staining with phospho-Acetyl-CoA Carboxylase (pACC) in WT and Panx1-KO gp33⁺ CD8⁺ T cells are shown. In the right, average gMFI values for pACC for total, Tcm, Tem and LLEC gp33⁺ CD8⁺ T cells are shown. (**a-d**) Data are from 2-3 independent experiments, n=4-10 per experimental group. €

Data are from three independent experiments, n=7 per experimental group. (**a-e**) * $p<0.05$, ** $p<0.01$, *** $p<0.001$, **** $p<0.0001$, One-way ANOVA with Tukey post-test.

Panx1 expression oppositely regulate the intracellular metabolism of effector and memory-programmed CD8$^+$ T cells

We found that Panx1 regulates CD8$^+$ T cell activation quickly after priming (**Fig. 3**). We also found that Panx1 promotes sustained effector and memory responses *in vivo*, via P2RX7-independent and P2RX7-dependent pathways, respectively (**Fig. 4**). Because each one of these three stages of CD8$^+$ T cell function are regulated by intracellular metabolic pathways [42, 43], we used *in vitro* systems to track CD8$^+$ T cells after initial activation, with effector-like conditions (in the presence of IL-2) or with memory-like (with IL-15) conditions (**Fig. 5a**) [44]. After 72h of *in vitro* activation, Panx1-KO CD8$^+$ T cells display reduced engagement of bioenergetic pathways needed for complete CD8$^+$ T cell activation [43]: aerobic glycolysis and mitochondrial respiration (**Fig. 5b-c**). A more nuanced scenario is observed for effector-like and memory-like cells. Our RNA-seq analyses of these populations pointed to unique transcriptional signatures regulated by Panx1 expression in effector- versus memory-like cells. Effector-like Panx1-KO CD8$^+$ T cells displayed reduced expression of most genes of the glycolytic pathway, which was not true for memory-like Panx1-KO CD8$^+$ T cells (**Fig. 5d**). In contrast, memory-like Panx1-KO CD8$^+$ T cells had defective expression of genes from pro-mitochondrial function pathways, such as AMPK and FOXO1 signaling (**Fig. 5d**). In line with the transcriptional data, the effects of Panx1-KO in CD8$^+$ T cell metabolism depend on the cell functional stage: while effector-like Panx1-KO CD8$^+$ T cells displayed reduced glycolytic function (**Fig. 5e**), memory-like Panx1-KO negatively affected engagement of mitochondrial respiration (**Fig. 5f**). The opposite pathways were not affected in Panx1-KO, i.e., mitochondrial respiration in effector-like or glycolysis in memory-like Panx1-KO CD8$^+$ T cells (**Figs. 5e-f**). Agreeing with these results, mitochondrial membrane

potential was reduced in memory-like, but not effector-like, Panx1-KO $CD8^+$ T cells (**Fig. 5g**). No differences in mitochondrial mass were observed (**Fig. 5g**).

To test if a similar trend is found *in vivo*, we sorted $gp33^+$ $CD8^+$ TE and MP cells from LCMV-infected mice (WT versus T cell-Panx1-KO) and performed the same metabolic assessments. Panx1-KO TE cells had reduced glycolysis but not mitochondrial respiration, while Panx1-KO MP cells had less mitochondrial respiration rates, but no difference in glycolysis (**Fig. 5h**). These results indicate that Panx1 oppositely controls the metabolic state of effector- and memory-phenotype $CD8^+$ T cells. They also suggest that Panx1 promotes the dominant metabolic pathway used by antigen-specific $CD8^+$ T cells at either effector or memory phases.

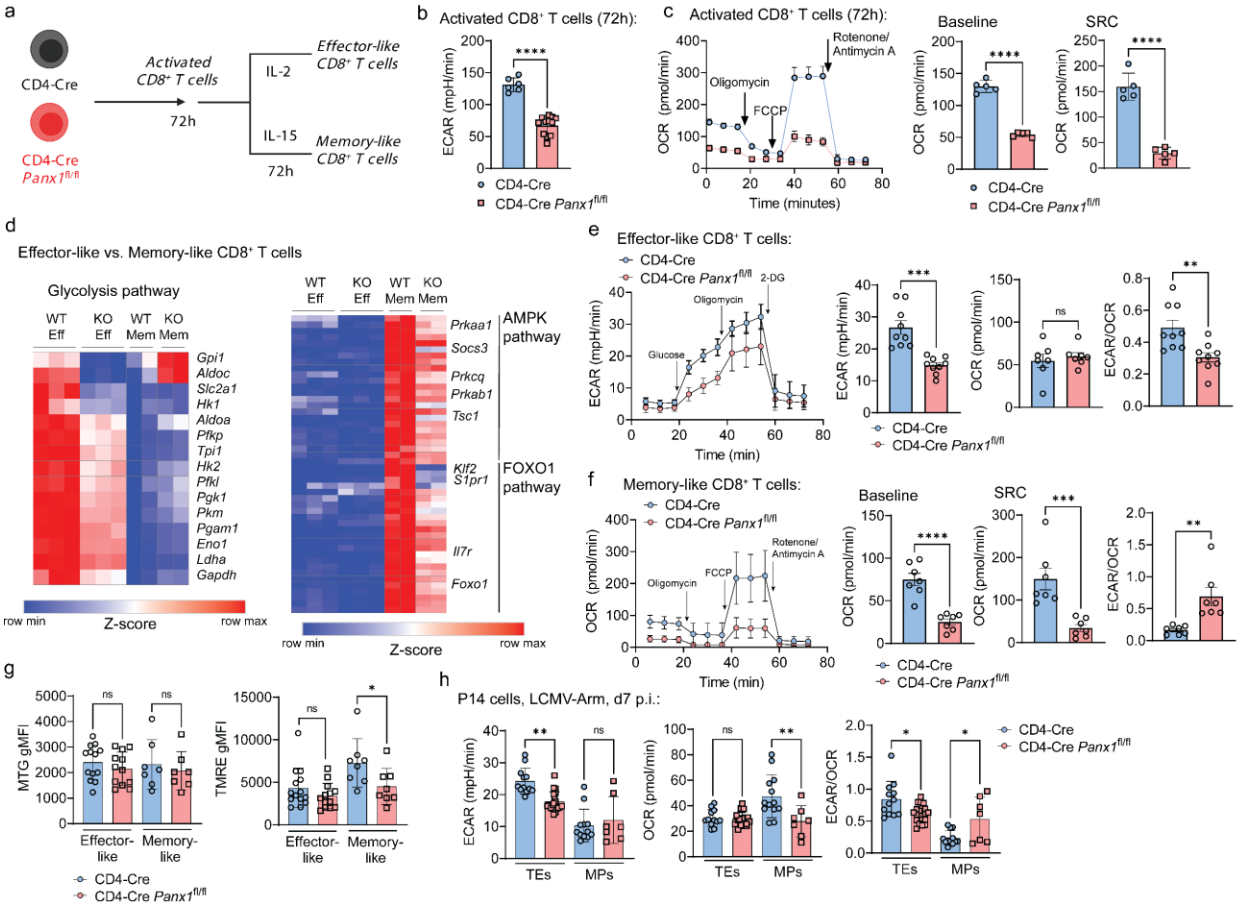

Fig. 5. Panx1 oppositely control the metabolic fate of effector and memory-phenotype CD8⁺ T cells. (**a-g**) WT (CD4-Cre) and Panx1-KO (KO; CD4-Cre *Panx1*$^{fl/fl}$) CD8⁺ T cells were *in vitro* activated for 72h; some cells were further polarized into effector-like (with IL-2) or memory-like (with IL-15) populations. Cells were collected at these three conditions and examined by Extracellular Flux Analyses (**b-c, e-f**), RNA-seq (**d**) and flow cytometry (**g**). (**a**) Experimental design. (**b**) Average measurements of Extracellular Acidification Rate (ECAR) levels from activated CD8⁺ T cells (72h). (**c**) Measurements of Oxygen Consumption Rate (OCR) levels after sequential addition of Oligomycin, FCCP and Rotenone/Antimycin A (left); on the right, average OCR values at baseline (measurement #3 of the kinetics on the left) and Spare Respiratory Capacity (SRC; see methods) from activated CD8⁺ T cells (72h). (**d**) In the left, heatmap showing expression of genes from the Glycolysis pathway in effector-like and memory-like CD8⁺ T cells. In the right, heatmap showing expression of selected genes from the AMPK and FoxO signaling pathways in effector-like and memory-like CD8⁺ T cells. (**e**) Measurements of Extracellular Acidification Rate (ECAR) levels from effector-like CD8⁺ T cells after sequential addition of Glucose, Oligomycin and 2-DG (left); on the right, ECAR values (from measurement

#6 of the above kinetics) and ratios between ECAR and OCR values from effector-like CD8$^+$ T cells. (**f**) Measurements of OCR values from memory-like CD8$^+$ T cells after sequential addition of Oligomycin, FCCP and Rotenone/ Antimycin A (left); on the right, baseline and SRC OCR values from memory-like CD8$^+$ T cells. (**g**) Average MTG and TMRE gMFI values for effector-like and memory-like CD8$^+$ T cells. (**h**) WT (CD4-Cre) and CD4-Cre *Panx1*$^{fl/fl}$ mice were infected with LCMV-Arm. At day 7 post-infection, TE and MP gp33$^+$ CD8$^+$ T cells were sorted. ECAR values, OCR values and ECAR/OCR ratios from sorted TE and MP gp33$^+$ CD8$^+$ T cells. (**b-c, e-h**) Data from three independent experiments, n=6-12 per experimental group. (**d**) Data from 2-3 biological replicates per experimental group (from n=5-8 mice per group). * $p<0.05$, ** $p<0.01$, *** $p<0.001$, **** $p<0.0001$, Unpaired t-test (**b-c, e-f**), One-way ANOVA with Tukey's post-test (**g-h**).

Panx1 promotes effector CD8$^+$ T cell activation through extracellular lactate accumulation

The P2RX7-independent role of Panx1 in effector CD8$^+$ T cells suggests that Panx1 either acts together with another eATP receptor [28, 45], or it works independently of eATP. Both effector-like and memory-like CD8$^+$ T cells export ATP via Panx1 (**Extended Data Fig. 5a**). We added exogenous eATP into Panx1-KO CD8$^+$ T cell cultures. Exogenous eATP completely rescued defective mitochondrial parameters of memory-like cells (**Fig. 6a**). In contrast, eATP did not rescue the activation defects of Panx1-KO CD8$^+$ T cells (**Fig. 6b**). Exogenous eATP also failed to rescue Panx1-KO defects in effector-like glycolytic engagement and CD69 expression (**Fig. 6c**). These results suggest that Panx1 controls the activation and effector differentiation of CD8$^+$ T cells independently of eATP accumulation.

Next, we used untargeted metabolomics to simultaneously identify the intracellular metabolic pathways and the extracellular metabolites affected by Panx1-KO in effector- or memory-like CD8$^+$ T cells (**Extended Data Fig. 5b-c**). We found >250 extracellular metabolites with

decreased levels in effector-like Panx1-KO supernatants (top 100 depicted in **Extended Data Fig. 5d**), and >300 in memory-like Panx1-KO supernatants (top 100 depicted in **Extended Data Fig. 5d**). Among the metabolites decreased in Panx1-KO effector-like CD8$^+$ T cell supernatants, we found amino acids, fatty acids, and metabolites from the glycolysis pathway (**Fig. 6d**). One of these metabolites, lactate (**Fig. 6e**), has been recently suggested to promote effector CD8$^+$ T cell activation [46, 47, 48], despite past contrary evidence [49]. Panx1 inhibition decreased extracellular lactate accumulation by activated CD8$^+$ T cells (**Fig. 6f**). Lactate also accumulate extracellularly via Panx1 from memory-like CD8$^+$ T cells (**Extended Data Fig. 5d**). The Panx1-mediated extracellular lactate accumulation by CD8$^+$ T cells could occur through control of the canonical lactate importer MCT-1 (encoded by *Slc16a1*), which is known to promote CD8$^+$ T cell proliferation [48], or its exporter MCT-4 (encoded by *Slc16a3*). Activated CD8$^+$ T cells express both MCT-1 and MCT-4 [50, 51, 52], and *Slc16a3* expression is reduced in Panx1-KO effector-like CD8$^+$ T cells (**Extended Data Fig. 5e**). MCT-4 blockade did not decrease proliferation or activation of CD8$^+$ T cells (**Fig. 6g**), nor altered extracellular lactate accumulation (**Extended Data Fig. 5f**). We then tested whether exogenous lactate would rescue the activation and proliferation of Panx1-KO CD8$^+$ T cells. Sodium lactate (a pH neutral lactate salt) significantly rescued Panx1-KO CD8$^+$ T cell proliferation and activation (**Fig. 6h**). Sodium lactate also significantly restored the glycolysis and mitochondrial respiration of activated Panx1-KO CD8$^+$ T cells (**Fig. 6i**). The restoring effects of sodium lactate are abolished when the OXPHOS inhibitor Oligomycin is concomitantly present (**Fig. 6j**), further indicating that Panx1 promotes CD8$^+$ T cell activation through bioenergetic metabolic pathways. Many TCA cycle intermediates were decreased in Panx1-KO effector-like CD8$^+$ T cells (**Extended Data Fig. 5g**).

In addition to lactate, effector CD8$^+$ T cells use Panx1 for the accumulation of many other extracellular metabolites (**Extended Data Fig. 5c-d**). In screenings to identify additional metabolites that rescue Panx1-KO CD8$^+$ T cell activation (**Extended Data Fig. 5h**), among the

few other candidates found was Hydroxylauric Acid, a medium-chain fatty acid [53]. Medium-chain fatty acids are used by CD8$^+$ T cells for fatty acid biosynthesis, a fundamental step in effector CD8$^+$ T cell activation [54]. Intracellular phospholipid biosynthesis metabolites were sharply decreased in Panx1-KO effector-like CD8$^+$ T cells (**Fig. 6k**), including phosphatidylinositol (PIs) (**Fig. 6l**). PIs compose the immunological synapse [55], and saturated (i.e., with less than 2 double bonds) phosphatidylinositol phosphates (PIPs) compose lipid rafts found during late activation, to sustain effector function [54]. Panx1-KO effector-like CD8$^+$ T cells had specific defects in saturated PIs (**Fig. 6l-m, Extended Data Fig. 5i**), and decreased lipid raft formation as depicted by Cholera Toxin B (CTB) staining (**Fig. 6n**). Additionally, oleic acid, a PI biosynthesis-forming medium-chain fatty acid [54], had decreased intracellular levels in Panx1-KO CD8$^+$ T cells (**Extended Data Fig. 5j**). Exogenous oleic acid significantly restored Panx1-KO CD8$^+$ T cell activation (**Fig. 6o**), suggesting that Panx1-mediated accumulation of this fatty acid plays a role in effector CD8$^+$ T cell activation.

In effector CD8$^+$ T cells, fatty acid biosynthesis is dependent on extracellular carbon sources, and lactate has been recently suggested as an important carbon source during CD8$^+$ T cell activation [46]. The restoring effects of lactate for Panx1-KO CD8$^+$ T cell activation are abolished when an inhibitor of CDIPT, the enzyme that catalyzes the biosynthesis of saturated fatty acids, is present (**Fig. 6p**). Lipid raft formation is restored in Panx1-KO CD8$^+$ T cells exposed to sodium lactate (**Fig. 6n**), which does not occur in the presence of MCT-1 inhibition (**Extended Data Fig. 5k**) or CDIPT inhibition (**Extended Data Fig. 5l**). Saturated PI biosynthesis leads to activation of the MAP-kinase (MAPK) signaling pathway to sustain CD8$^+$ T cell activation and effector function [54]. RNA expression of some MAPK pathway genes is decreased in Panx1-KO effector-like CD8$^+$ T cells (**Fig. 6q**), and phosphorylated ERK1/2 levels are diminished in Panx1-KO CD8$^+$ T cells – which is restored in the presence of lactate (**Fig. 6r**). Likewise, IFN-γ production is decreased in Panx1-KO CD8$^+$ T cells and rescued by lactate, in an MCT-1-

dependent way (**Fig. 6s**). Finally, sodium lactate treatment significantly rescued the effector expansion of Panx1-KO P14 cells in LCMV-infected mice (**Fig. 6t, Extended Data Fig. 6**). These findings indicate that Panx1 induces the full activation of effector $CD8^+$ T cells through extracellular lactate accumulation, which is recycled to induce optimal biosynthesis of saturated PIs that compose the immunological synapse to sustain effector function (**Extended Data Fig. 7**).

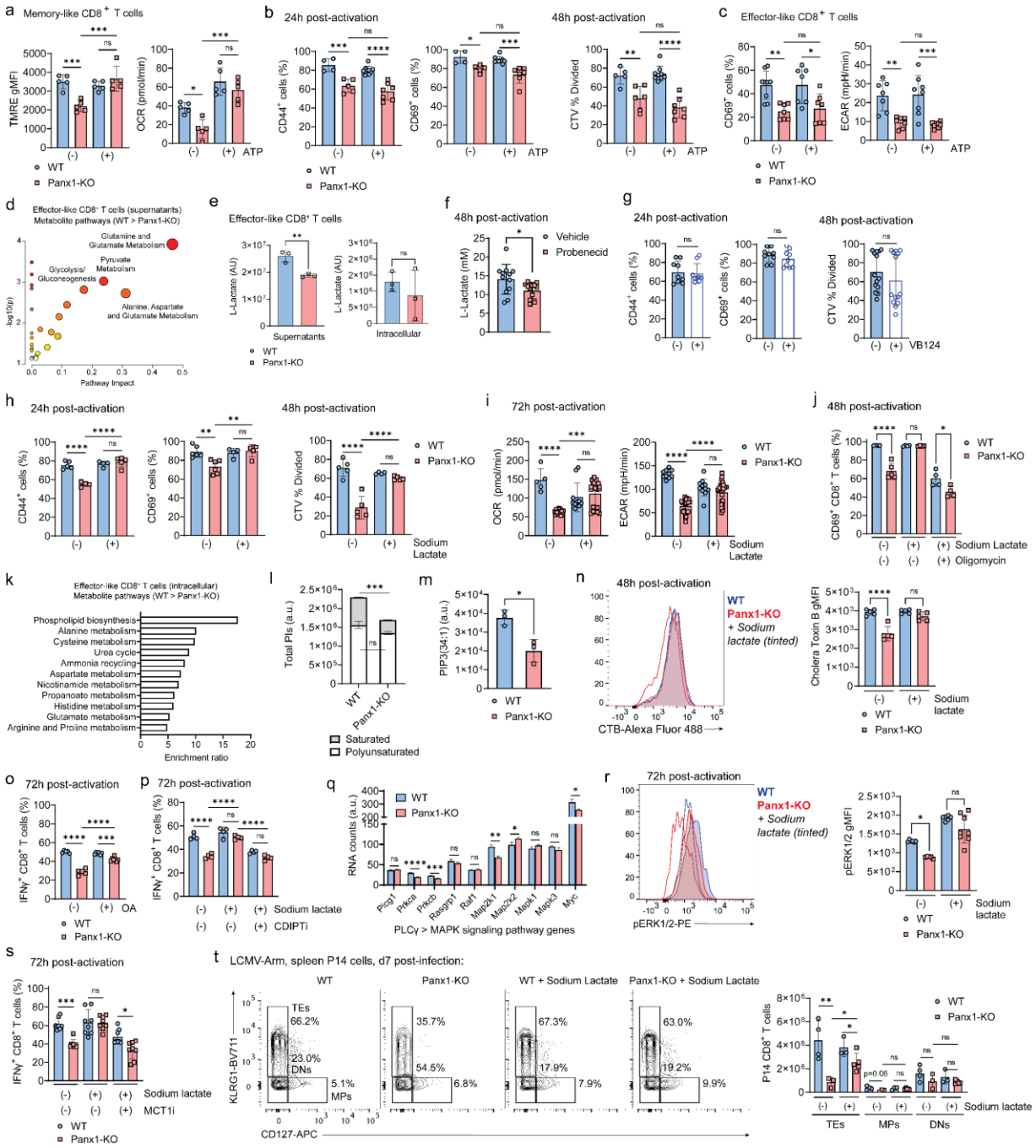

Fig. 6. Panx1 promotes the activation of effector CD8⁺ T cells through accumulation of extracellular lactate. (**a-c**) WT (CD4-Cre) and Panx1-KO (CD4-Cre *Panx1*$^{fl/fl}$) CD8⁺ T cells were activated *in vitro* (α-CD3 + α-CD28 + IL-2, 72h). In some cases, cells were further incubated with IL-2 (effector-like) or IL-15 (memory-like). In these cultures, ATP (50 μM) or vehicle (PBS) was added at the beginning of IL-2 vs IL-15 polarization (**a, c**) or at priming (0h post-activation; **b**). (**a**) TMRE gMFI values (left) and baseline OCR values (right) for memory-like CD8⁺ T cells. (**b**) Percentages of CD44⁺ cells and CD69⁺ cells at 24h post-activation (left) and of

CTV divided cells at 48h post-activation (right). (**c**) Percentages of CD69$^+$ (left) and baseline ECAR values (right) for effector-like CD8$^+$ T cells. (**d**) WT or Panx1-KO effector-like and memory-like CD8$^+$ T cell cultures were harvested, and intracellular lysates and supernatants were submitted for untargeted metabolomics (GC-MS) analysis. Enrichment analysis showing pathways preferentially represented in the metabolites from the supernatants of WT effector-like CD8$^+$ T cells (WT>Panx1-KO). (**e**) Levels (arbitrary units – AU) of l-lactate in the supernatants (left) and intracellular lysates (right) of effector-like WT and Panx1-KO CD8$^+$ T cells. (**f**) WT CD8$^+$ T cells were *in vitro* activated, and the Panx1 inhibitor Probenecid (100 μM) or vehicle (0.1% DMSO) was added after 24h. L-lactate supernatant concentrations were measured at 48h post-activation. (**g**) WT CD8$^+$ T cells were activated *in vitro*. In these cultures, the MCT-4 inhibitor VB124 (10 μM) or vehicle (0.1% DMSO) was added at priming. Percentages of CD44$^+$ and CD69$^+$ cells at 24h post-activation (left) and of CTV divided cells at 48h post-activation (right) are shown. (**h-i**) WT and Panx1-KO CD8$^+$ T cells were activated *in vitro*. In these cultures, Sodium Lactate (1 mM) or vehicle (0.1% DMSO) was added at priming. (**h**) Percentages of CD44$^+$ cells, CD69$^+$ cells (left) and of CTV divided cells (right) at the indicated time points after activation are shown. (**i**) OCR (left) and ECAR (right) values at 72h post-activation are shown. (**j**) In some *in vitro* activation cultures, WT and Panx1-KO CD8$^+$ T cells were treated with Sodium Lactate in the presence or not of Oligomycin (1.37 nM). Percentages of CD69$^+$ cells at 48h post-activation are shown. (**k**) Top enriched intracellular pathways in WT effector-like CD8$^+$ T cells (compared to Panx1-KO), depicted from the untargeted metabolomics from (d). (**l**) Levels (AU) of total PIs in WT versus Panx1-KO effector-like CD8$^+$ T cells; polyunsaturated (2 or more double bonds) or saturated (1 or less double bonds) PIs are depicted in white and grey, respectively. (**m**) Levels (AU) of PIP(34:1) in WT versus Panx1-KO effector-like CD8$^+$ T cells. (**n**) WT and Panx1-KO CD8$^+$ T cells were activated in the presence or not of Sodium Lactate as described above. Representative histograms (left) and average gMFI values (right) for Cholera Toxin B are shown. (**o**) WT and Panx1-KO CD8$^+$ T cells were activated in the presence or not of BSA-conjugated Oleic Acid (OA; 100 μM). Average percentages of IFNγ$^+$ CD8$^+$ T cells are shown. (**p**) WT and Panx1-KO CD8$^+$ T cells were activated in the presence or not of Sodium Lactate and/or the CDIPT inhibitor Inostamycin (CDIPTi; 0.2 μg/ml). Average percentages of IFNγ$^+$ CD8$^+$ T cells are shown. (**q**) RNA expression levels (AU) of the indicated PLCγ-MAPK signaling pathway genes in WT and Panx1-KO effector-like CD8$^+$ T cells. (**r**) WT and Panx1-KO CD8$^+$ T cells were activated in the presence or not of Sodium Lactate as described above. Representative histograms (left) and average gMFI values (right) for phosphorylated ERK1/2 (pERK1/2) are shown. (**s**) WT and

Panx1-KO CD8$^+$ T cells were activated in the presence or not of Sodium Lactate and/or the MCT1 inhibitor AZD3985 (MCT1i; 10 nM). Average percentages of IFNγ$^+$ CD8$^+$ T cells are shown. (**t**) WT or Panx1-KO P14 cells (CD45.2$^+$) were transferred into WT CD45.1$^+$ mice, which were infected with LCMV-Arm. Some mice were treated with sodium lactate between days 1-3 post-infection. Spleen P14 cells were analyzed at day 7 post-infection. Representative flow cytometry plots showing expression of CD127 and KLRG1, and identifying TE, MP and DN cells are shown in the left. In the right, average numbers of TE, MP and DN P14 cells per spleen are shown. (**a-c**, **f-j**, **n-p**, **r-t**) Data from 2-3 independent experiments, n=3-14 per experimental group. (**d-e**, **k-m**, **q**) Data from 3 biological replicates per experimental group (from n=3 mice per group). * p<0.05, ** p<0.01, *** p<0.001, **** p<0.0001, Unpaired t-test (**e-g**, **l-m**, **q**), One-way ANOVA with Tukey's post-test (**a-c**, **h-j**, **n-p**, **r-t**).

Panx1 deficiency hinders tumor control by CD8$^+$ T cells

Given the importance of CD8$^+$ T cell responses for the control of solid tumors such as melanoma [56, 57, 58], we assessed the role of Panx1 in melanoma control. Global Panx1-KO mice did not display any differences in the control of B16 melanomas (**Fig. 7a-b**). To avoid the potential confusion caused by non-CD8$^+$ T cell-specific effects, we used an adoptive cell therapy (ACT) model [59, 60] to test if CD8$^+$ T cell-specific Panx1 is needed for activated CD8$^+$ T cells to infiltrate and control solid tumors. *In vitro*-activated Panx1-KO P14 cells are defective in limiting B16-gp33 tumor growth (**Fig. 7c-d**) and promoting survival of B16-gp33 tumor-bearing mice (**Fig. 7e**), in comparison to activated WT P14 cells. We next evaluated the numbers and phenotype of adoptively transferred WT and Panx1-KO P14 cells in tumor-bearing mice, in co-transfer experiments. In these experiments, we found significant underrepresentation of Panx1-KO P14 cells infiltrating B16 tumors, and no differences in draining lymph nodes or spleen (**Fig. 7f, left**). Among tumor-infiltrating P14 cells, Panx1-KO cells display signs of mitochondrial dysfunction, such as increased percentages of cells with depolarized mitochondria, decreased mitochondrial mass and decreased mitochondrial membrane potential (**Fig. 7f, right panels**).

Overall, these results suggest that expression of Panx1 is important for CD8⁺ T cells to infiltrate tumors, maintain their metabolic homeostasis, and perform optimal antitumor function upon activation.

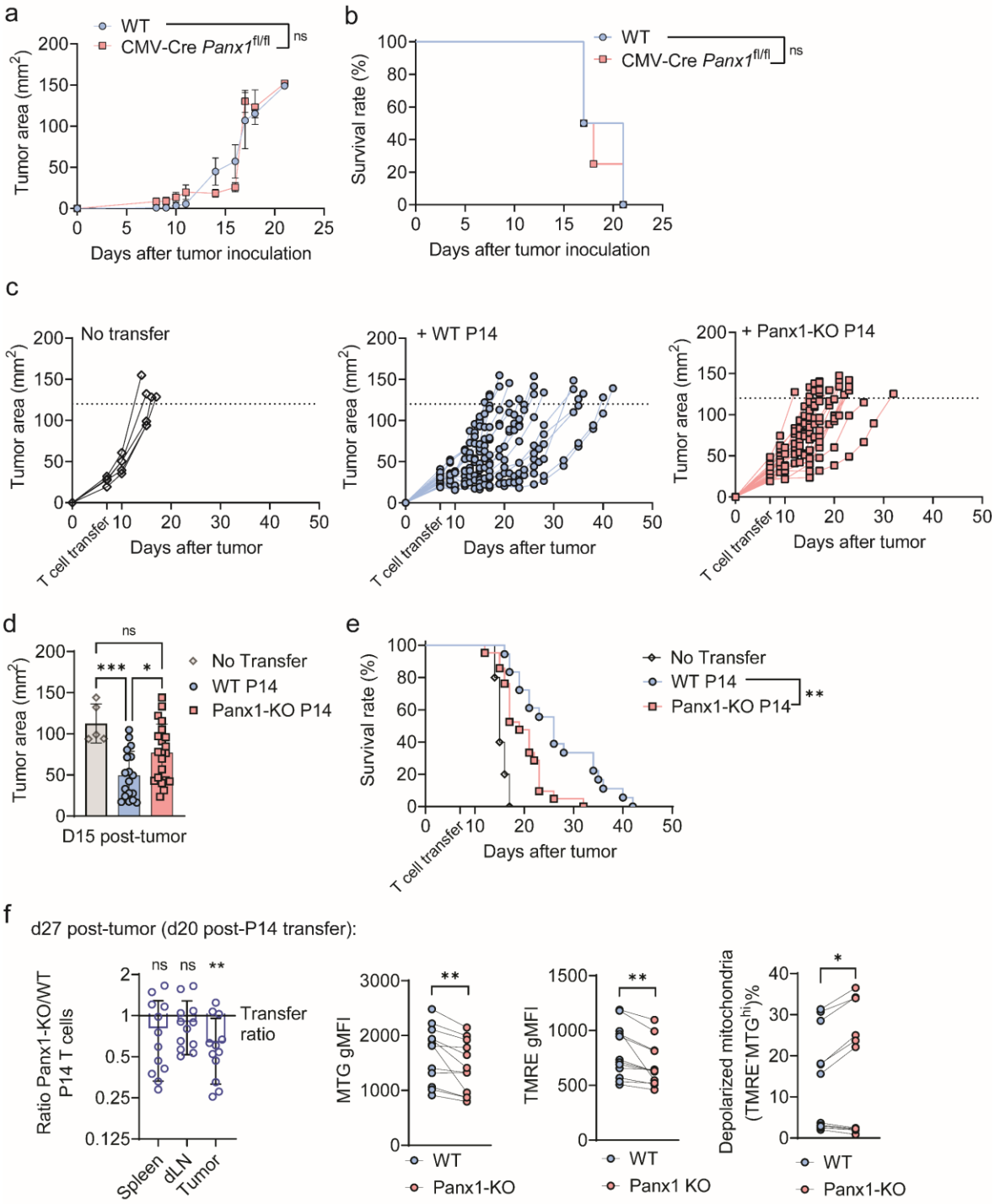

Fig. 7. CD8-specific Panx1 harnesses the antitumor ability of CD8$^+$ T cells. (**a-b**) WT (CMV-Cre) and CMV-Cre *Panx1*$^{fl/fl}$ mice were inoculated with B16.F10 melanoma cells. The tumor sizes and survival of mice were tracked over time post-tumor inoculation. (**a**) Average tumor growth values over time. (**b**) Survival curves over time. (**c-e**) In other experiments, WT (CD4-Cre) and Panx1-KO (CD4-Cre *Panx1*$^{fl/fl}$) P14 cells were activated *in vitro* (α-CD3, α-CD28, IL-2 and IL-12 – refs.49-50) for 72h. After this period, P14 cells were transferred (individually or co-transferred) into B16.gp33 tumor-bearing mice. The tumor sizes and survival of individually transferred mice were tracked over time post-tumor inoculation; the numbers and phenotype of transferred P14 cells were assessed at 20 days post-tumor inoculation in co-transferred mice. (**c**) Individual tumor growth values over time. (**d**) Average tumor areas at day 14 post-tumor inoculation are shown. (**e**) Survival curves of individually transferred mice over time. (**f**) Average Panx1-KO/WT P14 cell number ratios in the indicated organs are shown in the left; in the right three panels, the respective values for percent of P14 cells with depolarized mitochondria (MTG^{hi}TMRE$^-$), gMFI for MTG and gMFI for TMRE are displayed. (**a-b**) Data from 2 independent experiments, n=8 per experimental group. (**c-f**) Data from 3 independent experiments, n=5-20 per experimental group. * $p<0.05$, ** $p<0.01$, *** $p<0.001$, Unpaired t-test (**d, f**), Kaplan-Meier Survival curve analysis (**a, e**).

Discussion

Sensing of extracellular metabolites promotes CD8$^+$ T cell metabolism, homeostasis, and function [61, 62, 63]. The precise sources of these metabolites and how they affect CD8$^+$ T cell intracellular pathways are still not fully understood. Our work suggests that, through the action of Panx1, CD8$^+$ T cells provide multiple metabolites for their own sensing. Panx1 is a well-known eATP exporter [20], but our work shows that Panx1 is a “master transporter” in healthy CD8$^+$ T cells, promoting the extracellular accumulation of many metabolites that can promote either memory (eATP) or effector (lactate) CD8$^+$ T cell responses. Our results suggest that effector and memory-phenotype CD8$^+$ T cells use Panx1 to export similar levels of eATP and lactate, ruling out differential metabolite export as a reason why Panx1 oppositely controls their

metabolism. Rather, what dictates the outcome of the Panx1 role are the signaling pathways and requirements specific for effector or memory $CD8^+$ T cells. In future studies, we will investigate if this is generalizable for all metabolites exported via Panx1, or if there are certain molecules that are exported differentially in effector versus memory $CD8^+$ T cells.

Panx1 promotes the survival of memory $CD8^+$ T cells. Our data suggested that Panx1 favors the homeostasis of memory $CD8^+$ T cells through export of eATP that is, in turn, sensed by P2RX7. These results resembled previous reports on *in vitro*-stimulated T cells [31, 39]. Moreover, they corroborated our speculation that, at the memory phase, eATP levels are tightly regulated around the pericellular space of memory $CD8^+$ T cells [32, 64]. This process can be, at first, viewed as energetically futile: export of ATP would result in a decrease in intracellular levels and subsequent lower availability for energy demanding processes. However, there are possible advantages to Panx1-induced eATP export. First, that would ensure constant engagement of P2RX7 to sustain Ca^{2+} influx and subsequent mitochondrial health and function [65]. Indeed, Panx1-KO memory-phenotype $CD8^+$ T cells display defective mitochondrial respiration. The exceptions were Trm cells forming in tissues where potential alternative eATP sources are present: the SI-IEL, where eATP can be microbiota-derived [37, 66], and the influenza-infected lung, where release of eATP by tissue damage may occur. These results reinforce the notion that Panx1 induces memory $CD8^+$ T cell survival as an eATP exporter (**Extended Data Fig. 7**).

We also found a fundamental role of Panx1 in promoting effector $CD8^+$ T cell responses to antigen. Unexpectedly, the role of Panx1 was shown to be eATP- and P2RX7-independent. This contrasts with previous reports, which have suggested Panx1-induced ATP export as an important step in T cell activation [45, 67]. These studies, however, used readouts such as Ca^{2+} influx, early mitochondrial activity, or T cell migration. Our current work does not dispute the fact that Panx1 promotes ATP export at this stage of immune response, neither that it can induce

such effects on CD8$^+$ T cells. However, these readouts may not fully capture the steps needed for full CD8$^+$ T cell effector differentiation. It is possible, therefore, that some initial steps of CD8$^+$ T cell priming occur through Panx1-mediated eATP release, but full differentiation of effector CD8$^+$ T cells may rely on other metabolites exported via Panx1 [24, 68].

Apoptotic T cells secrete many distinct metabolites via Panx1 [21]. Our work is the first one, to our knowledge, showing Panx1-mediated broad metabolite export in healthy activated CD8$^+$ T cells. Our data suggested that one of these metabolites, lactate, plays a substantial role in Panx1-induced CD8$^+$ T cell activation. Glycolytic activity in activated CD8$^+$ T cells induce production and export of lactate [69], leading to its extracellular accumulation [70]. Because its export is coupled with acidosis, lactate has been considered a CD8$^+$ T cell suppressor [49, 71]. Lactate-induced acidosis, however, is only observed in hypoxia, such as in the tumor microenvironment [72]. During T cell priming, lactate is likely present in a pH neutral condition, which is well-tolerated by cells [73]. Our results indicate that Panx1-induced extracellular lactate can be recycled by activated CD8$^+$ T cells via MCT-1, which leads, in sequence, to: saturated PI biosynthesis, lipid raft formation, induction of MAPK pathway activation, and reinforcement of the effector CD8$^+$ T cell program (**Extended Data Fig. 7**). Our work provides additional evidence that (a) carbon sources induce the generation of optimal lipid raft structures for sustained CD8$^+$ T cell activation [54], and that glucose-independent sources such as lactate is a relevant carbon source for CD8$^+$ T cell activation and effector differentiation [46, 47, 69]. Panx1, therefore, may be a “link” between these two concepts, by promoting the accumulation of an extracellular lactate pool, that in turn is used by activated CD8$^+$ T cells to sustain its effector differentiation. Our results showing that inhibition of CDIPT not only blocks the rescuing effects of sodium lactate, but also phenocopied Panx1 deficiency in WT CD8$^+$ T cells (**Fig. 6p, Extended Data Fig. 5l**), further suggest a direct connection between Panx1 function and lipid rafts formation.

CD8$^+$ T cell-specific Panx1 also promotes melanoma control. At first, these results conflict with human cancer data, which shows high *PANX1* gene expression linked with poor prognosis in multiple tumors [74], including melanoma [75]. Our data, however, focus on the CD8$^+$ T cell-specific roles of Panx1. The ACT experiments, therefore, reinforce a model where Panx1 expression in CD8$^+$ T cells promote efficient immune responses mediated by these cells and better tumor control. Because of the mitochondrial defects observed in intratumoral CD8$^+$ T cells lacking Panx1, we speculate that, in the context of melanoma, the dominant role of Panx1 is to promote the longevity and homeostasis of CD8$^+$ T cells once inside tumors. Additional studies will be necessary to further understand this mechanism. It is also unclear if the role of Panx1 for CD8$^+$ T cell antitumor activity is related to eATP or lactate export. We recently reported that sensing of eATP through P2RX7 promotes CD8$^+$ T cell antitumor function and increased mitochondrial homeostasis in the same adoptive cell transfer model of melanoma [60], like what we observed for Panx1. Thus, Panx1 may serve as an eATP source in IL-12-treated CD8$^+$ T cells, which in turn are better equipped to withstand the tumor microenvironment. Extracellular lactate may not play a role in Panx1-induced CD8$^+$ T cell antitumor function, mainly because of the acidosis associated with its tumor extracellular accumulation [76]. However, a possible role of pH-independent lactate on promoting CD8$^+$ T cell tumor control has been suggested recently [72]. Whether Panx1-mediated lactate export helps CD8$^+$ T cell effector function against melanoma – perhaps together with eATP accumulation – remains to be defined.

Panx1 research often focus on the effect of extracellular metabolite export. However, Panx1 export of molecules leads to their intracellular decrease. This is true for ATP [32] and we have previously speculated the possible consequences of Panx1-mediated intracellular ATP decrease for CD8$^+$ T cells [64]. Promotion of the AMPK pathway due to decreased intracellular ATP in an LKB-dependent pathway is known to favor memory CD8$^+$ T cell homeostasis [77], which we have shown to rely on P2RX7 [32]. Here, we found that Panx1-KO memory CD8$^+$ T cells

have diminished AMPK activity. This suggests that $CD8^+$ T cell Panx1 is part of the P2RX7/AMPK circuit: Panx1 export of ATP in memory $CD8^+$ T cells induces a decrease in intracellular ATP, which leads to increased AMP/ATP ratios and subsequent AMPK activation [32]. Panx1-mediated intracellular metabolite alterations could also have effects on lactate. Excess intracellular lactate can hinder T cell activation [78], therefore Panx1-mediated lactate export can prevent this shutdown. We will investigate this possibility in the future, which would suggest Panx1 also acts as a "metabolite escape valve" for effector or memory $CD8^+$ T cells.

Here, we demonstrated that $CD8^+$ T cells need Panx1 channels for their proper activation, expansion, and survival into memory phase. Beyond the classical nucleotide exporter role of Panx1, our results unveiled an unexpected link between expression of Panx1 and extracellular accumulation of many metabolites including lactate – which is necessary for proper activation of $CD8^+$ T cells. Defining how Panx1 acts as an amplifier of $CD8^+$ T cell responses will open new directions on our understanding of how adaptive immune cells interact with their surrounding milieu in response to disease. Our data suggests that, at least in part, $CD8^+$ T cells can use Panx1 to generate a favorable extracellular microenvironment by recycling products of their own intracellular metabolic pathways.

Acknowledgments: We thank the Borges da Silva and Lancaster labs (Mayo Clinic Arizona) for their intellectual input. We are thankful to the animal facilities at Mayo Clinic Arizona and at the University of Minnesota for technical assistance and mouse husbandry; T. Brehm-Gibson, C. Viso and I. Silva-Junior for cell sorting and Flow Cytometry Core Facility maintenance at Mayo Clinic Arizona. We thank K. Ravichandran (U-Virginia, now Washington University) for providing the *Panx1*$^{fl/fl}$ mice. We thank G. Hasko (Rutgers University) and Matyas Sandor (U-Wisconsin) for providing the *P2rx7*$^{fl/fl}$ mice. BGI Americas provided bioinformatic support and resources that helped achieve the results reported within this paper. This work was supported

by an individual predoctoral F30 fellowship from the National Institutes of Health (NIH) (F30CA250321) to K.M.W.; NIH grants R01AI038903 and R01AI145147 to S.C.J.; Mayo Clinic Center for Biomedical Discovery Pilot Grant-2021, and NIH grants K99/R00A139381 and R01A170649 to H.BdS.

Article contributions

Conceptualization, H.BdS.; Methodology, H.BdS.; Formal Analysis, T.V-K., A.B., M.G-P., K.M.W., S.C.J. and H.BdS.; Investigation, T.V-K., A.B., M.G-P, K.M.W., M.H.Z., S.vD., B.G.M., C.L.S., I.S-C., C.P., and H.BdS.; Resources, S.C.J. and H.BdS.; Data Curation, H.BdS.; Writing – Original Draft, T.V-K. and H.BdS.; Writing – Review & Editing, T.V-K., A.B., M.G-P., K.M.W., S.C.J, and H.BdS.; Supervision, H.BdS.; Project Administration, H.BdS.; Funding Acquisition, S.C.J. and H.BdS.

Conflicts of interest

H.BdS. is an advisor for International Genomics Consortium. The remaining authors have no financial disclosures.

Materials and Methods

Mice

Male and female 6- to 8-week-old adult C57BL/6 (B6) and B6.SJL (expressing the CD45.1 allele) mice were purchased from Jackson and Charles River and were allowed to acclimate to our housing facilities for at least one week. CD4-Cre, ERT2-Cre, CMV-Cre and R26-EYFP (LSL-YFP) mice were obtained from Jackson Laboratories. *P2rx7*$^{fl/fl}$ mice were obtained from Drs. Gyorgy Hasko (Rutgers University) and Matyas Sandor (U-Wisconsin). *Panx1*$^{fl/fl}$ mice were

obtained from Dr. Kodi Ravichandran (U-Virginia; now Washington University). OVA-K^b SIINFEKL-specific TCR transgenic OTI and LCMV-D^b GP33-specific TCR transgenic P14 mice were bred in-house at the University of Minnesota and then transferred to Mayo Clinic Arizona. OTI and P14 mice were fully backcrossed to B6 and CD4-Cre *Panx1*$^{fl/fl}$ mice, with introduction of CD45.1 and CD45.2 congenic markers for identification. Animals were maintained under specific-pathogen-free conditions at Mayo Clinic Arizona and at the University of Minnesota. In all experiments, mice were randomly assigned to experimental groups. All experimental procedures were approved by the institutional animal care and use committee at Mayo Clinic Arizona (IACUC A00005542-20) and at the University of Minnesota (IACUC 1709-35136A).

Viral strains

LCMV (Armstrong strain) was maintained at −80°C until infection and diluted to $2x10^6$ PFU/ml in PBS. Influenza (PR8 strain) was maintained at −80°C and diluted to $7x10^4$ PFU/ml in PBS at the time of infection studies.

Infection studies

WT (CD4-Cre, ERT2-Cre-LSL-YFP), CD4-Cre *Panx1*$^{fl/fl}$, ERT2-Cre-LSL-YFP-*Panx1*$^{fl/fl}$, and CD4-Cre *P2rx7*$^{fl/fl}$ P14 cells were adoptively transferred into naive wild-type mice, which were infected with LCMV-Armstrong (2×10^5 PFU, intraperitoneally (i.p.)). Sometimes, wild-type (CD4-Cre, CMV-Cre), CMV-Cre *Panx1*$^{fl/fl}$ or CD4-Cre *Panx1*$^{fl/fl}$ mice were infected with LCMV Armstrong. In other experiments, wild-type (CD4-Cre) or CD4-Cre *Panx1*$^{fl/fl}$ mice were infected with Influenza-PR8 (1400 PFU, intranasally (i.n.)). In some experiments, LCMV-infected mice were treated with Trovafloxacin (4.2 mg x kg^{-1} mouse, Sigma-Aldrich) or Sodium Lactate (1.68 g x kg^{-1} mouse, Sigma-Aldrich)[72] between days 1-7 after infection.

Tumor inoculations

WT or CMV-Cre *Panx1*$^{fl/fl}$ mice were injected subcutaneously with 1.5 x 10^5 B16.F10 or 3 x 10^5 B16.F10.gp33 cells in the right flank. In some experiments, after tumors became palpable (~7 days), tumor-bearing mice received 5 x 10^5 activated CD4-Cre or CD4-Cre *Panx1*$^{fl/fl}$ P14 cells (or 2.5 x 10^5 of a 1:1 mix of these two P14 populations for co-transfer experiments). Tumor growth was monitored by measuring height and width with calipers until mice reached an endpoint criterion of 144 mm^2 or ulceration. When indicated in the figures, tumor-bearing mice were sacrificed for flow cytometry analysis.

Bone marrow chimeras

CD45.1/2$^+$ WT mice were reconstituted with a 1:1 mixture of CD4-Cre (CD45.1$^+$) and CD4-Cre *Panx1*$^{fl/fl}$ (Panx1-KO, CD45.2$^+$) following lethal irradiation (2 x 450 Rad). Two months following irradiation, mice were infected with LCMV-Armstrong.

Administration of tamoxifen in mice

Tamoxifen (Sigma-Aldrich, diluted in Sunflower Oil) was administered to mice i.p. at a daily dose of 1 mg [37]. Two different treatment periods were used, in which Tamoxifen was given between days 1-4 or between days 28-35 after LCMV-Armstrong infection.

Primary cell cultures

Total CD8$^+$ T cells or P14 cells were obtained from 6- to 8-week-old mice with a C57BL/6 background. Cells were cultured in complete RPMI media: RPMI 1640 (Corning) supplemented with 10% Fetal Bovine Serum (Atlanta Biologicals), 100 U/ml penicillin/streptomycin (Thermo Fisher Scientific) and 2 mM L-glutamine (Corning). All cells were cultured at 37°C in a humidified atmosphere containing 5% CO_2.

In vitro activation of CD8$^+$ T cells

P14 and/or polyclonal WT (CD4-Cre), P2RX7-KO (CD4-Cre *P2rx7*$^{fl/fl}$) or Panx1-KO (CD4-Cre *Panx1*$^{fl/fl}$) CD8$^+$ T cells were isolated from naïve mice with the Mouse CD8$^+$ T cell isolation kit (Miltenyi Biotec). Cells were stimulated for 24h, 48h or 72h with plate-bound αCD3 (10 µg/ml), plate-bound αCD28 (20 µg/ml) and soluble IL-2 (10 ng/ml). When indicated, ATP (50 µM, Sigma-Aldrich), Sodium Lactate (1 mM, Sigma-Aldrich), VB-124 (10 µM, Tocris), Oligomycin (1.39 nM, Agilent), BSA-conjugated Oleic Acid (100 µM, ThermoFisher), Inostamycin (0.2 µg/ml, Cayman Chemical) or AZD3965 (10 nM, Cayman Chemical) were added to the cultures at the beginning of activation. In screening experiments, multiple other compounds were added to the cultures, or in alternative their respective vehicles. A complete list of screening compounds is depicted in **Extended Data Table 1**. In some experiments, after 72h of activation, CD8$^+$ T cells were incubated for an additional 72h with either recombinant IL-2 (10 ng/ml) or IL-15 (10 ng/ml).

Flow cytometry

Lymphocytes were isolated from tissues including spleen, inguinal lymph nodes, cervical lymph nodes, blood, small intestine epithelium (SI IEL), salivary glands (SG), tumors, lungs and kidneys as previously described [32, 37, 60]. In summary, organs were removed and cut in small pieces into Erlenmeyer flasks containing 30 mL of 0.5 mg/ml Collagenase type I solution (tumor, kidney, and SG), 0.5 mg/ml Collagenase type IV (lung) or 0.15 mg/ml Dithioerythritol (SI IEL). Following this period, lymphocytes were isolated by 44/67% Percoll gradient isolation. During isolation of lymphocytes from non-lymphoid tissues, in all experiments, 50 µg of Treg-Protector (anti-ARTC2.2) nanobodies (BioLegend) were injected i.v. 30 minutes prior to mouse sacrifice [35]. Direct *ex vivo* staining and intracellular staining were performed as described [32]. To identify LCMV-specific or Flu-specific CD8$^+$ T cells, tetramers were obtained from the Yerkes NIH Tetramer Core: D^b-gp33 and D^b-NP-flu tetramers conjugated with APC- or PE-Streptavidin were used. For detection of vascular-associated lymphocytes in non-lymphoid organs, *in vivo* i.v. injection of PerCP-Cy5.5-conjugated CD8α antibody was performed [79]. Among LCMV- or Flu-

specific $CD8^+$ T cells, the following markers were used to distinguish these respective populations: naïve ($CD44^-CD62L^+$), Tcm ($CD44^+CD62L^+$), Tem ($CD44^+CD62L^-CD127^+$), LLEC ($CD44^+CD62L^-CD127^-KLRG1^{hi}$), Trm (i.v.$CD8\alpha^-CD69^{+/-}CD103^{hi/int/lo}$), MPs ($CD127^+KLRG1^{-)}$, TEs ($CD127^-KLRG1^+$). Adoptively transferred P14 cells and LCMV-specific $CD8^+$ T cells in mixed bone marrow chimeras were identified using a combination of CD45.1 and CD45.2 monoclonal antibodies. In some experiments, To-Pro 3 (Sigma-Aldrich) was added right before flow cytometry [22]. From *in vitro*-activated $CD8^+$ T cells, we used antibodies for CD44, CD69, CD25; in some experiments, $CD8^+$ T cells were stained with Cell Trace Violet (Life Technologies) according to manufacturer's instructions, for tracking of proliferation cycles. In all flow cytometry experiments, Live/Dead Near-IR was used to distinguish between live and dead cells. Intracellular detection of Ki-67 and IFNγ was done as described before [32]. For mitochondrial mass and membrane potential measurements, cells were incubated with MTG (Thermo Fisher Scientific) and Mitotracker Deep Red (Thermo Fisher Scientific) or TMRE (Cell Signaling Technology) simultaneously for 15 min at 37°C prior to staining. For intracellular detection of phosphorylated Acetyl-CoA Carboxylase (pACC; Cell Signaling Technology) or phosphorylated ERK1/2 (pERK1/2; Biolegend), cells were stained with surface markers then fixed with Paraformaldehyde 1%, permeabilized with 90% Methanol and stained with pACC or pERK1/2-PE for 20 min at room temperature. A secondary antibody (Alexa Fluor 647 anti-rabbit IgG) was used for detection of pACC. Alexa Fluor 488-conjugated Cholera Toxin B was used for detection of lipid rafts and stained as described in [54]. Flow cytometric analyses were performed on FACS Symphony or LSR Fortessa (BD Biosciences) and data was analyzed using FlowJo software (Treestar).

Cell sorting

Cell sorting was performed on a FACS Aria III device (BD Biosciences). RNA-seq analysis experiments were performed on WT (CD4-Cre) and Panx1-KO (CD4-Cre *Panx1*$^{fl/fl}$) TE

(KLRG1^{+}CD127^{-}) and MP (KLRG1^{-}CD127^{+}) P14 cells sorted from mice 7 days post-LCMV infection. The population purity after cell sorting was > 98% in all experiments.

Intracellular and extracellular ATP measurements

Intracellular ATP concentrations were measured by using the ATP determination kit (Life Technologies). To assess the levels of extracellular ATP, WT CD8^{+} T cells were activated *in vitro* as described above, and further incubated with IL-2 for 24h; IL-2 incubation cultures were performed in Transwells (Corning). After 24 h of IL-2 incubation, the transwells were transferred to new wells and the plates were centrifuged at 50 rpm for 1 min. The supernatant below the transwells was quantified for ATP concentration as described above. In all transwells, a combination of the plasma membrane ATPase inhibitor ebselen (30 μM; Cayman Chemical) and the ecto-ATPase inhibitor ARL 67156 trisodium salt hydrate (100 μM; Sigma-Aldrich) was added 1 h before evaluation, to inhibit ATPase activity [32]. In some samples, Trovafloxacin (10 μM) was added 24 h before assessment.

Crispr-Cas9 experiments

Cas9/RNP nucleofection of P14 cells was performed as previously described [40]. Briefly, WT (CD4-Cre) and CD4-Cre *P2rx7*$^{fl/fl}$ P14 cells were isolated and activated as described above. After 24h of activation, single guide RNAs (sgRNA) for either *Cd4* (sg*Cd4*) or *Panx1* (sg*Panx1*) and Cas9 protein were pre-complexed at room temperature for at least 10 mins. Following this, 1-10 million of pre-activated P14 cells were resuspended in 20 μl of P4 Nucleofection Buffer (Lonza). This cell suspension was then mixed with sgRNA/Cas9 and then incubated at room temperature for 2 mins. The P14 cell/Cas9/RNP mixes were transferred to Nucleofection cuvette strips (4D-Nucleofector X kit S; Lonza). Cells were electroporated using a 4D nucleofector (4D-Nucleofector Core Unit; Lonza). After nucleofection, prewarmed complete RPMI was used to transfer transfected P14 cells in 96-well plates. After 2 h, P14 cells were

cultured in 24-well plates in complete RPMI for 48 h, before adoptive transfer into recipient mice.

RNA-seq and bioinformatics analyses

WT (CD4-Cre) or CD4-Cre *Panx1*$^{fl/fl}$ P14 cells were *in vitro* activated for 72h ("effector-like") or activated and subsequently treated with recombinant IL-15 ("memory-like"). In another experiment, CD4-Cre or CD4-Cre *Panx1*$^{fl/fl}$ TE or MP cells were sorted from mice infected with LCMV-Arm (7 days p.i.). These cells were homogenized using QIAshredder columns (Qiagen), and RNA was extracted using the RNeasy Plus Mini Kit (Qiagen) following the manufacturer's instructions. Library preparation and RNA-seq (BGI-Seq platform, PE 100-bp paired-end read length) was done by BGI Americas. RNA-seq reads were mapped, and raw count matrix was generated. DEG analysis was done using DESeq2, and genes with greater than twofold changes and false discovery rate <0.05 were considered for gene cluster analysis. BGI provided customized analysis of DEGs, principal component analysis plots, and Pathway analyses between groups. Some heatmaps were generated using the Morpheus software (Broad Institute; https://software.broadinstitute.org/morpheus/). Some RNA-seq expression value counts were collected from the public database ImmGen (immgen.org), and from previous RNA-seq analysis performed by our group [32, 34]. These RNA-seq analyses can be accessed at GEO Omnibus with the accession numbers GSE217292 and GSE218643.

Extracellular flux analyses

In the indicated *in vitro*-activated or *ex vivo*-sorted CD8^{+} T cell populations, OCR and ECAR values were measured using a 96-well XF Extracellular flux analyzer, following manufacturer instructions (Agilent). Spare respiratory capacity (SRC) was defined as the subtraction between the maximum OCR values and the baseline OCR values [32, 37].

Untargeted metabolomics

When indicated, *in vitro*-activated $CD8^+$ T cell populations were isolated. We separated cell pellets and supernatants and sent them to the Mayo Clinic Metabolomics Core Laboratory for Liquid Chromatography-Mass Spectrometry (LC-MS) metabolome assessments. Primary analyses and comparisons of differentially expressed metabolites (DEMs) were done by the Metabolomics Core. Pathway enrichment analyses of DEMs were done using the MetaboAnalyst tool (metaboanalyst.ca/MetaboAnalyst/ModuleView.xhtml). Heatmaps of the top-100 DEMs for each comparison were generated using the Morpheus software.

L-lactate detection assays

When indicated, the supernatants from *in vitro*-activated $CD8^+$ T cell populations were collected, and the concentrations of extracellular L-lactate were measured using the L-Lactate Assay Kit (Sigma-Aldrich), following the manufacturer's instructions.

Statistical Analyses

Details on statistics used can be found in figure legends. Data were subjected to the Kolmogorov-Smirnov test to assess normality of samples. Statistical differences were calculated by using unpaired two-tailed Student's t-test (or one-way ANOVA with Tukey post-test, where indicated). All experiments were analyzed using Prism 9 (GraphPad Software). Graphical data was shown as mean values with error bars indicating the SD. P values of < 0.05 (*), < 0.01 (*), < 0.001 (***) or < 0.0001 (****) indicated significant differences between groups.

Supplementary Materials: This article includes Extended Data Figs.1 to 7, and Extended Data Table 1.

References and Notes

1. Harty, J.T., Tvinnereim, A.R. & White, D.W. CD8+ T cell effector mechanisms in resistance to infection. *Annu Rev Immunol* **18**, 275-308 (2000).

2. Williams, M.A. & Bevan, M.J. Effector and memory CTL differentiation. *Annu Rev Immunol* **25**, 171-192 (2007).

3. Renkema, K.R. *et al.* KLRG1(+) Memory CD8 T Cells Combine Properties of Short-Lived Effectors and Long-Lived Memory. *J Immunol* **205**, 1059-1069 (2020).

4. Milner, J.J. *et al.* Delineation of a molecularly distinct terminally differentiated memory CD8 T cell population. *Proc Natl Acad Sci U S A* **117**, 25667-25678 (2020).

5. Jameson, S.C. & Masopust, D. Understanding Subset Diversity in T Cell Memory. *Immunity* **48**, 214-226 (2018).

6. Masopust, D. & Soerens, A.G. Tissue-Resident T Cells and Other Resident Leukocytes. *Annu Rev Immunol* **37**, 521-546 (2019).

7. Chen, L. & Flies, D.B. Molecular mechanisms of T cell co-stimulation and co-inhibition. *Nat Rev Immunol* **13**, 227-242 (2013).

8. Leal, J.M. *et al.* Innate cell microenvironments in lymph nodes shape the generation of T cell responses during type I inflammation. *Sci Immunol* **6** (2021).

9. Kapsenberg, M.L. Dendritic-cell control of pathogen-driven T-cell polarization. *Nat Rev Immunol* **3**, 984-993 (2003).

10. Williams, M.A., Tyznik, A.J. & Bevan, M.J. Interleukin-2 signals during priming are required for secondary expansion of CD8+ memory T cells. *Nature* **441**, 890-893 (2006).

11. Kaech, S.M. *et al.* Selective expression of the interleukin 7 receptor identifies effector CD8 T cells that give rise to long-lived memory cells. *Nat Immunol* **4**, 1191-1198 (2003).

12. Ku, C.C., Murakami, M., Sakamoto, A., Kappler, J. & Marrack, P. Control of homeostasis of CD8+ memory T cells by opposing cytokines. *Science* **288**, 675-678 (2000).

13. Zhang, N. & Bevan, M.J. Transforming growth factor-beta signaling controls the formation and maintenance of gut-resident memory T cells by regulating migration and retention. *Immunity* **39**, 687-696 (2013).

14. Chan, F.K., Luz, N.F. & Moriwaki, K. Programmed necrosis in the cross talk of cell death and inflammation. *Annu Rev Immunol* **33**, 79-106 (2015).

15. Syrjanen, J., Michalski, K., Kawate, T. & Furukawa, H. On the molecular nature of large-pore channels. *J Mol Biol* **433**, 166994 (2021).

16. Molica, F., Figueroa, X.F., Kwak, B.R., Isakson, B.E. & Gibbins, J.M. Connexins and Pannexins in Vascular Function and Disease. *Int J Mol Sci* **19** (2018).

17. Mese, G., Richard, G. & White, T.W. Gap junctions: basic structure and function. *J Invest Dermatol* **127**, 2516-2524 (2007).

18. Bhat, E.A. & Sajjad, N. Human Pannexin 1 channel: Insight in structure-function mechanism and its potential physiological roles. *Mol Cell Biochem* **476**, 1529-1540 (2021).

19. Narahari, A.K. *et al.* ATP and large signaling metabolites flux through caspase-activated Pannexin 1 channels. *Elife* **10** (2021).

20. Chekeni, F.B. *et al.* Pannexin 1 channels mediate 'find-me' signal release and membrane permeability during apoptosis. *Nature* **467**, 863-867 (2010).

21. Medina, C.B. *et al.* Metabolites released from apoptotic cells act as tissue messengers. *Nature* **580**, 130-135 (2020).

22. Poon, I.K. *et al.* Unexpected link between an antibiotic, pannexin channels and apoptosis. *Nature* **507**, 329-334 (2014).

23. Beckel, J.M. *et al.* Pannexin 1 channels mediate the release of ATP into the lumen of the rat urinary bladder. *J Physiol* **593**, 1857-1871 (2015).

24. Chiu, Y.H. *et al.* A quantized mechanism for activation of pannexin channels. *Nat Commun* **8**, 14324 (2017).

25. Iglesias, R. *et al.* P2X7 receptor-Pannexin1 complex: pharmacology and signaling. *Am J Physiol Cell Physiol* **295**, C752-760 (2008).

26. Silverman, W.R. *et al.* The pannexin 1 channel activates the inflammasome in neurons and astrocytes. *J Biol Chem* **284**, 18143-18151 (2009).

27. Weilinger, N.L. *et al.* Metabotropic NMDA receptor signaling couples Src family kinases to pannexin-1 during excitotoxicity. *Nat Neurosci* **19**, 432-442 (2016).

28. Woehrle, T. *et al.* Pannexin-1 hemichannel-mediated ATP release together with P2X1 and P2X4 receptors regulate T-cell activation at the immune synapse. *Blood* **116**, 3475-3484 (2010).

29. Woehrle, T. *et al.* Hypertonic stress regulates T cell function via pannexin-1 hemichannels and P2X receptors. *J Leukoc Biol* **88**, 1181-1189 (2010).

30. Medina, C.B. *et al.* Pannexin 1 channels facilitate communication between T cells to restrict the severity of airway inflammation. *Immunity* **54**, 1715-1727 e1717 (2021).

31. Schenk, U. *et al.* Purinergic control of T cell activation by ATP released through pannexin-1 hemichannels. *Sci Signal* **1**, ra6 (2008).

32. Borges da Silva, H. *et al.* The purinergic receptor P2RX7 directs metabolic fitness of long-lived memory CD8(+) T cells. *Nature* **559**, 264-268 (2018).

33. Di Virgilio, F., Dal Ben, D., Sarti, A.C., Giuliani, A.L. & Falzoni, S. The P2X7 Receptor in Infection and Inflammation. *Immunity* **47**, 15-31 (2017).

34. Vardam-Kaur, T. *et al.* The Extracellular ATP Receptor P2RX7 Imprints a Promemory Transcriptional Signature in Effector CD8(+) T Cells. *J Immunol* **208**, 1686-1699 (2022).

35. Borges da Silva, H., Wang, H., Qian, L.J., Hogquist, K.A. & Jameson, S.C. ARTC2.2/P2RX7 Signaling during Cell Isolation Distorts Function and Quantification of Tissue-Resident CD8(+) T Cell and Invariant NKT Subsets. *J Immunol* **202**, 2153-2163 (2019).

36. Stark, R. *et al.* T RM maintenance is regulated by tissue damage via P2RX7. *Sci Immunol* **3** (2018).

37. Borges da Silva, H. *et al.* Sensing of ATP via the Purinergic Receptor P2RX7 Promotes CD8(+) Trm Cell Generation by Enhancing Their Sensitivity to the Cytokine TGF-beta. *Immunity* **53**, 158-171 e156 (2020).

38. Taruno, A. ATP Release Channels. *Int J Mol Sci* **19** (2018).

39. Yip, L. *et al.* Autocrine regulation of T-cell activation by ATP release and P2X7 receptors. *FASEB J* **23**, 1685-1693 (2009).

40. Seki, A. & Rutz, S. Optimized RNP transfection for highly efficient CRISPR/Cas9-mediated gene knockout in primary T cells. *J Exp Med* **215**, 985-997 (2018).

41. Blagih, J. *et al.* The energy sensor AMPK regulates T cell metabolic adaptation and effector responses in vivo. *Immunity* **42**, 41-54 (2015).

42. Pearce, E.L., Poffenberger, M.C., Chang, C.H. & Jones, R.G. Fueling immunity: insights into metabolism and lymphocyte function. *Science* **342**, 1242454 (2013).

43. Chang, C.H. *et al.* Posttranscriptional control of T cell effector function by aerobic glycolysis. *Cell* **153**, 1239-1251 (2013).

44. Carrio, R., Bathe, O.F. & Malek, T.R. Initial antigen encounter programs CD8+ T cells competent to develop into memory cells that are activated in an antigen-free, IL-7- and IL-15-rich environment. *J Immunol* **172**, 7315-7323 (2004).

45. Brock, V.J. *et al.* P2X4 and P2X7 are essential players in basal T cell activity and Ca(2+) signaling milliseconds after T cell activation. *Sci Adv* **8**, eabl9770 (2022).

46. Kaymak, I. *et al.* Carbon source availability drives nutrient utilization in CD8(+) T cells. *Cell Metab* **34**, 1298-1311 e1296 (2022).

47. Barbieri, L. *et al.* Lactate exposure shapes the metabolic and transcriptomic profile of CD8+ T cells. *Front Immunol* **14**, 1101433 (2023).

48. Macchi, C. *et al.* Monocarboxylate transporter 1 deficiency impacts CD8(+) T lymphocytes proliferation and recruitment to adipose tissue during obesity. *iScience* **25**, 104435 (2022).

49. Brand, A. *et al.* LDHA-Associated Lactic Acid Production Blunts Tumor Immunosurveillance by T and NK Cells. *Cell Metab* **24**, 657-671 (2016).

50. Hukelmann, J.L. *et al.* The cytotoxic T cell proteome and its shaping by the kinase mTOR. *Nat Immunol* **17**, 104-112 (2016).

51. Heng, T.S., Painter, M.W. & Immunological Genome Project, C. The Immunological Genome Project: networks of gene expression in immune cells. *Nat Immunol* **9**, 1091-1094 (2008).

52. Wang, R. & Green, D.R. Metabolic reprogramming and metabolic dependency in T cells. *Immunol Rev* **249**, 14-26 (2012).

53. Rowlatt, B. *et al.* Chain length-dependent cooperativity in fatty acid binding and oxidation by cytochrome P450BM3 (CYP102A1). *Protein Cell* **2**, 656-671 (2011).

54. Edwards-Hicks, J. *et al.* Phosphoinositide acyl chain saturation drives CD8(+) effector T cell signaling and function. *Nat Immunol* **24**, 516-530 (2023).

55. Huang, Y.H. & Sauer, K. Lipid signaling in T-cell development and function. *Cold Spring Harb Perspect Biol* **2**, a002428 (2010).

56. Huang, A.C. *et al.* T-cell invigoration to tumour burden ratio associated with anti-PD-1 response. *Nature* **545**, 60-65 (2017).

57. Pentcheva-Hoang, T., Simpson, T.R., Montalvo-Ortiz, W. & Allison, J.P. Cytotoxic T lymphocyte antigen-4 blockade enhances antitumor immunity by stimulating melanoma-specific T-cell motility. *Cancer Immunol Res* **2**, 970-980 (2014).

58. Yuan, J. *et al.* Integrated NY-ESO-1 antibody and CD8+ T-cell responses correlate with clinical benefit in advanced melanoma patients treated with ipilimumab. *Proc Natl Acad Sci U S A* **108**, 16723-16728 (2011).

59. Curtsinger, J.M., Gerner, M.Y., Lins, D.C. & Mescher, M.F. Signal 3 availability limits the CD8 T cell response to a solid tumor. *J Immunol* **178**, 6752-6760 (2007).

60. Wanhainen, K.M. *et al.* P2RX7 Enhances Tumor Control by CD8+ T Cells in Adoptive Cell Therapy. *Cancer Immunol Res* **10**, 871-884 (2022).

61. Carr, E.L. *et al.* Glutamine uptake and metabolism are coordinately regulated by ERK/MAPK during T lymphocyte activation. *J Immunol* **185**, 1037-1044 (2010).

62. Hayashi, K., Jutabha, P., Endou, H., Sagara, H. & Anzai, N. LAT1 is a critical transporter of essential amino acids for immune reactions in activated human T cells. *J Immunol* **191**, 4080-4085 (2013).

63. Ma, E.H. *et al.* Metabolic Profiling Using Stable Isotope Tracing Reveals Distinct Patterns of Glucose Utilization by Physiologically Activated CD8(+) T Cells. *Immunity* **51**, 856-870 e855 (2019).

64. Wanhainen, K.M., Jameson, S.C. & da Silva, H.B. Self-Regulation of Memory CD8 T Cell Metabolism through Extracellular ATP Signaling. *Immunometabolism* **1** (2019).

65. Denton, R.M. Regulation of mitochondrial dehydrogenases by calcium ions. *Biochim Biophys Acta* **1787**, 1309-1316 (2009).

66. Proietti, M. *et al.* ATP released by intestinal bacteria limits the generation of protective IgA against enteropathogens. *Nat Commun* **10**, 250 (2019).

67. Ledderose, C., Bromberger, S., Slubowski, C.J., Sueyoshi, K. & Junger, W.G. Frontline Science: P2Y11 receptors support T cell activation by directing mitochondrial trafficking to the immune synapse. *J Leukoc Biol* **109**, 497-508 (2021).

68. Boyd-Tressler, A.M., Lane, G.S. & Dubyak, G.R. Up-regulated Ectonucleotidases in Fas-Associated Death Domain Protein- and Receptor-Interacting Protein Kinase 1-Deficient Jurkat Leukemia Cells Counteract Extracellular ATP/AMP Accumulation via Pannexin-1 Channels during Chemotherapeutic Drug-Induced Apoptosis. *Mol Pharmacol* **92**, 30-47 (2017).

69. Menk, A.V. *et al.* Early TCR Signaling Induces Rapid Aerobic Glycolysis Enabling Distinct Acute T Cell Effector Functions. *Cell Rep* **22**, 1509-1521 (2018).

70. Grist, J.T. *et al.* Extracellular Lactate: A Novel Measure of T Cell Proliferation. *J Immunol* **200**, 1220-1226 (2018).

71. Haas, R. *et al.* Lactate Regulates Metabolic and Pro-inflammatory Circuits in Control of T Cell Migration and Effector Functions. *PLoS Biol* **13**, e1002202 (2015).

72. Feng, Q. *et al.* Lactate increases stemness of CD8 + T cells to augment anti-tumor immunity. *Nat Commun* **13**, 4981 (2022).

73. Robergs, R.A., Ghiasvand, F. & Parker, D. Biochemistry of exercise-induced metabolic acidosis. *Am J Physiol Regul Integr Comp Physiol* **287**, R502-516 (2004).

74. Bao, L., Sun, K. & Zhang, X. PANX1 is a potential prognostic biomarker associated with immune infiltration in pancreatic adenocarcinoma: A pan-cancer analysis. *Channels (Austin)* **15**, 680-696 (2021).

75. Penuela, S. *et al.* Loss of pannexin 1 attenuates melanoma progression by reversion to a melanocytic phenotype. *J Biol Chem* **287**, 29184-29193 (2012).

76. Elia, I. *et al.* Tumor cells dictate anti-tumor immune responses by altering pyruvate utilization and succinate signaling in CD8(+) T cells. *Cell Metab* **34**, 1137-1150 e1136 (2022).

77. Rolf, J. *et al.* AMPKalpha1: a glucose sensor that controls CD8 T-cell memory. *Eur J Immunol* **43**, 889-896 (2013).

78. Quinn, W.J., 3rd *et al.* Lactate Limits T Cell Proliferation via the NAD(H) Redox State. *Cell Rep* **33**, 108500 (2020).

79. Anderson, K.G. *et al.* Intravascular staining for discrimination of vascular and tissue leukocytes. *Nat Protoc* **9**, 209-222 (2014).

Extended Data Figures and Table

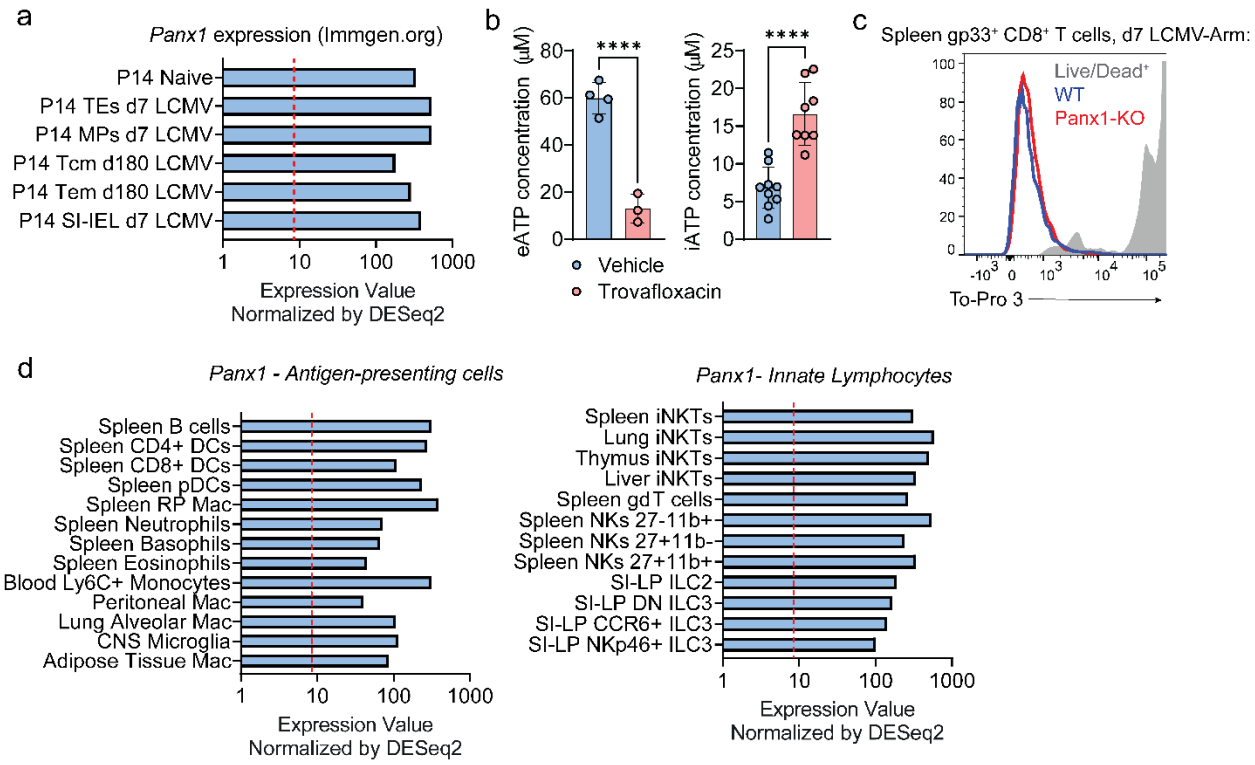

Extended Data Fig. 1. Functional Panx1 hemichannels are expressed constitutively by CD8⁺ T cells and other immune cells. (**a**) Panx1 mRNA expression (data from *Immgen.org*) in the indicated subsets of P14 cells. (**b**) CD8⁺ T cells were *in vitro* activated (αCD3/αCD28/IL-2); after 48h, vehicle or Trovafloxacin was added to the activation cultures. The ATP concentration of the supernatants of the pericellular space (eATP; collected as described in ref. 32) and the intracellular lysate of CD8⁺ T cells (iATP) were quantified. (**c**) WT and global Panx1-KO (CMV-Cre *Panx1*$^{fl/fl}$) mice were infected with LCMV-Arm; at day 7 post-infection, spleens were collected and incubated with To-Pro 3 dye. Histograms showing the internalization of To-Pro 3 in WT versus Panx1-KO gp33⁺ CD8⁺ T cells are shown. As positive control of To-Pro 3 internalization, Live/Dead⁺ CD8⁺ T cells from WT mice is represented. (**d**) Panx1 mRNA expression (from Immgen.org) of several subsets of antigen-presenting cells (left) and innate lymphocytes (right) is shown. (**b-c**) Data from three independent experiments, n=6-9 per experimental group. **** $p<0.0001$, Unpaired t-test.

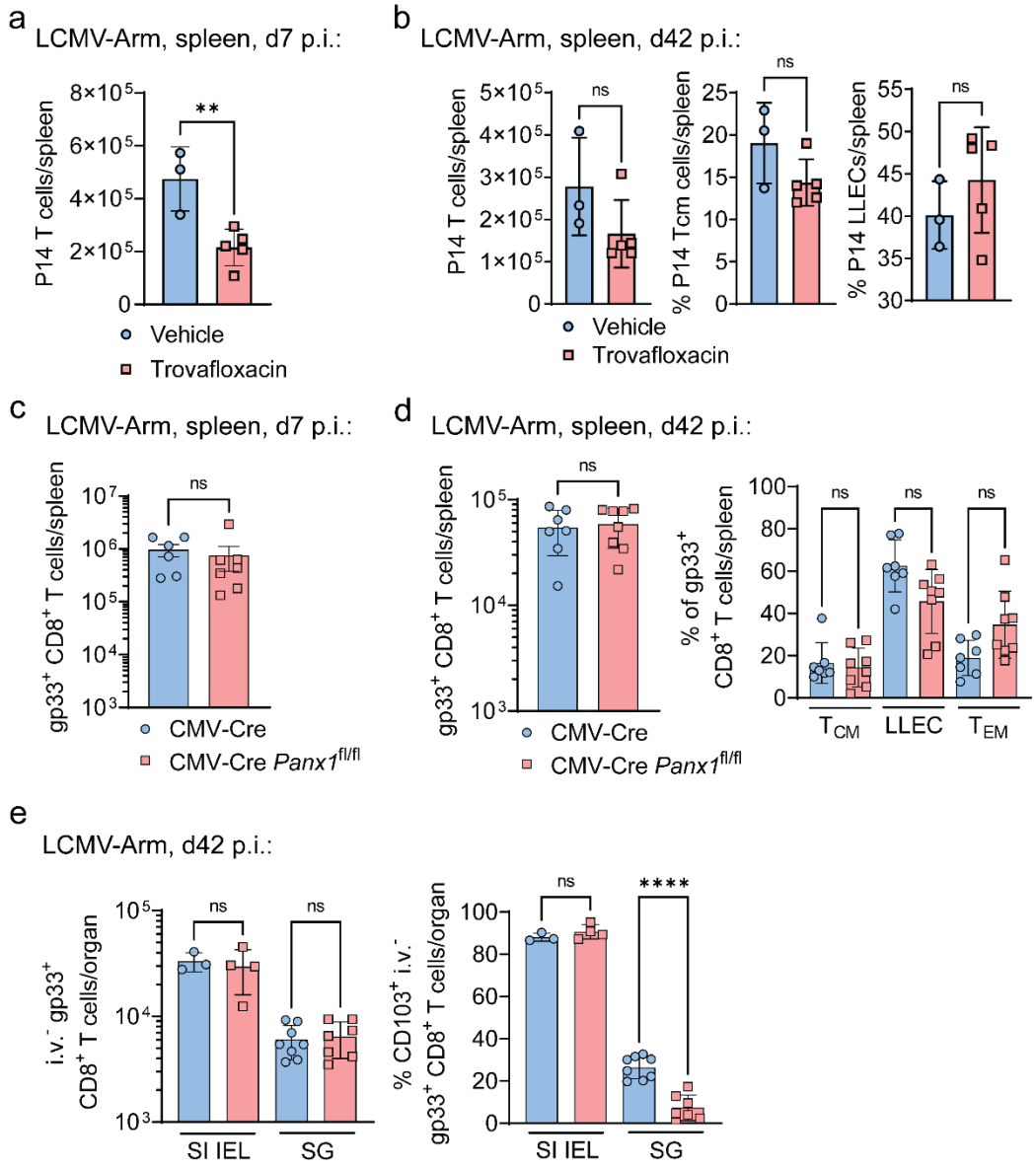

Extended Data Fig. 2. Global Pannexin-1 deficiency minimally impacts the establishment of effector and memory CD8⁺ T cells. (**a-b**) C57BL/6 mice (adoptively transferred with P14 cells and infected with LCMV-Arm) were treated between days 1-7 post-infection (p.i.) with Vehicle or Trovafloxacin. (**a**) Numbers of TE (left) and MP (right) P14 cells per spleen, at day 7 p.i.. (**b**) Numbers of spleen P14 cells (left), and percentages of spleen P14 Tcm (center) and P14 LLEC (right) cells. (**c-e**) CMV-Cre (WT) and CMV-Cre *Panx1*$^{fl/fl}$ mice were infected with LCMV-Arm. (**c**) Numbers of spleen gp33⁺ CD8⁺ T cells (left) and percentages of TE and MP spleen gp33⁺ CD8⁺ T cells (right), at day 7 p.i.. (**d**) Numbers of spleen gp33⁺ CD8⁺ T cells (left)

and percentages of Tcm, LLEC and Tem spleen gp33^{+} CD8^{+} T cells (right), at day 42 p.i.. (**e**) Numbers (left) and percentages of CD103^{+} (right) of intravenous labeling negative (i.v.$^{-}$) SI IEL and SG gp33^{+} CD8^{+} T cells, at day 42 p.i.. (**a-e**) Data from two independent experiments, n=3-8 per experimental group. * $p<0.05$, ** $p<0.01$, **** $p<0.0001$, Unpaired t-test (**a-d**) or One-Way ANOVA with Tukey's post-test (**c-e**).

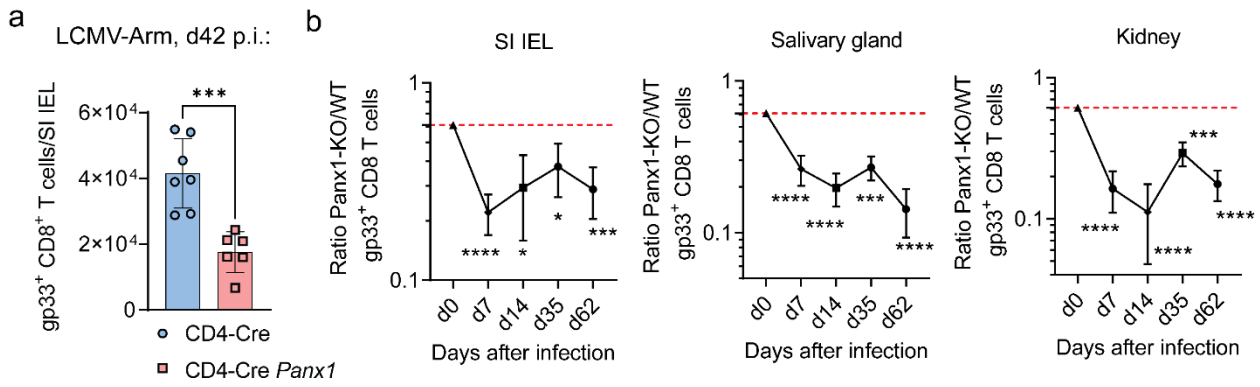

Extended Data Fig. 3. T cell-specific Panx1 is needed for the accumulation of CD8⁺ Trm cells. (**a**) WT (CD4-Cre) and T cell-Panx1-KO (CD4-Cre *Panx1*$^{fl/fl}$) mice were infected with LCMV-Arm. At 42 days p.i., mice were sacrificed, and the SI IEL tissues collected. The average numbers of gp33⁺ CD8⁺ T cells per SI IEL are shown. (**b**) WT/Panx1-KO BM chimeric mice (1:1 mix of CD4-Cre and CD4-Cre *Panx1*$^{fl/fl}$ BM cells transferred) were infected with LCMV-Arm. Panx1-KO/WT ratios of total SI IEL, Salivary gland, and Kidney gp33⁺ CD8⁺ T cells over time post-infection are shown. (**a-b**) Data from three independent experiments, n=6-12 per time point. (**a**) *** $p<0.001$, Unpaired t-test. (**b**) * $p<0.05$, *** $p<0.001$, **** $p<0.0001$, Two-way ANOVA with Bonferroni post-test.

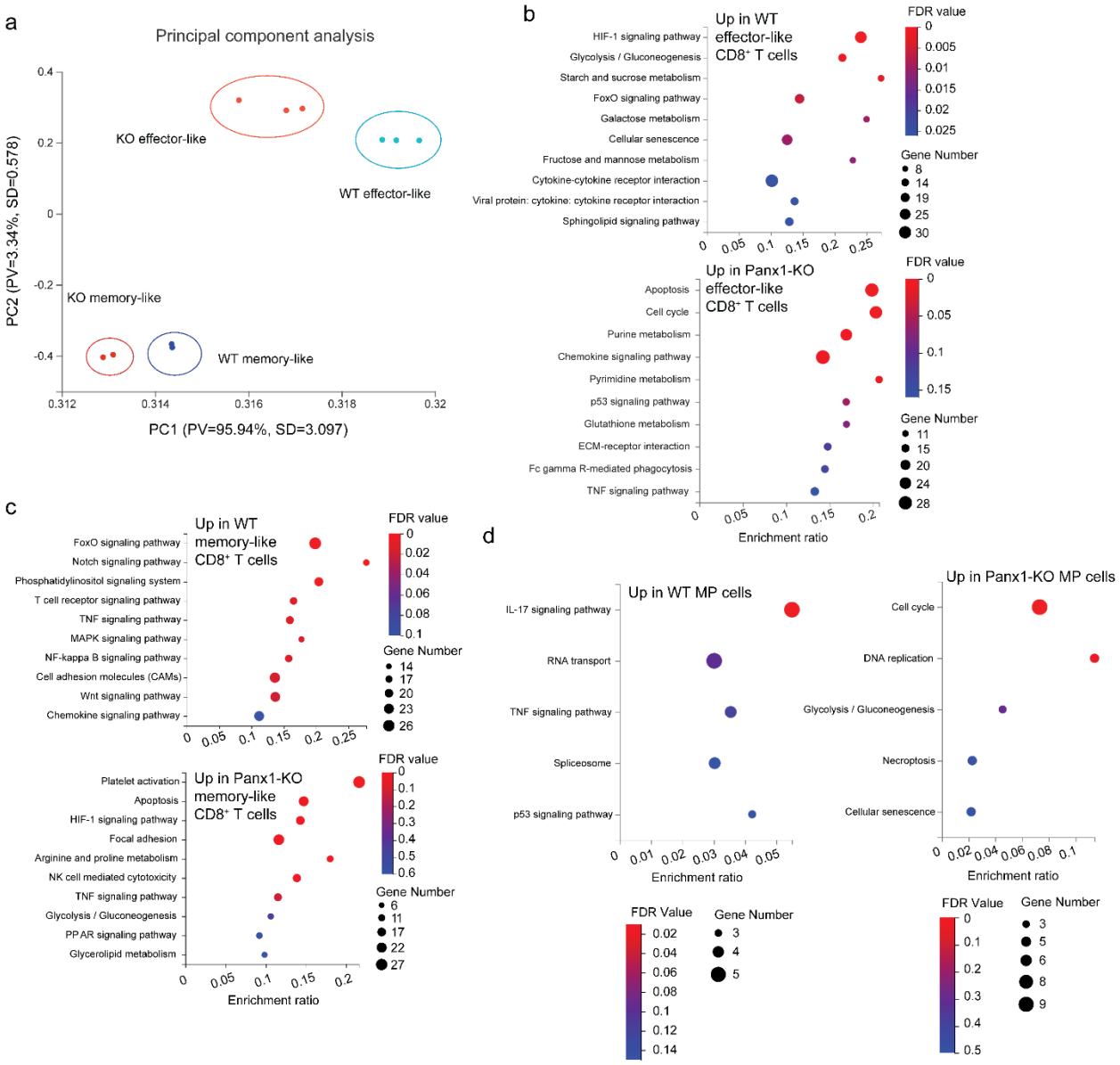

Extended Data Fig. 4. Transcriptional signatures of WT and Panx1-KO effector and memory-phenotype CD8⁺ T cells. (**a-c**) WT (CD4-Cre) and Panx1-KO (KO; CD4-Cre *Panx1*$^{fl/fl}$) CD8⁺ T cells were *in vitro* activated for 72h, then further polarized into effector-like (with IL-2) or memory-like (with IL-15) populations. Cells were collected and examined by RNA-seq. (**a**) Principal component analysis (PCA) plot showing the relative distribution of WT and Panx1-KO effector-like and memory-like populations. (**b**) Gene expression pathways enriched in WT effector-like (top) or Panx1-KO effector-like (bottom) cells. (**c**) Gene expression pathways

enriched in WT memory-like (top) or Panx1-KO memory-like (bottom) cells. (**d**) Gene expression pathways enriched in gp33^{+} WT MP cells (KLRG1^{-}CD127^{+}) compared to Panx1-KO MP cells (left). In the right, pathways enriched in Panx1-KO MP cells compared to WT MP cells. (**a-c**) Each replicate is a pool of activated CD8^{+} T cells from three mice; n=3 replicates per experimental group. (**d**) Each replicate is a pool of gp33^{+} TE or MP cells from three mice; n=3 replicates per experimental group.

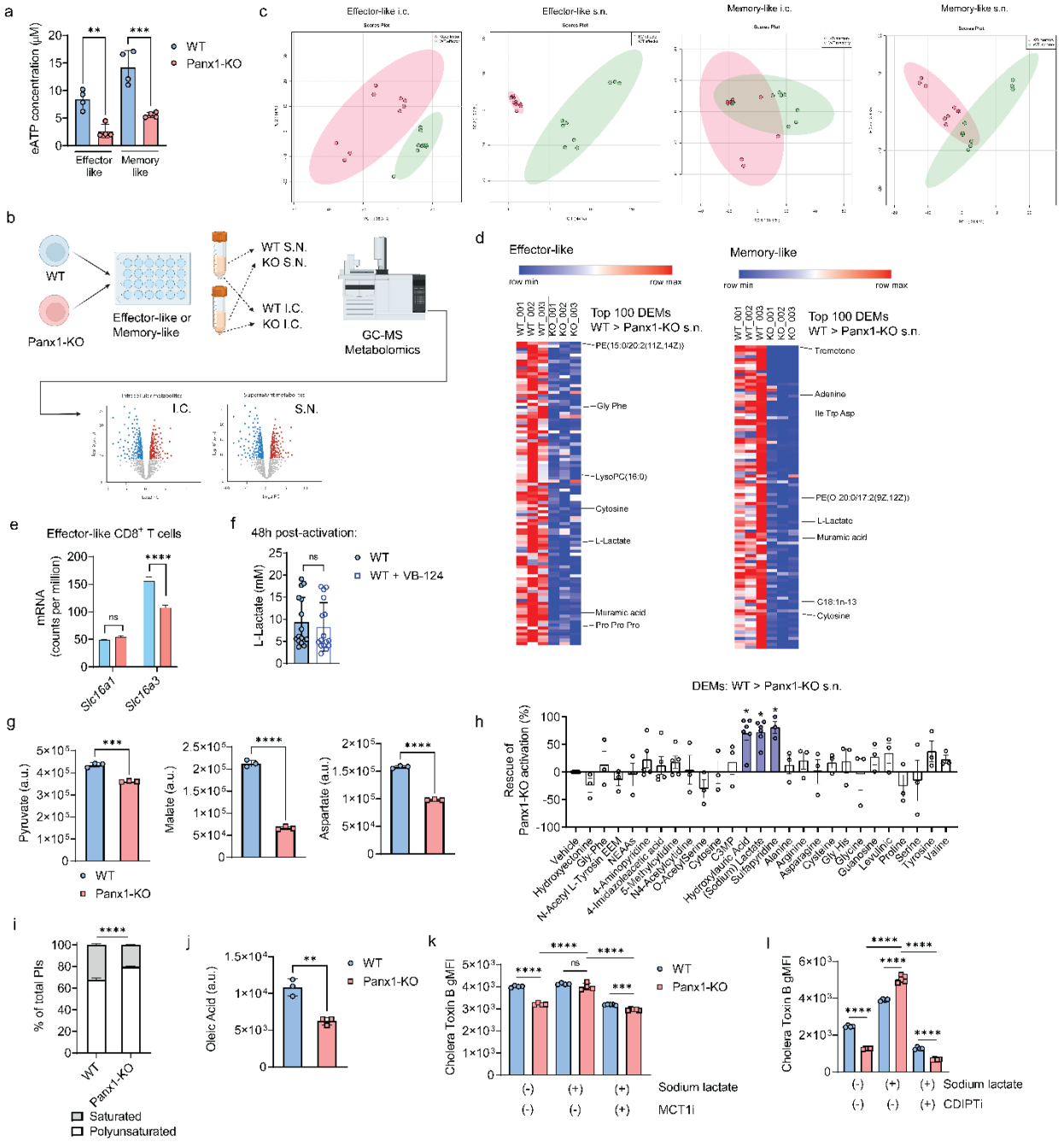

Extended Data Fig. 5. Panx1 effects on the extracellular and intracellular metabolism of CD8⁺ T cells. (**a**) WT or Panx1-KO effector-like and memory-like CD8⁺ T cell supernatants were harvested, and the levels of eATP were measured. (**b-d**) WT or Panx1-KO effector-like and memory-like CD8⁺ T cell cultures were harvested, and intracellular lysates and supernatants were submitted for untargeted metabolomics (GC-MS) analysis. (**b**) Experimental design. (**c**)

PCA plots comparing WT and Panx1-KO CD8$^+$ T cell samples. (**d**) Heatmaps showing the top 100 differentially expressed metabolites (DEMs) with increased representation in the supernatants of effector-like (left) or memory-like (right) WT cells, in comparison to Panx1-KO cells. (**e**) mRNA counts per million of *Slc16a1* (MCT-1-encoding gene) and *Slc16a3* (MCT-4-encoding gene) genes in WT and Panx1-KO effector-like (left) and memory-like cells. (**f**) Average lactate values (arbitrary units) in supernatants of *in vitro*-activated WT CD8$^+$ T cells in the presence or not of VB124 (MCT-4 inhibitor). (**g**) Intracellular levels (arbitrary units – a.u.) of pyruvate, malate, and aspartate in WT versus Panx1-KO effector-like CD8$^+$ T cells (depicted from the GC-MS experiments described above). (**h**) In some experiments, the top DEMs depicted in Fig. S5d (effector-like; left) were added exogenously in WT versus Panx1-KO CD8$^+$ T cell *in vitro* activation cultures. The percentage of Panx1-KO activation rescue (inferred as percentage of increase in activation compared to WT cells) is depicted for these metabolites. (**i**) Percentages, within total intracellular PIs, of saturated (one or less double bonds) and unsaturated (2 or more double bonds) PIs in WT versus Panx1-KO effector-like CD8$^+$ T cells. Data from the GC-MS experiments described above. (**j**) Intracellular levels (a.u.) of oleic acid in WT versus Panx1-KO effector-like CD8$^+$ T cells (from the GC-MS experiments). (**k**) In some experiments, WT and Panx1-KO CD8$^+$ T cells were *in vitro* activated in the presence or not of sodium lactate and/or AZD3965 (MCT1i); the average gMFI values of Cholera Toxin B per group are shown. (**l**) WT and Panx1-KO CD8$^+$ T cells were activated in the presence or not of sodium lactate and/or Inostamycin (CDIPTi); the average gMFI values of Cholera Toxin B per group are shown. (**b-e, g, i-j**) Data from 2-3 biological replicates per experimental group (from n=3 mice per group). (**a, f, h, k-l**) Data from 2-3 independent experiments (from n=3-16 mice per group). (**a, e, h, k-l**) ** $p<0.01$, *** $p<0.001$, **** $p<0.0001$, One-way ANOVA with Tukey's post-test. (f-g, i-j) ** $p<0.01$, *** $p<0.001$, **** $p<0.0001$, Unpaired t-test.

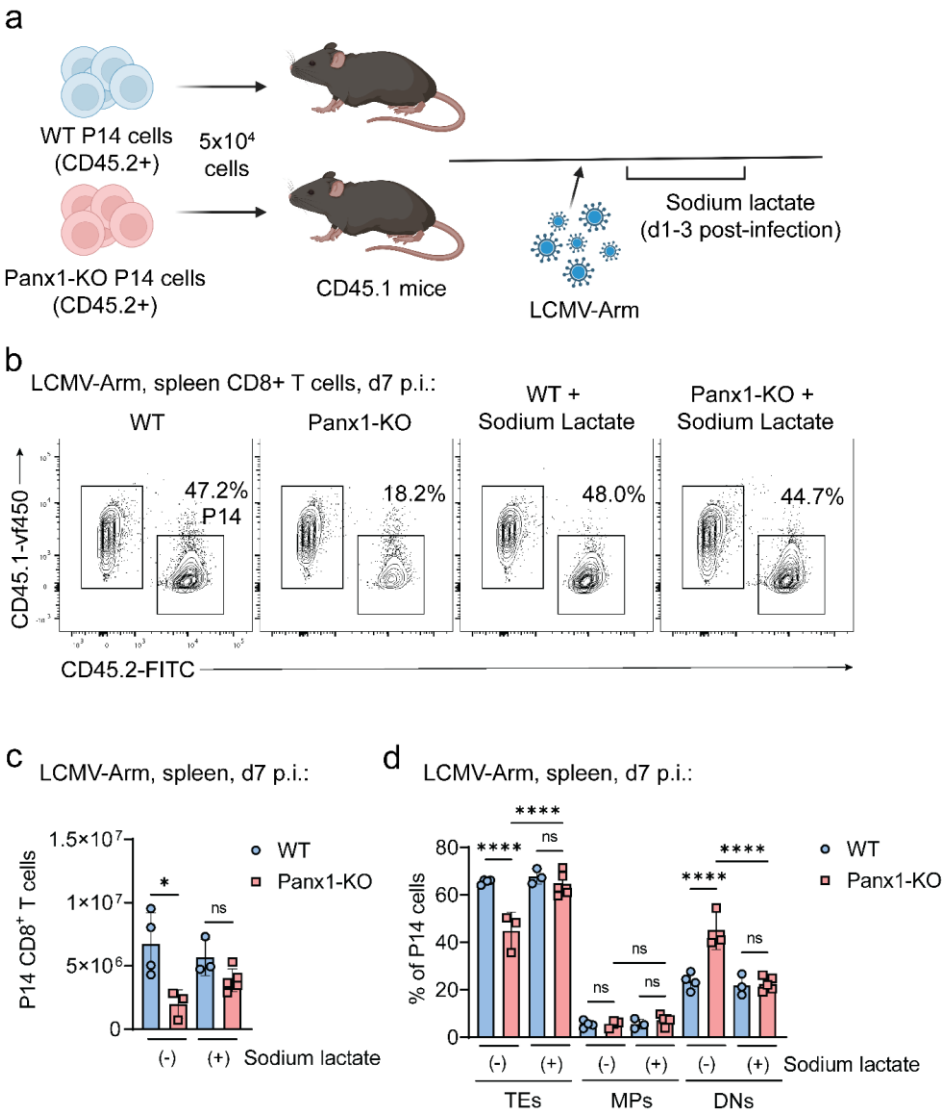

Extended Data Fig. 6. Panx1-KO *in vivo* effector CD8⁺ T cell expansion is rescued by exogenous sodium lactate. (**a-d**) WT or Panx1-KO P14 cells (CD45.2⁺) were transferred into WT CD45.1⁺ mice, which were infected with LCMV-Arm. Some mice were treated with sodium lactate between days 1-3 post-infection. Spleen P14 cells were analyzed at day 7 post-infection. (**a**) Experimental design. (**b**) Representative flow cytometry plots showing P14 cell percentages (CD45.2⁺) in the indicated groups. (**c**) Average numbers of total spleen P14 cells at day 7 post-infection. (**d**) Average percentages of TE, MP and DN P14 cells per spleen are shown. (**c-d**) Data from two independent experiments, n=3-5 per time point. (**c-d**) * $p<0.05$, **** $p<0.0001$, One-way ANOVA with Tukey's post-test.

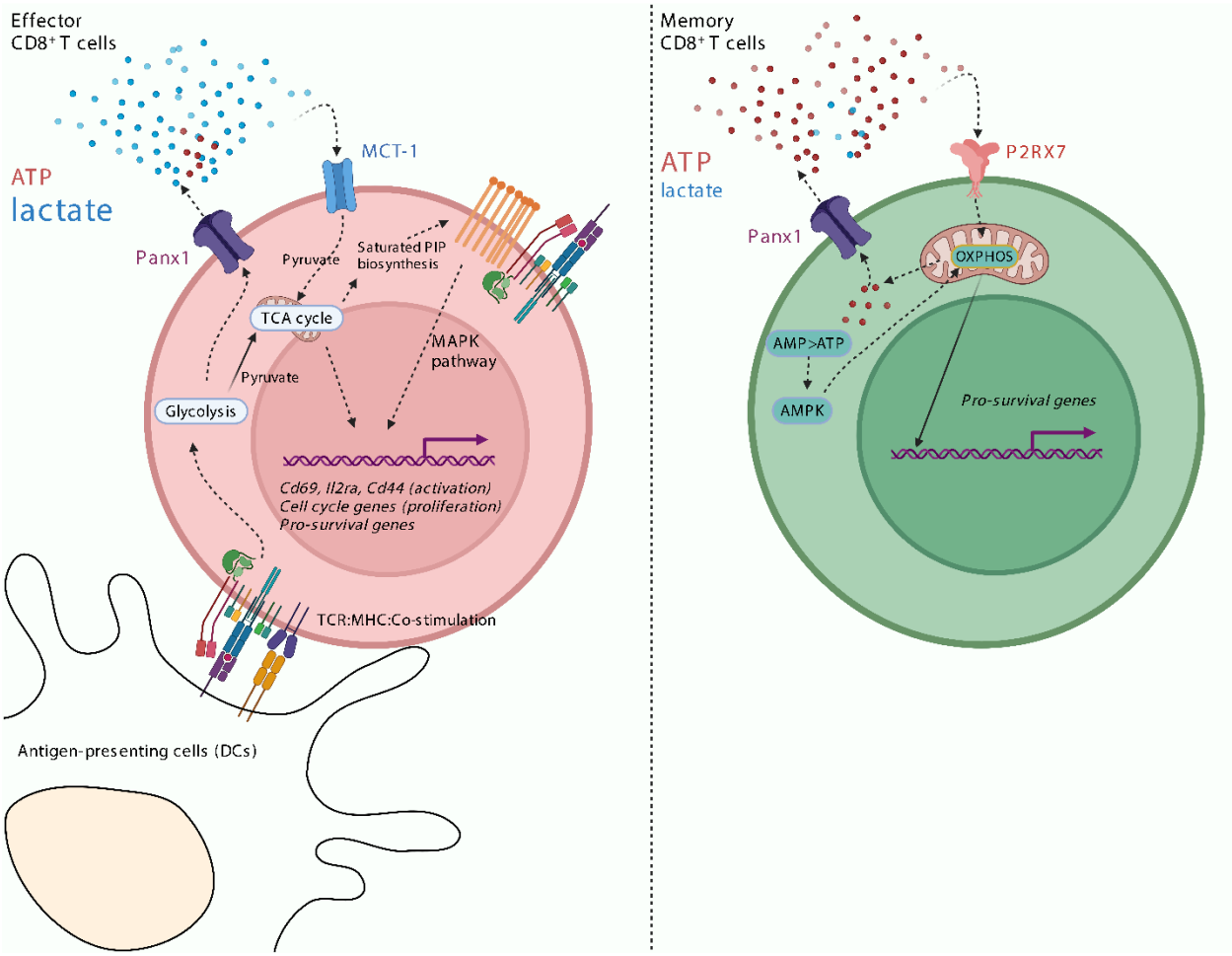

Extended Data Fig. 7. Working model on how Panx1 regulates effector and memory CD8⁺ T cell responses. Our results suggest that Panx1 controls CD8⁺ T cell immune responses in two phases. First (left), during effector CD8⁺ T cell differentiation, Panx1 is important in the coordination of extracellular lactate accumulation. In turn, lactate is internalized via MCT-1, and participates in the TCA cycle and biosynthesis of saturated PIs. Consequently, Panx1-lactate is important in the establishment of lipid rafts, which in turn sustains the MAPK signaling pathway and reinforces the effector differentiation and function of CD8⁺ T cells. During the memory phase (right), Panx1 is linked to the induction of mitochondrial metabolism. Our results suggest this occur through export of ATP, which in turn is sensed via P2RX7 and directly promotes OXPHOS. Simultaneously, ATP export leads to increased AMPK activation, which also works to maintain mitochondrial function and, consequently, memory CD8⁺ T cell survival. Thus, Panx1,

working as a “master exporter”, regulates distinct phases of $CD8^+$ T cell responses through different metabolites and intracellular pathways.

Name	Short Name	Vehicle	Final Concentration (uM)	
4-imidazoleacetic acid hydrochloride	4-imidazol	H2O (100mg/mL)	100	
Cytosine	cytosine	0.5 M HCl	100	
5-Methylcytidine	5-methyl	H2O (25mg/mL)	100	
4-aminopyridine	4-amino	H2O (50mg/mL)	100	
DL-B-Hydroxylauric Acid (3-hydroxy-dodecanoic acid)	lauric	Ethanol (100%)	100	Panx1-KO r.
Hydroxyectonine	ectoine	H2O	100	
N6,N6-Dimethyladenosine	N6-Dimethyl	DMSO	10	
O-Acetylserine	O-Aceytl	DMSO	100	
Gly-Phe	Gly Phe	H2O	100	
N-Aceytl-L-tyrosin ethyl ester monohydrate	N-Aceytl	H2O	100	
Cytidine 3-monophosphate	C3MP	PBS	100	
Cdk5/Cdk2 inhibitor (N-[5-(1-methylethyl)2-thiazolyl]-benzeneacetamide (Cay10554)	Cay10554	PBS and DMSO (1:5)	10	
FKGK 11 (1,1,1,2,2-pentafluoro-7-phenyl-3-heptanone)	FKGK	(0.5% ethanol) and PBS	100	
N4-Acetylcytidine	N4-Aceytl	DMSO	100	
Sodium Lactate	Sodium Lactate	PBS	1000	Panx1-KO r.
5-Aminolevulinic Acid Hydrochloride	Leuvulinic	dH2O	100	
Gly-His	Gly-His	dH2O	100	
L-Valine	Valine	dH2O	100	
L-Proline	Proline	dH2O	100	
L-Alanine	Alanine	dH2O	100	
7-Methylguanosine	Guanosine	dH2O	100	
L-Cyeteine	Cyeteine	dH2O	100	
L-Asparagine	Aspara	dH2O	100	
L-Arginine	Argin	dH2O	100	
L-Serine	Serine	dH2O	100	
Glycine	Glycine	dH2O	100	
2-(Aziridin-1-yl)ethanol	Azindrin	dH2O	100	
1-docosahexaenoyl-2-hydroxy-sn-glycero-3-PC	Docosa	Chloroform (10mg/ml) & dH2O	100	
N-Aceytl sulfapyridine-d4	Sulfa	DMSO	100	Panx1-KO r.
4-AminoMethyllindole	Amino Methyl	DMSO	100	

2-Octanamidoacetic Acid	**Octana**	**DMSO**	**100**	
MEM Non-essential Amino Acid	**MEM**	**dH2O -- aliquot from stock bottle**	**100**	
1-Palmitoyl-sn-glycero-3-phosphocholine	**Palmitoyl**	**Methanol (slighly, heated)**	**100**	
Phosphorylcholine	**Phospho**	**arrived in oil**	**100**	
L-Tyrosine	**Tyro**	**H2O**	**100**	

Extended Data Table 1. List of metabolites used in the experiments depicted on Extended Data Fig. 5h.

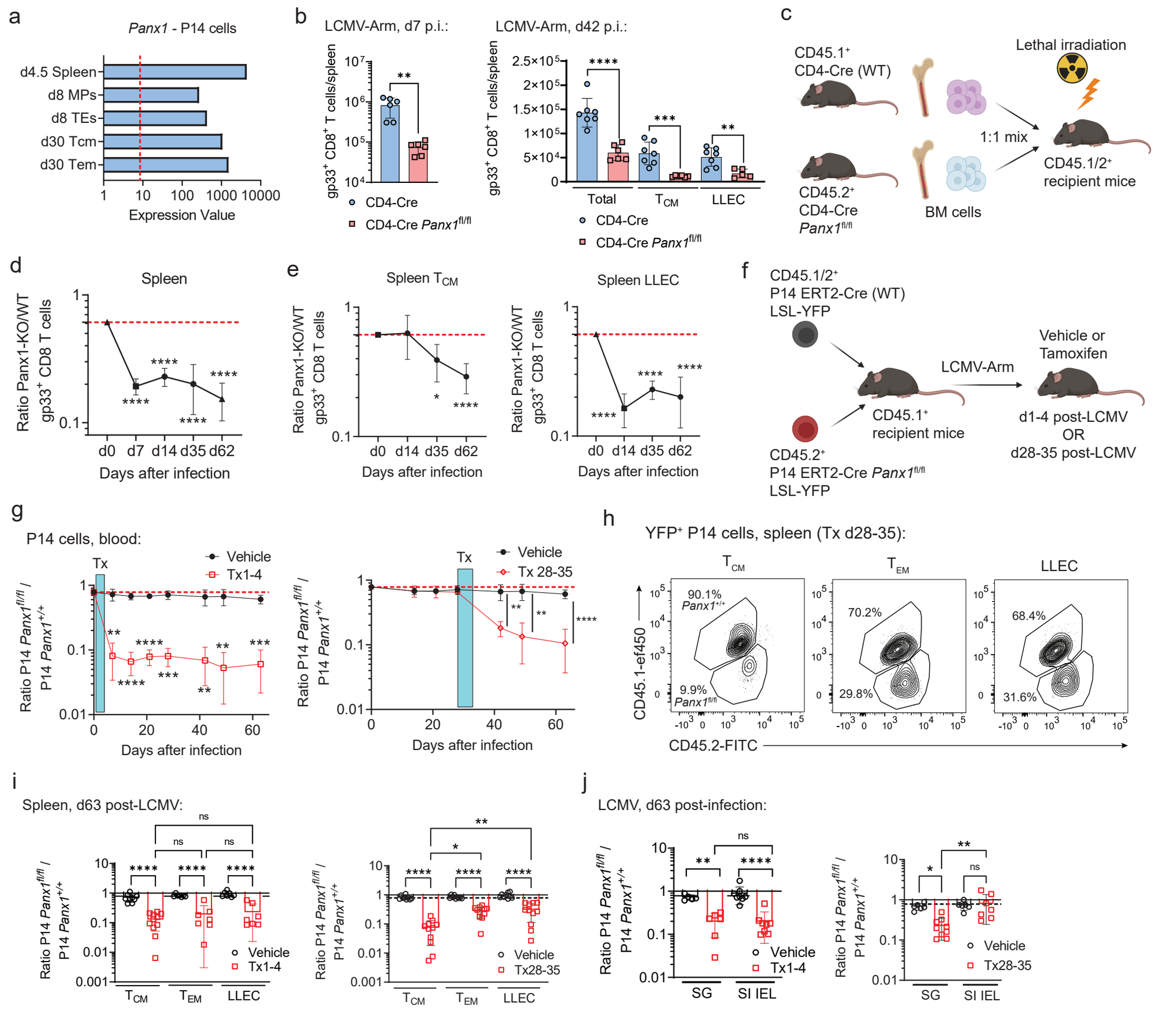
a
Panx1 - P14 cells
d4.5 Spleen
d8 MPs
d8 TEs
d30 Tcm
d30 Tem
1 10 100 1000 10000
Expression Value
b
LCMV-Arm, d7 p.i.:
gp33+ CD8+ T cells/spleen
CD4-Cre
CD4-Cre Panx1fl/fl
LCMV-Arm, d42 p.i.:
Total
TCM
LLEC
c
CD45.1+
CD4-Cre (WT)
Lethal irradiation
1:1 mix
CD45.2+
CD4-Cre
Panx1fl/fl
BM cells
CD45.1/2+
recipient mice
d
Spleen
Ratio Panx1-KO/WT
gp33+ CD8 T cells
d0 d7 d14 d35 d62
Days after infection
e
Spleen TCM
Spleen LLEC
f
CD45.1/2+
P14 ERT2-Cre (WT)
LSL-YFP
LCMV-Arm
Vehicle or
Tamoxifen
CD45.1+
recipient mice
d1-4 post-LCMV
OR
d28-35 post-LCMV
CD45.2+
P14 ERT2-Cre Panx1fl/fl
LSL-YFP
g
P14 cells, blood:
Tx
Vehicle
Tx1-4
Tx 28-35
Ratio P14 Panx1fl/fl / P14 Panx1+/+
Days after infection
h
YFP+ P14 cells, spleen (Tx d28-35):
TCM
TEM
LLEC
90.1%
Panx1+/+
9.9%
Panx1fl/fl
70.2%
29.8%
68.4%
31.6%
CD45.1-ef450
CD45.2-FITC
i
Spleen, d63 post-LCMV:
ns
Vehicle
Tx1-4
Tx28-35
j
LCMV, d63 post-infection:
SG
SI IEL

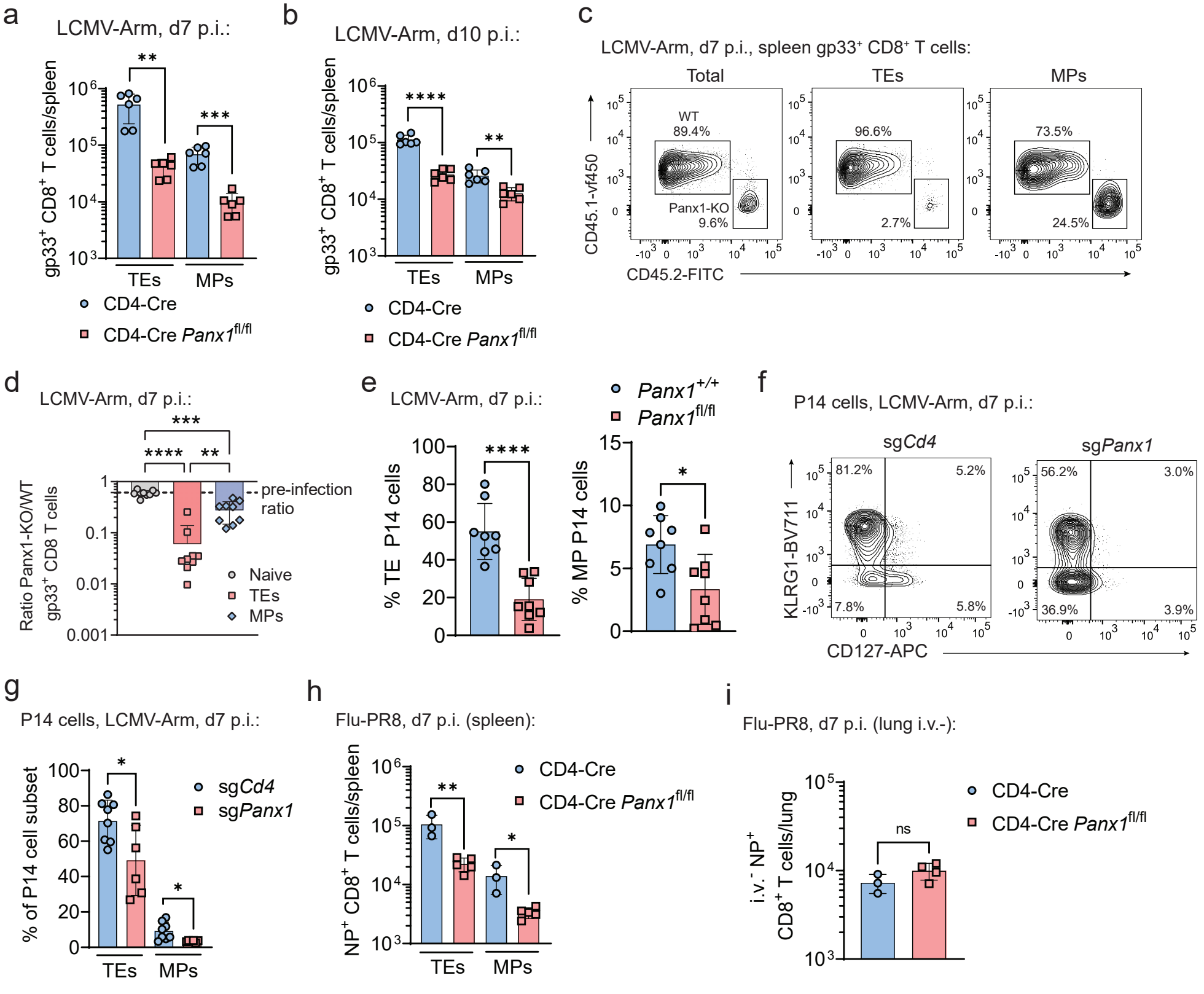
a
LCMV-Arm, d7 p.i.:
gp33+ CD8+ T cells/spleen
TEs
MPs
CD4-Cre
CD4-Cre Panx1fl/fl
b
LCMV-Arm, d10 p.i.:
gp33+ CD8+ T cells/spleen
TEs
MPs
CD4-Cre
CD4-Cre Panx1fl/fl
c
LCMV-Arm, d7 p.i., spleen gp33+ CD8+ T cells:
Total
TEs
MPs
WT
89.4%
Panx1-KO
9.6%
96.6%
2.7%
73.5%
24.5%
CD45.1-vf450
CD45.2-FITC
d
LCMV-Arm, d7 p.i.:
Ratio Panx1-KO/WT gp33+ CD8 T cells
pre-infection ratio
Naive
TEs
MPs
e
LCMV-Arm, d7 p.i.:
Panx1+/+
Panx1fl/fl
% TE P14 cells
% MP P14 cells
f
P14 cells, LCMV-Arm, d7 p.i.:
sgCd4
sgPanx1
81.2%
5.2%
7.8%
5.8%
56.2%
3.0%
36.9%
3.9%
KLRG1-BV711
CD127-APC
g
P14 cells, LCMV-Arm, d7 p.i.:
% of P14 cell subset
sgCd4
sgPanx1
TEs
MPs
h
Flu-PR8, d7 p.i. (spleen):
NP+ CD8+ T cells/spleen
CD4-Cre
CD4-Cre Panx1fl/fl
TEs
MPs
i
Flu-PR8, d7 p.i. (lung i.v.-):
i.v.- NP+ CD8+ T cells/lung
ns
CD4-Cre
CD4-Cre Panx1fl/fl

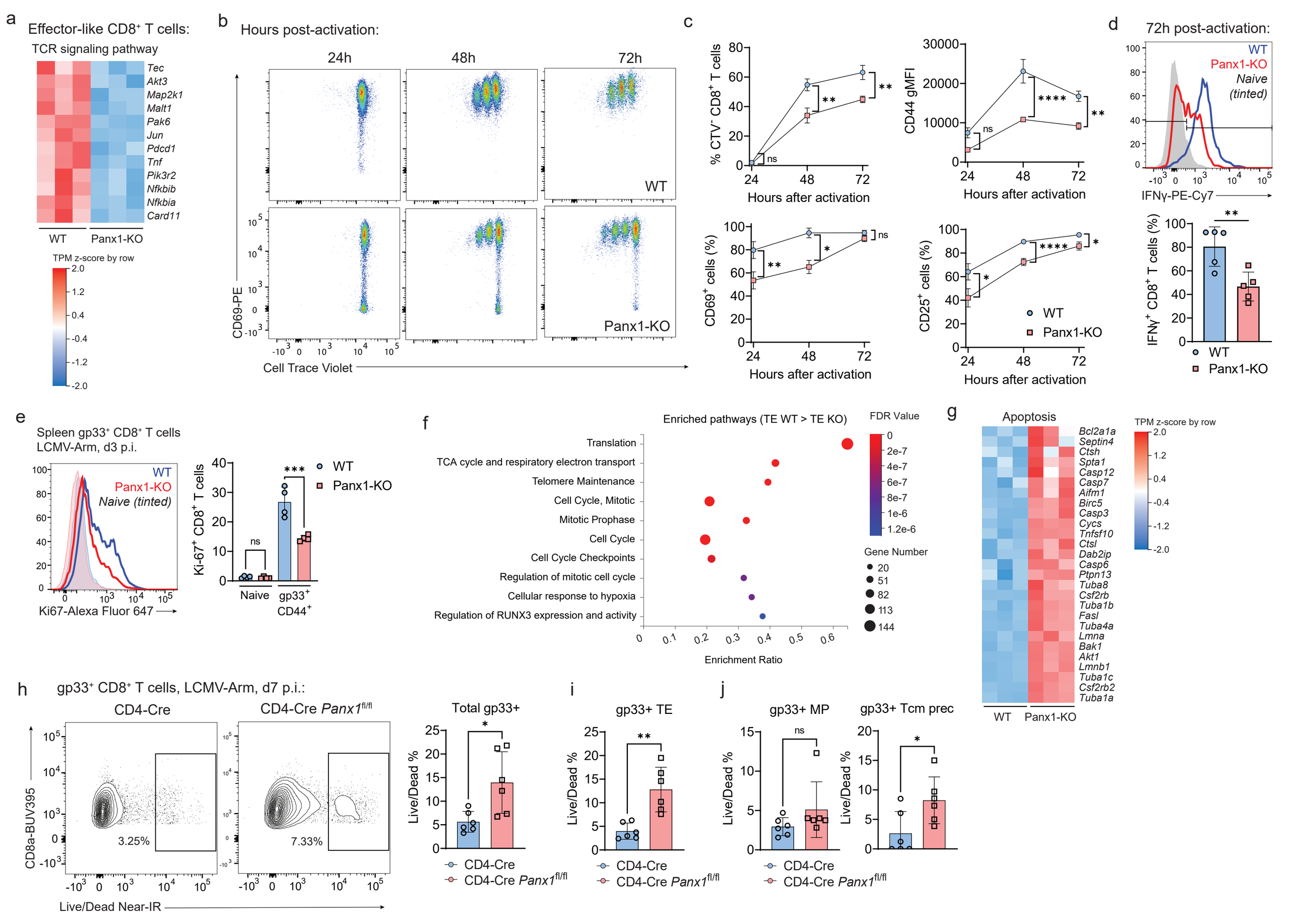
a
Effector-like CD8+ T cells:
TCR signaling pathway
Tec
Akt3
Map2k1
Malt1
Pak6
Jun
Pdcd1
Tnf
Pik3r2
Nfkbib
Nfkbia
Card11
WT
Panx1-KO
TPM z-score by row
b
Hours post-activation:
24h
48h
72h
WT
Panx1-KO
CD69-PE
Cell Trace Violet
c
% CTV- CD8+ T cells
CD44 gMFI
CD69+ cells (%)
CD25+ cells (%)
Hours after activation
ns
d
72h post-activation:
WT
Panx1-KO
Naive (tinted)
IFNγ-PE-Cy7
IFNγ+ CD8+ T cells (%)
e
Spleen gp33+ CD8+ T cells
LCMV-Arm, d3 p.i.
Ki67-Alexa Fluor 647
Ki-67+ CD8+ T cells
Naive
gp33+ CD44+
f
Enriched pathways (TE WT > TE KO)
FDR Value
Translation
TCA cycle and respiratory electron transport
Telomere Maintenance
Cell Cycle, Mitotic
Mitotic Prophase
Cell Cycle
Cell Cycle Checkpoints
Regulation of mitotic cell cycle
Cellular response to hypoxia
Regulation of RUNX3 expression and activity
Enrichment Ratio
Gene Number
g
Apoptosis
Bcl2a1a
Septin4
Ctsh
Spta1
Casp12
Casp7
Aifm1
Birc5
Casp3
Cycs
Tnfsf10
Ctsl
Dab2ip
Casp6
Ptpn13
Tuba8
Csf2rb
Tuba1b
Fasl
Tuba4a
Lmna
Bak1
Akt1
Lmnb1
Tuba1c
Csf2rb2
Tuba1a
h
gp33+ CD8+ T cells, LCMV-Arm, d7 p.i.:
CD4-Cre
CD4-Cre Panx1fl/fl
CD8a-BUV395
Live/Dead Near-IR
3.25%
7.33%
Total gp33+
i
gp33+ TE
j
gp33+ MP
gp33+ Tcm prec
Live/Dead %
CD4-Cre
CD4-Cre Panx1fl/fl

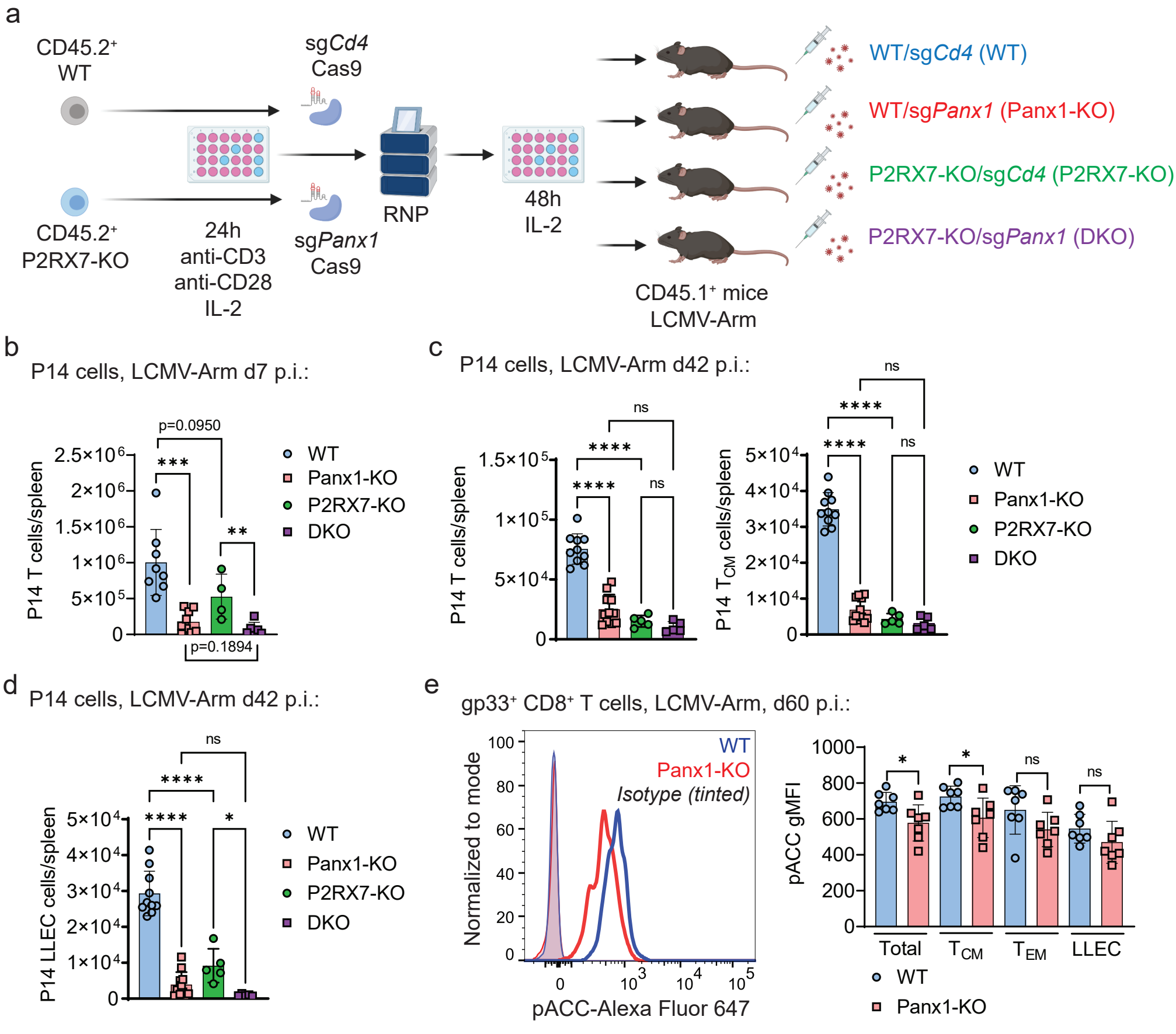
a
CD45.2+ WT
CD45.2+ P2RX7-KO
24h anti-CD3 anti-CD28 IL-2
sgCd4 Cas9
sgPanx1 Cas9
RNP
48h IL-2
CD45.1+ mice LCMV-Arm
WT/sgCd4 (WT)
WT/sgPanx1 (Panx1-KO)
P2RX7-KO/sgCd4 (P2RX7-KO)
P2RX7-KO/sgPanx1 (DKO)
b
P14 cells, LCMV-Arm d7 p.i.:
P14 T cells/spleen
p=0.0950
p=0.1894
WT
Panx1-KO
P2RX7-KO
DKO
c
P14 cells, LCMV-Arm d42 p.i.:
P14 T cells/spleen
P14 TCM cells/spleen
d
P14 cells, LCMV-Arm d42 p.i.:
P14 LLEC cells/spleen
e
gp33+ CD8+ T cells, LCMV-Arm, d60 p.i.:
Normalized to mode
pACC-Alexa Fluor 647
Isotype (tinted)
pACC gMFI
Total
TCM
TEM
LLEC

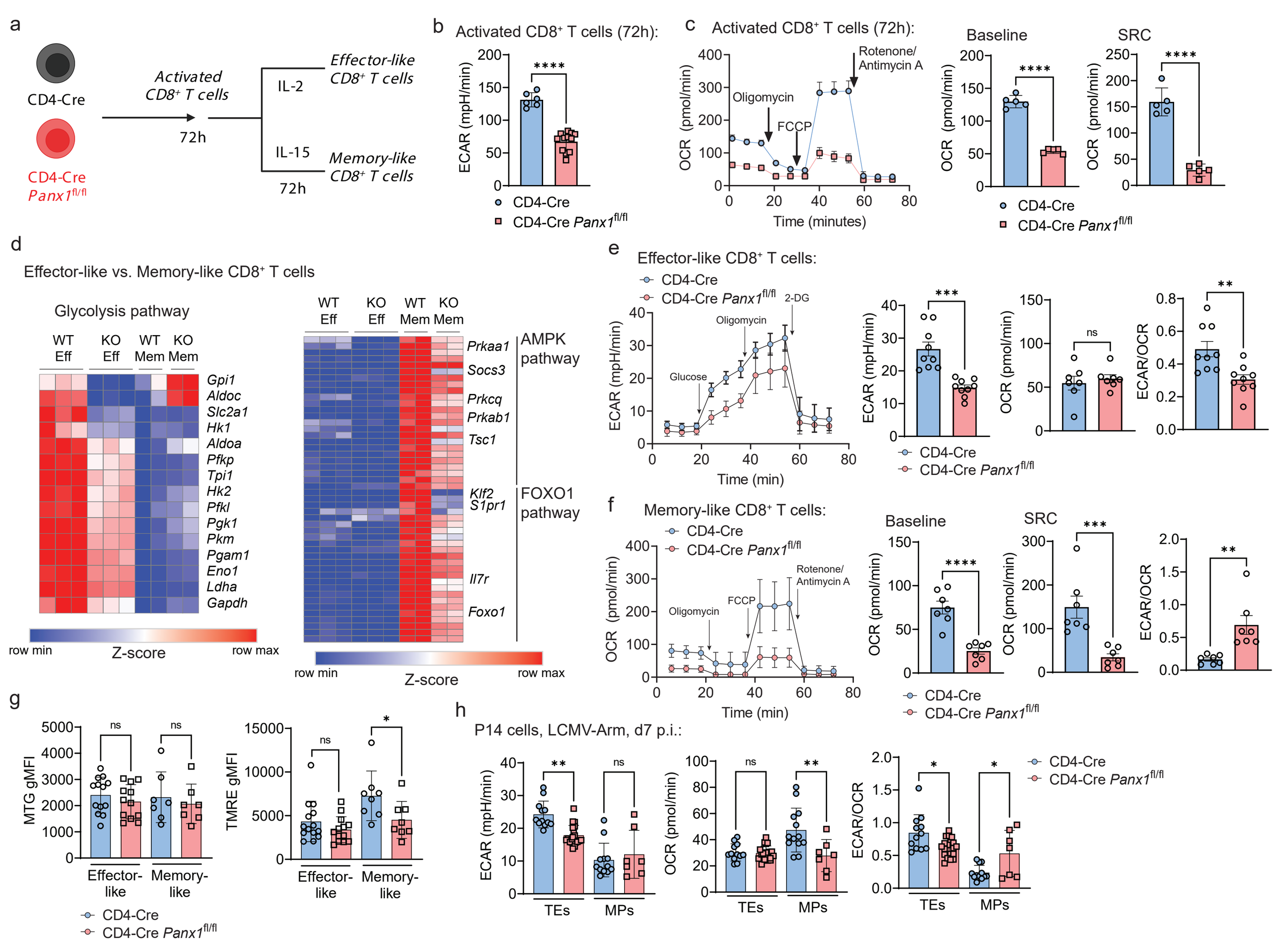
a
CD4-Cre
CD4-Cre Panx1fl/fl
Activated CD8+ T cells
72h
IL-2
IL-15
Effector-like CD8+ T cells
Memory-like CD8+ T cells
72h
b
Activated CD8+ T cells (72h):
ECAR (mpH/min)
****
CD4-Cre
CD4-Cre Panx1fl/fl
c
Activated CD8+ T cells (72h):
OCR (pmol/min)
Oligomycin
FCCP
Rotenone/ Antimycin A
Time (minutes)
Baseline
SRC
****
CD4-Cre
CD4-Cre Panx1fl/fl
d
Effector-like vs. Memory-like CD8+ T cells
Glycolysis pathway
WT Eff
KO Eff
WT Mem
KO Mem
Gpi1
Aldoc
Slc2a1
Hk1
Aldoa
Pfkp
Tpi1
Hk2
Pfkl
Pgk1
Pkm
Pgam1
Eno1
Ldha
Gapdh
row min
Z-score
row max
Prkaa1
Socs3
Prkcq
Prkab1
Tsc1
AMPK pathway
Klf2
S1pr1
Il7r
Foxo1
FOXO1 pathway
e
Effector-like CD8+ T cells:
CD4-Cre
CD4-Cre Panx1fl/fl
2-DG
Oligomycin
Glucose
ECAR (mpH/min)
Time (min)
***
OCR (pmol/min)
ns
ECAR/OCR
**
f
Memory-like CD8+ T cells:
Oligomycin
FCCP
Rotenone/ Antimycin A
Baseline
SRC
g
MTG gMFI
TMRE gMFI
ns
*
Effector-like
Memory-like
h
P14 cells, LCMV-Arm, d7 p.i.:
TEs
MPs

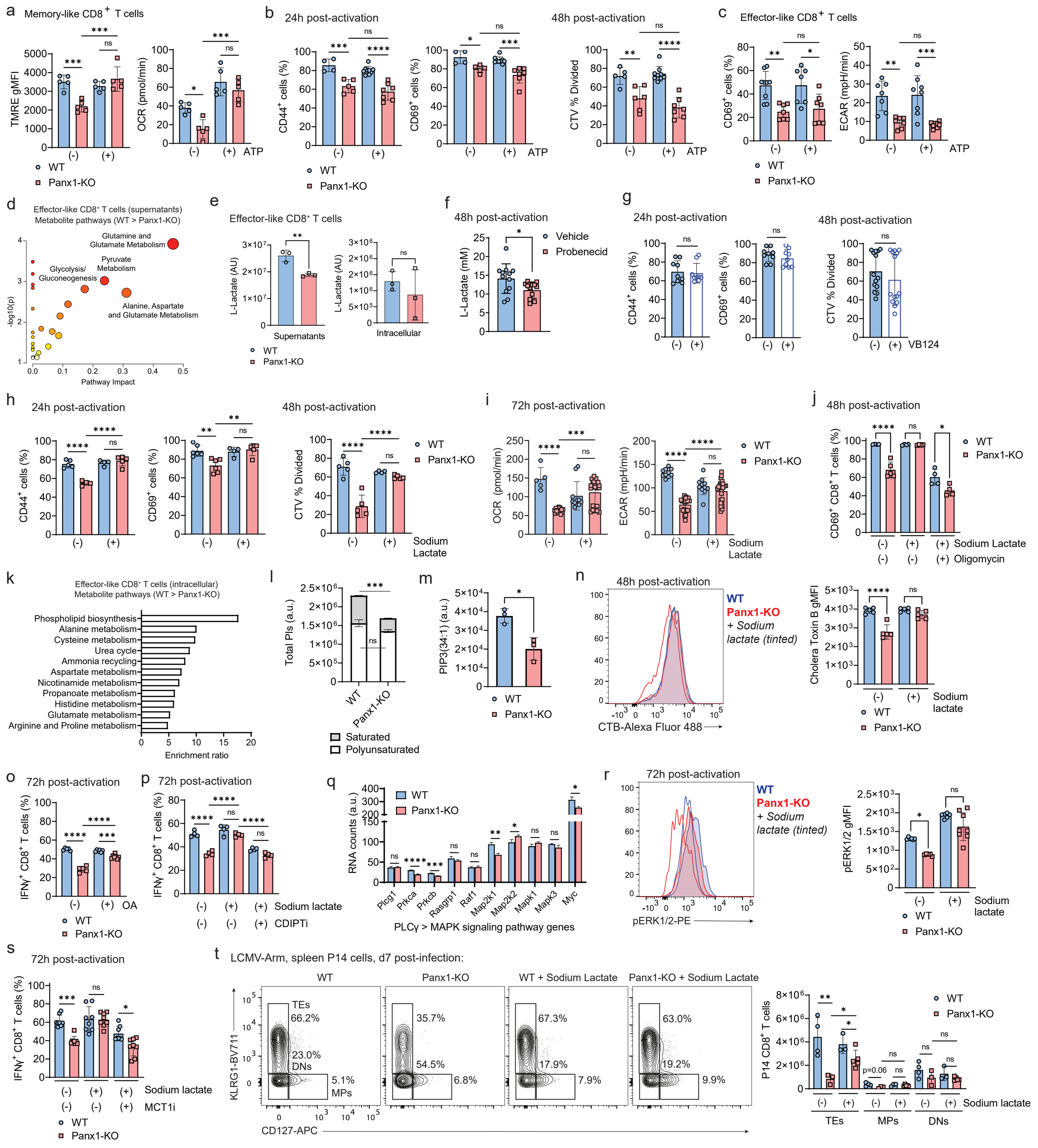
a
Memory-like CD8+ T cells
TMRE gMFI
OCR (pmol/min)
(-) (+) ATP
WT
Panx1-KO
b
24h post-activation
48h post-activation
CD44+ cells (%)
CD69+ cells (%)
CTV % Divided
c
Effector-like CD8+ T cells
CD69+ cells (%)
ECAR (mpH/min)
d
Effector-like CD8+ T cells (supernatants)
Metabolite pathways (WT > Panx1-KO)
Glutamine and Glutamate Metabolism
Pyruvate Metabolism
Glycolysis/ Gluconeogenesis
Alanine, Aspartate and Glutamate Metabolism
-log10(p)
Pathway Impact
e
Effector-like CD8+ T cells
L-Lactate (AU)
Supernatants
Intracellular
f
48h post-activation
L-Lactate (mM)
Vehicle
Probenecid
g
24h post-activation
48h post-activation
VB124
h
24h post-activation
48h post-activation
Sodium Lactate
i
72h post-activation
OCR (pmol/min)
ECAR (mpH/min)
j
48h post-activation
CD69+ CD8+ T cells (%)
Sodium Lactate
Oligomycin
k
Effector-like CD8+ T cells (intracellular)
Metabolite pathways (WT > Panx1-KO)
Phospholipid biosynthesis
Alanine metabolism
Cysteine metabolism
Urea cycle
Ammonia recycling
Aspartate metabolism
Nicotinamide metabolism
Propanoate metabolism
Histidine metabolism
Glutamate metabolism
Arginine and Proline metabolism
Enrichment ratio
l
Total PIs (a.u.)
Saturated
Polyunsaturated
m
PIP3(34:1) (a.u.)
n
48h post-activation
WT
Panx1-KO
+ Sodium lactate (tinted)
CTB-Alexa Fluor 488
Cholera Toxin B gMFI
o
72h post-activation
IFNγ+ CD8+ T cells (%)
OA
p
72h post-activation
Sodium lactate
CDIPTi
q
RNA counts (a.u.)
Plcg1
Prkca
Prkcb
Rasgrp1
Raf1
Map2k1
Map2k2
Mapk1
Mapk3
Myc
PLCγ > MAPK signaling pathway genes
r
72h post-activation
pERK1/2-PE
pERK1/2 gMFI
s
72h post-activation
MCT1i
t
LCMV-Arm, spleen P14 cells, d7 post-infection:
WT
Panx1-KO
WT + Sodium Lactate
Panx1-KO + Sodium Lactate
TEs
66.2%
23.0%
DNs
5.1%
MPs
35.7%
54.5%
6.8%
67.3%
17.9%
7.9%
63.0%
19.2%
9.9%
KLRG1-BV711
CD127-APC
P14 CD8+ T cells
p=0.06

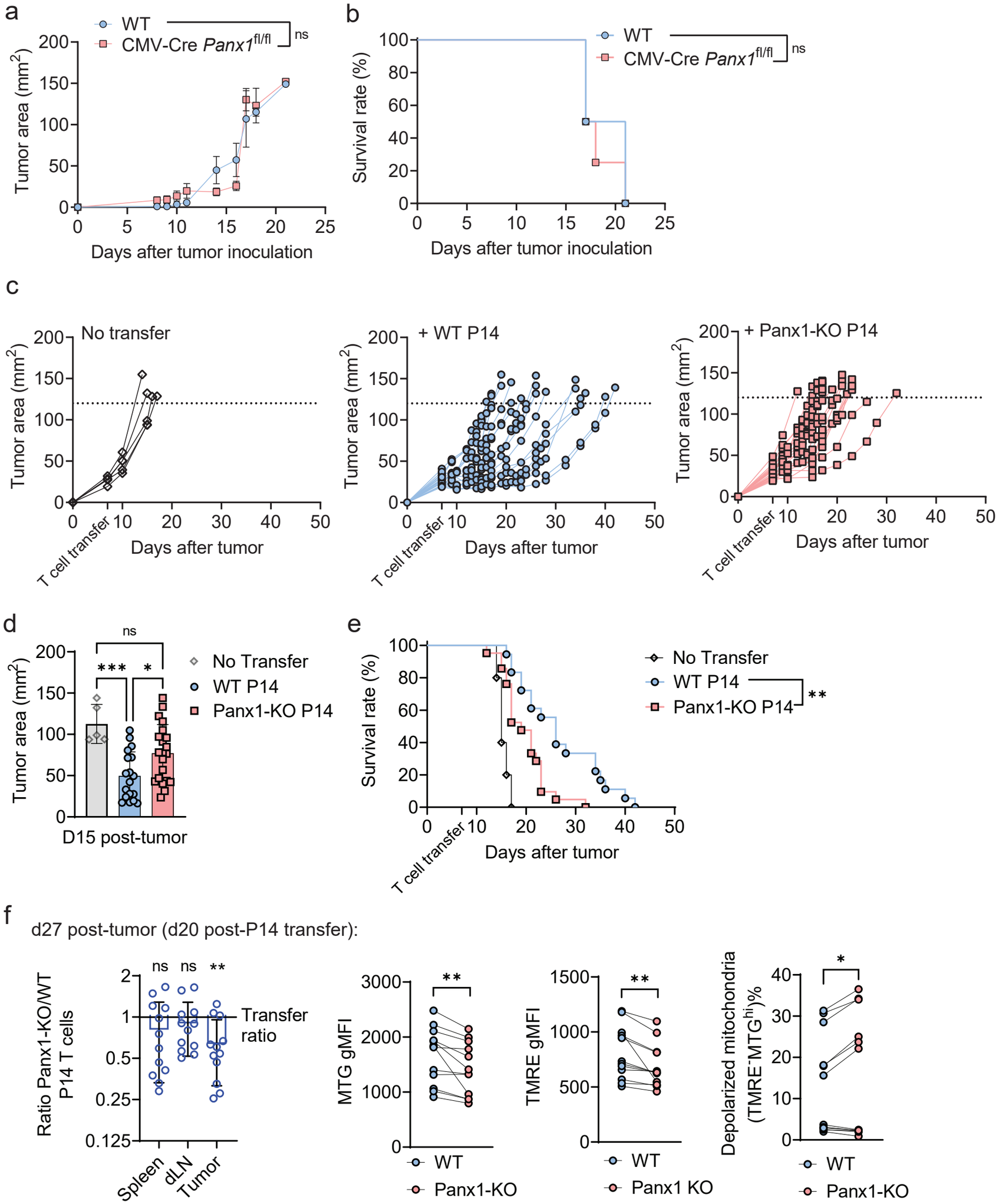
a
WT
CMV-Cre Panx1fl/fl
ns
Tumor area (mm2)
Days after tumor inoculation
b
WT
CMV-Cre Panx1fl/fl
ns
Survival rate (%)
Days after tumor inoculation
c
No transfer
+ WT P14
+ Panx1-KO P14
Tumor area (mm2)
T cell transfer
Days after tumor
d
ns
***
*
No Transfer
WT P14
Panx1-KO P14
Tumor area (mm2)
D15 post-tumor
e
No Transfer
WT P14
Panx1-KO P14
**
Survival rate (%)
T cell transfer
Days after tumor
f
d27 post-tumor (d20 post-P14 transfer):
ns
ns
**
Transfer ratio
Ratio Panx1-KO/WT P14 T cells
Spleen
dLN
Tumor
**
MTG gMFI
WT
Panx1-KO
**
TMRE gMFI
WT
Panx1 KO
*
Depolarized mitochondria (TMRE-MTGhi)%
WT
Panx1-KO

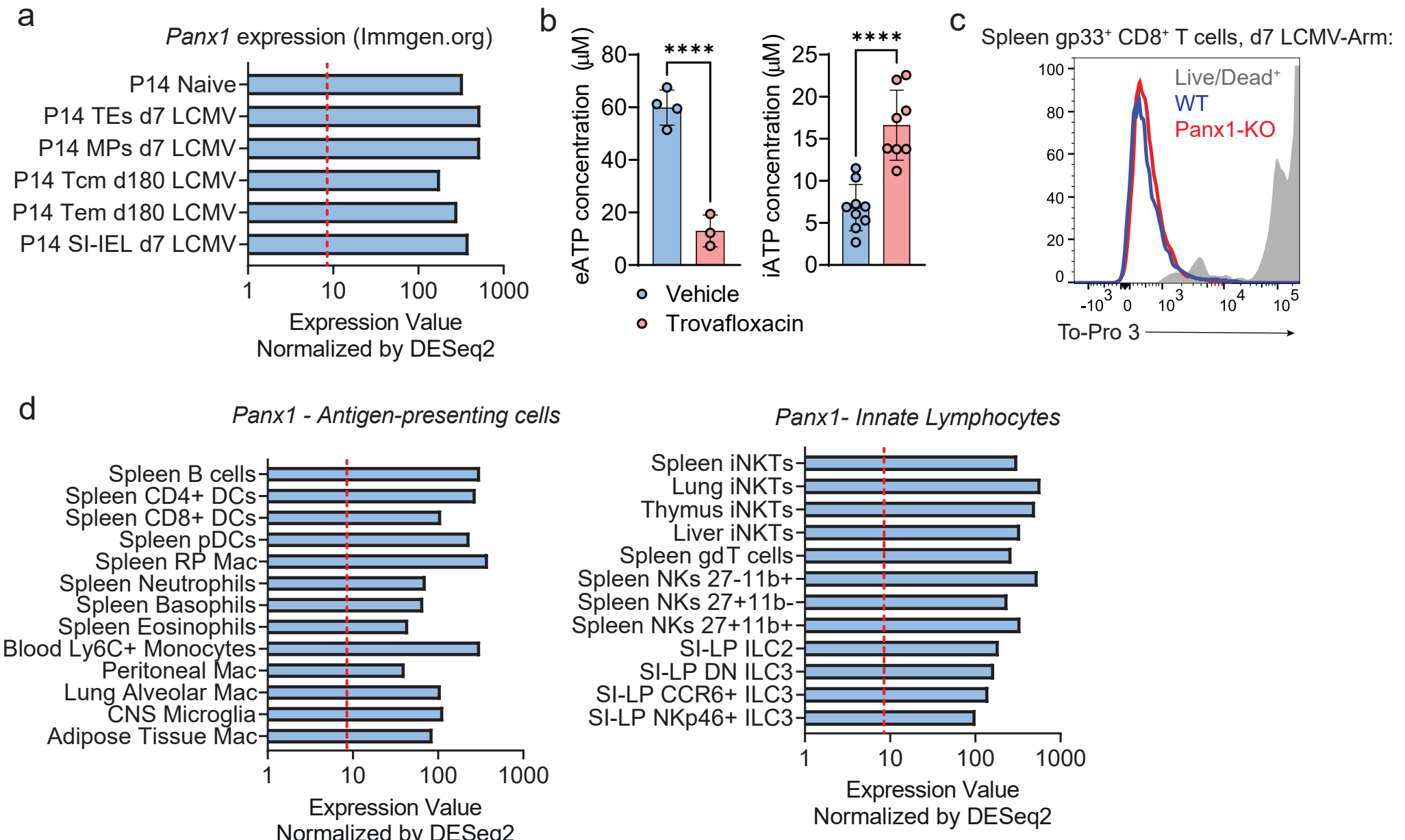
a
Panx1 expression (Immgen.org)
P14 Naive
P14 TEs d7 LCMV
P14 MPs d7 LCMV
P14 Tcm d180 LCMV
P14 Tem d180 LCMV
P14 SI-IEL d7 LCMV
1
10
100
1000
Expression Value
Normalized by DESeq2
b
eATP concentration (μM)
80
60
40
20
0
****
iATP concentration (μM)
25
20
15
10
5
0
****
Vehicle
Trovafloxacin
c
Spleen gp33+ CD8+ T cells, d7 LCMV-Arm:
Live/Dead+
WT
Panx1-KO
100
80
60
40
20
0
-10^3
0
10^3
10^4
10^5
To-Pro 3
d
Panx1 - Antigen-presenting cells
Spleen B cells
Spleen CD4+ DCs
Spleen CD8+ DCs
Spleen pDCs
Spleen RP Mac
Spleen Neutrophils
Spleen Basophils
Spleen Eosinophils
Blood Ly6C+ Monocytes
Peritoneal Mac
Lung Alveolar Mac
CNS Microglia
Adipose Tissue Mac
1
10
100
1000
Expression Value
Normalized by DESeq2
Panx1- Innate Lymphocytes
Spleen iNKTs
Lung iNKTs
Thymus iNKTs
Liver iNKTs
Spleen gdT cells
Spleen NKs 27-11b+
Spleen NKs 27+11b-
Spleen NKs 27+11b+
SI-LP ILC2
SI-LP DN ILC3
SI-LP CCR6+ ILC3
SI-LP NKp46+ ILC3
1
10
100
1000
Expression Value
Normalized by DESeq2

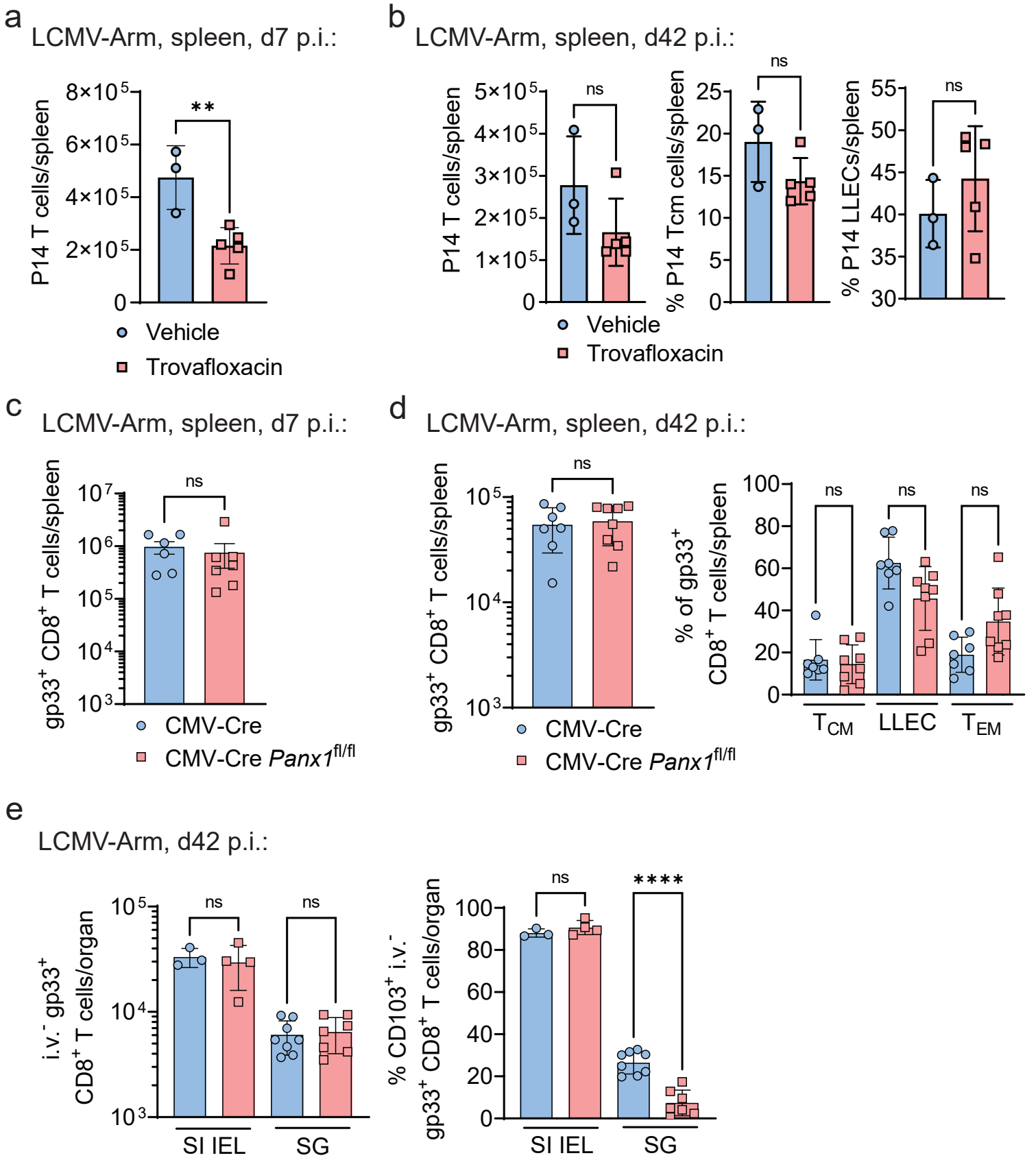
a
LCMV-Arm, spleen, d7 p.i.:
P14 T cells/spleen
8×10^5
6×10^5
4×10^5
2×10^5
0
**
Vehicle
Trovafloxacin
b
LCMV-Arm, spleen, d42 p.i.:
P14 T cells/spleen
5×10^5
4×10^5
3×10^5
2×10^5
1×10^5
0
ns
% P14 Tcm cells/spleen
25
20
15
10
5
0
ns
% P14 LLECs/spleen
55
50
45
40
35
30
ns
Vehicle
Trovafloxacin
c
LCMV-Arm, spleen, d7 p.i.:
gp33+ CD8+ T cells/spleen
10^7
10^6
10^5
10^4
10^3
ns
CMV-Cre
CMV-Cre Panx1fl/fl
d
LCMV-Arm, spleen, d42 p.i.:
gp33+ CD8+ T cells/spleen
10^5
10^4
10^3
ns
% of gp33+ CD8+ T cells/spleen
100
80
60
40
20
0
ns
ns
ns
TCM
LLEC
TEM
CMV-Cre
CMV-Cre Panx1fl/fl
e
LCMV-Arm, d42 p.i.:
i.v.- gp33+ CD8+ T cells/organ
10^5
10^4
10^3
ns
ns
SI IEL
SG
% CD103+ i.v.- gp33+ CD8+ T cells/organ
100
80
60
40
20
0
ns
****
SI IEL
SG

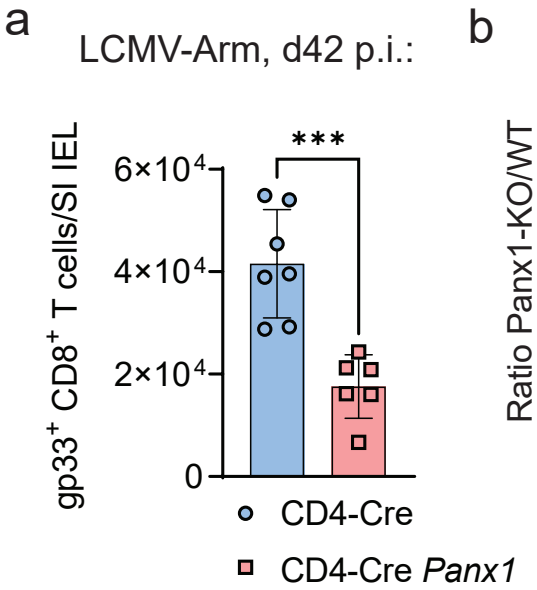
a
LCMV-Arm, d42 p.i.:
gp33+ CD8+ T cells/SI IEL
6×10^4
4×10^4
2×10^4
0
***
CD4-Cre
CD4-Cre Panx1

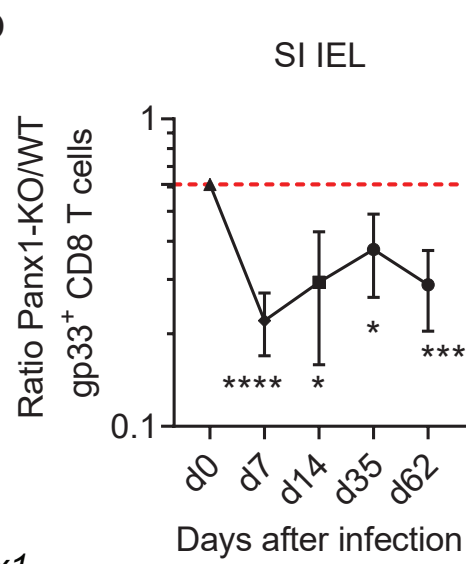
b
SI IEL
Ratio Panx1-KO/WT gp33+ CD8 T cells
1
0.1
****
*
*
***
d0
d7
d14
d35
d62
Days after infection

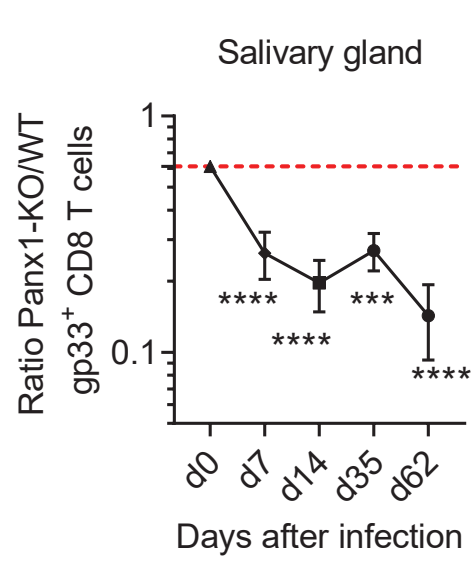
Salivary gland
Ratio Panx1-KO/WT gp33+ CD8 T cells
1
0.1
****
****
***
****
d0
d7
d14
d35
d62
Days after infection

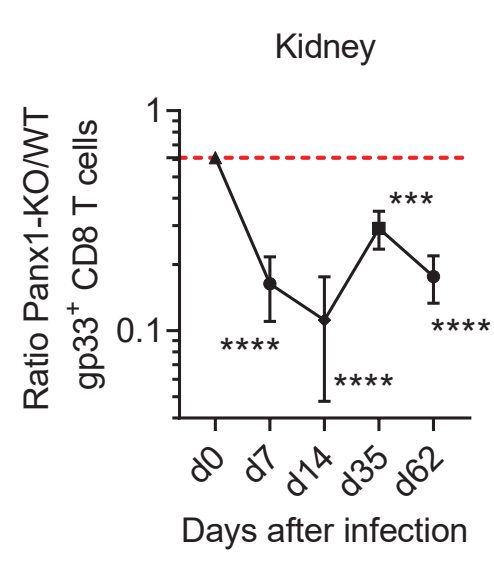
Kidney
Ratio Panx1-KO/WT gp33+ CD8 T cells
1
0.1
****
****
***
****
d0
d7
d14
d35
d62
Days after infection

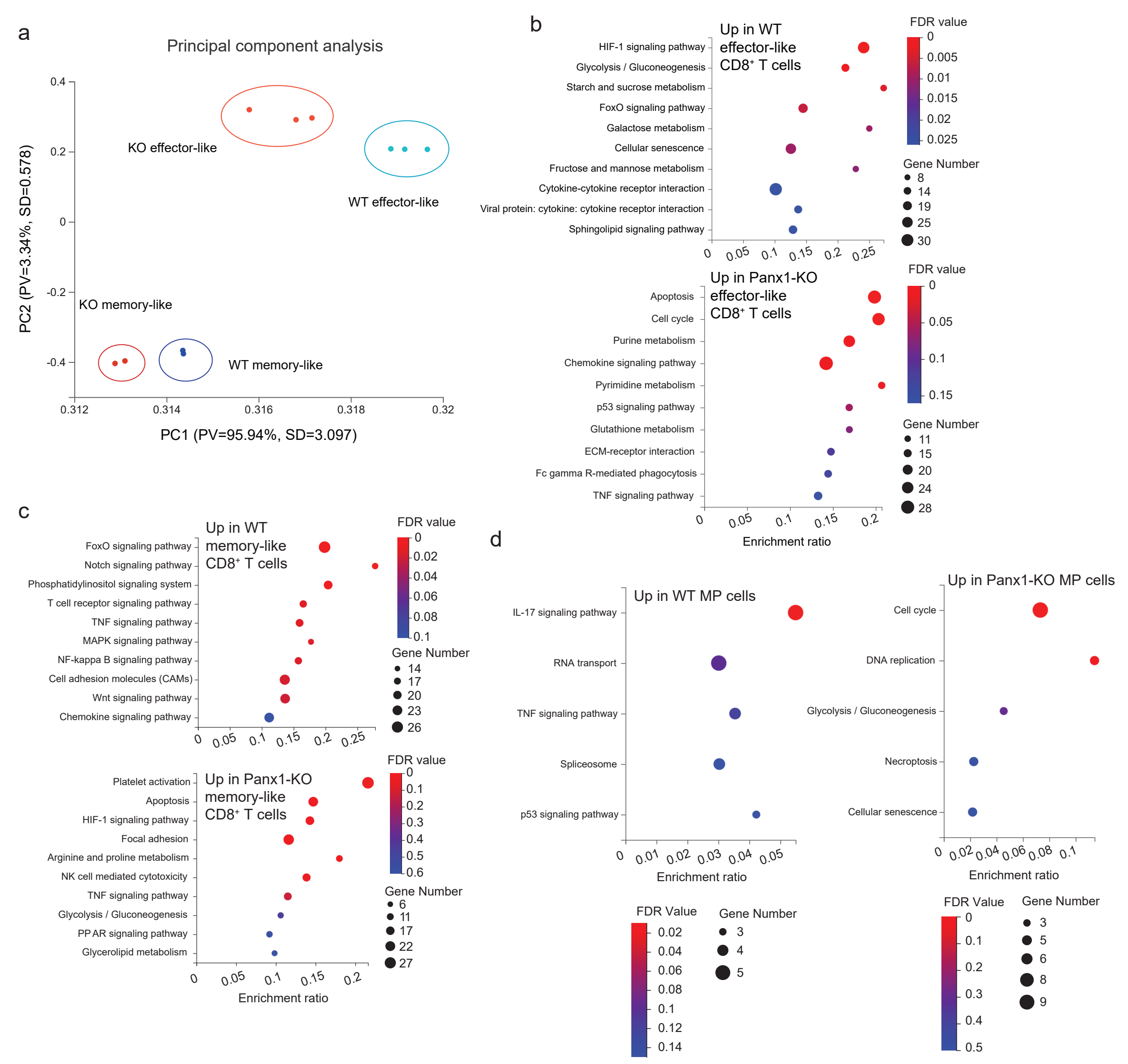
a
Principal component analysis
KO effector-like
WT effector-like
KO memory-like
WT memory-like
PC2 (PV=3.34%, SD=0.578)
PC1 (PV=95.94%, SD=3.097)
b
Up in WT effector-like CD8⁺ T cells
HIF-1 signaling pathway
Glycolysis / Gluconeogenesis
Starch and sucrose metabolism
FoxO signaling pathway
Galactose metabolism
Cellular senescence
Fructose and mannose metabolism
Cytokine-cytokine receptor interaction
Viral protein: cytokine: cytokine receptor interaction
Sphingolipid signaling pathway
FDR value
Gene Number
Up in Panx1-KO effector-like CD8⁺ T cells
Apoptosis
Cell cycle
Purine metabolism
Chemokine signaling pathway
Pyrimidine metabolism
p53 signaling pathway
Glutathione metabolism
ECM-receptor interaction
Fc gamma R-mediated phagocytosis
TNF signaling pathway
Enrichment ratio
c
Up in WT memory-like CD8⁺ T cells
FoxO signaling pathway
Notch signaling pathway
Phosphatidylinositol signaling system
T cell receptor signaling pathway
TNF signaling pathway
MAPK signaling pathway
NF-kappa B signaling pathway
Cell adhesion molecules (CAMs)
Wnt signaling pathway
Chemokine signaling pathway
Up in Panx1-KO memory-like CD8⁺ T cells
Platelet activation
Apoptosis
HIF-1 signaling pathway
Focal adhesion
Arginine and proline metabolism
NK cell mediated cytotoxicity
TNF signaling pathway
Glycolysis / Gluconeogenesis
PPAR signaling pathway
Glycerolipid metabolism
Enrichment ratio
d
Up in WT MP cells
IL-17 signaling pathway
RNA transport
TNF signaling pathway
Spliceosome
p53 signaling pathway
Up in Panx1-KO MP cells
Cell cycle
DNA replication
Glycolysis / Gluconeogenesis
Necroptosis
Cellular senescence
Enrichment ratio
FDR Value
Gene Number

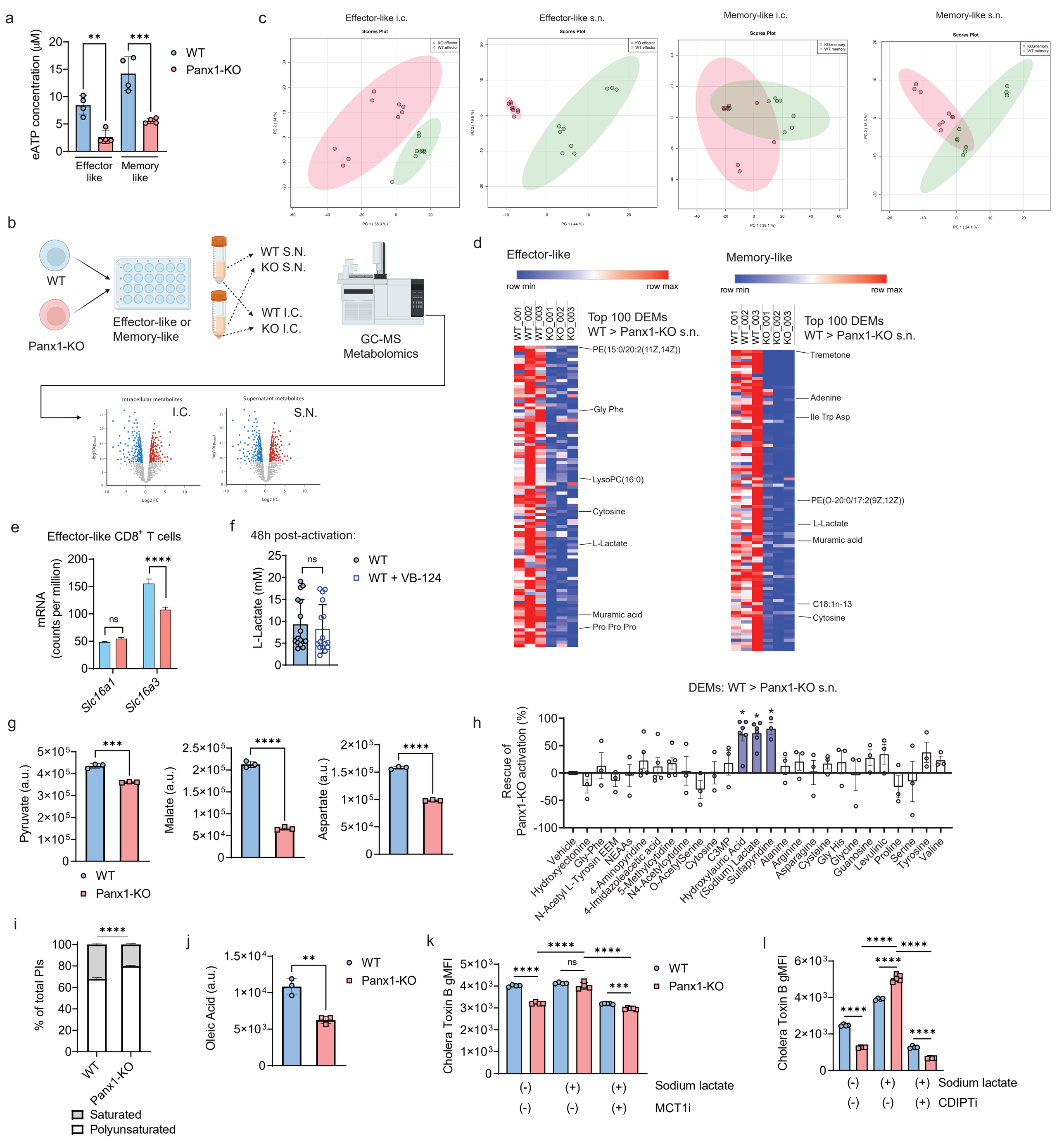
a
eATP concentration (μM)
WT
Panx1-KO
Effector like
Memory like
b
WT
Panx1-KO
Effector-like or Memory-like
WT S.N.
KO S.N.
WT I.C.
KO I.C.
GC-MS Metabolomics
Intracellular metabolites
I.C.
Supernatant metabolites
S.N.
c
Effector-like i.c.
Effector-like s.n.
Memory-like i.c.
Memory-like s.n.
Scores Plot
d
Effector-like
Memory-like
row min
row max
Top 100 DEMs WT > Panx1-KO s.n.
PE(15:0/20:2(11Z,14Z))
Gly Phe
LysoPC(16:0)
Cytosine
L-Lactate
Muramic acid
Pro Pro Pro
Tremetone
Adenine
Ile Trp Asp
PE(O-20:0/17:2(9Z,12Z))
L-Lactate
Muramic acid
C18:1n-13
Cytosine
e
Effector-like CD8+ T cells
mRNA (counts per million)
Slc16a1
Slc16a3
f
48h post-activation:
L-Lactate (mM)
WT
WT + VB-124
g
Pyruvate (a.u.)
Malate (a.u.)
Aspartate (a.u.)
WT
Panx1-KO
h
DEMs: WT > Panx1-KO s.n.
Rescue of Panx1-KO activation (%)
Vehicle
Hydroxyectonine
N-Acetyl L-Tyrosin
Gly-Phe
EEM
NEAAs
4-Aminopyridine
4-Imidazoleacetic acid
5-Methylcytidine
N4-Acetylcytidine
O-AcetylSerine
Cytosine
C3MP
Hydroxylauric Acid
(Sodium) Lactate
Sulfapyridine
Alanine
Arginine
Asparagine
Cysteine
Gly His
Glycine
Guanosine
Levulinic
Proline
Serine
Tyrosine
Valine
i
% of total PIs
WT
Panx1-KO
Saturated
Polyunsaturated
j
Oleic Acid (a.u.)
k
Cholera Toxin B gMFI
Sodium lactate
MCT1i
l
Cholera Toxin B gMFI
Sodium lactate
CDIPTi

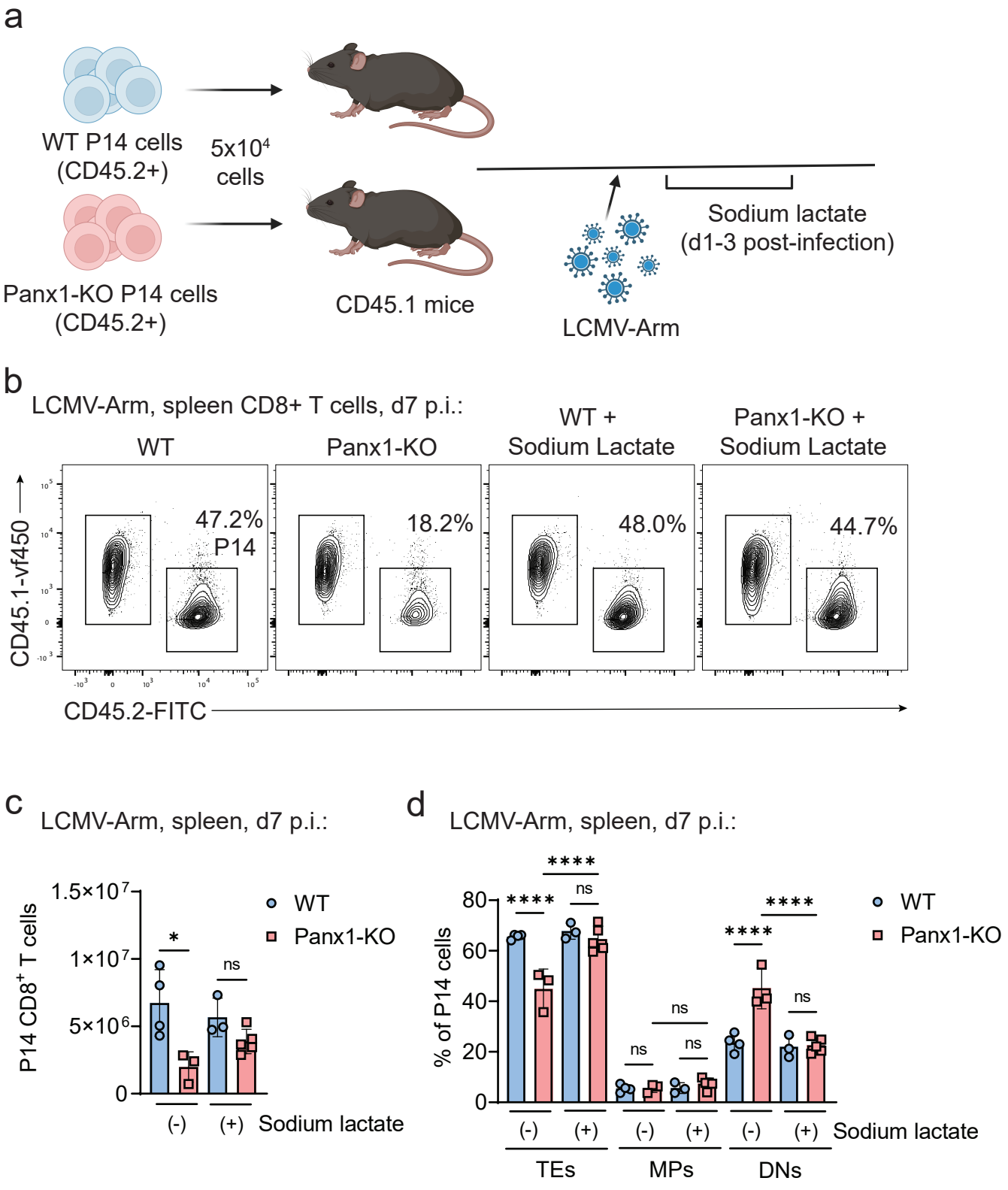
a
WT P14 cells
(CD45.2+)
5x10⁴
cells
Panx1-KO P14 cells
(CD45.2+)
CD45.1 mice
LCMV-Arm
Sodium lactate
(d1-3 post-infection)
b
LCMV-Arm, spleen CD8+ T cells, d7 p.i.:
WT
Panx1-KO
WT +
Sodium Lactate
Panx1-KO +
Sodium Lactate
47.2%
P14
18.2%
48.0%
44.7%
CD45.1-vf450
CD45.2-FITC
c
LCMV-Arm, spleen, d7 p.i.:
P14 CD8⁺ T cells
1.5×10⁷
1×10⁷
5×10⁶
0
*
ns
WT
Panx1-KO
(-)
(+)
Sodium lactate
d
LCMV-Arm, spleen, d7 p.i.:
% of P14 cells
80
60
40
20
0
****
ns
TEs
MPs
DNs

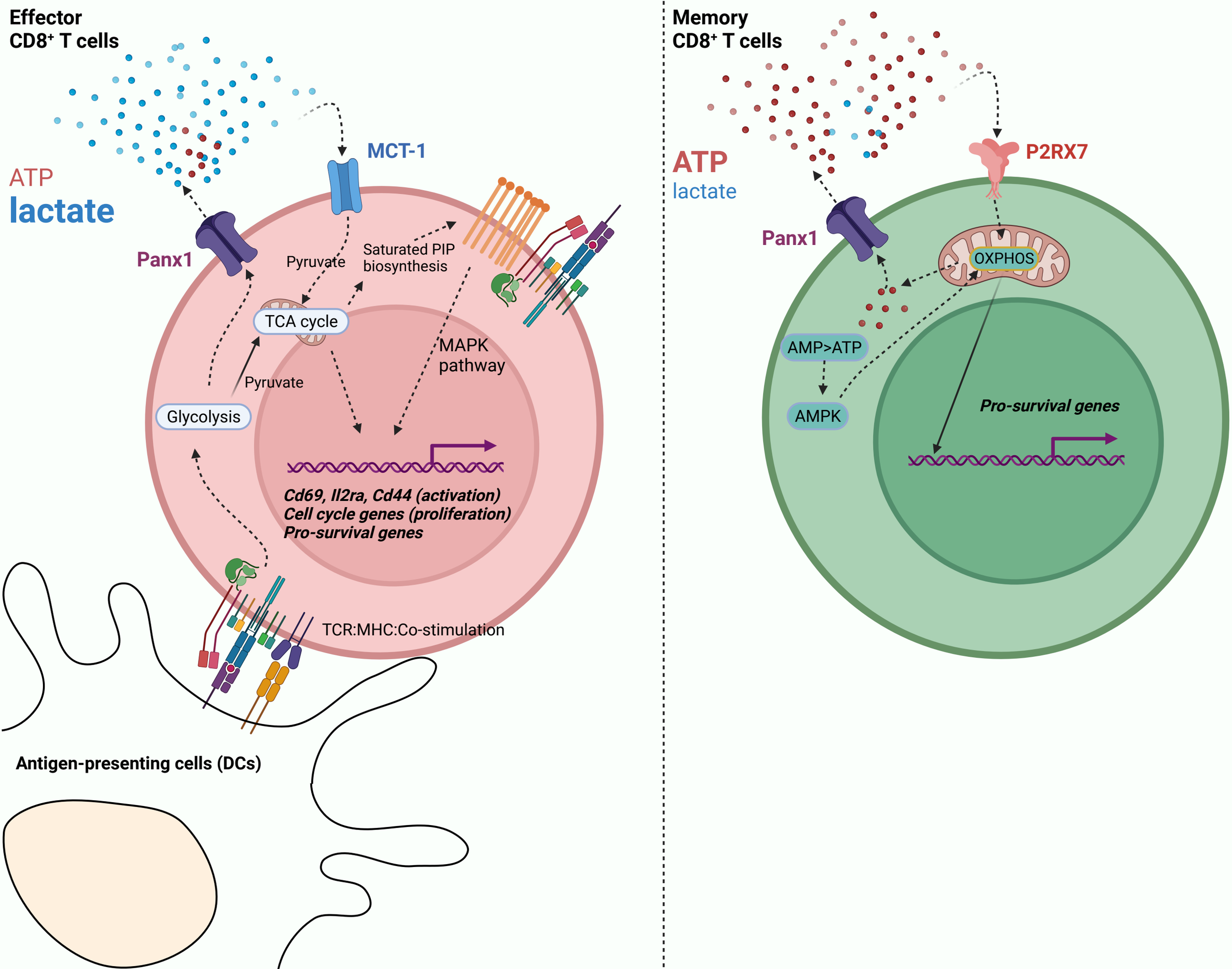
Effector
CD8+ T cells
ATP
lactate
MCT-1
Panx1
Pyruvate
Saturated PIP
biosynthesis
TCA cycle
MAPK
pathway
Pyruvate
Glycolysis
Cd69, Il2ra, Cd44 (activation)
Cell cycle genes (proliferation)
Pro-survival genes
TCR:MHC:Co-stimulation
Antigen-presenting cells (DCs)
Memory
CD8+ T cells
ATP
lactate
P2RX7
Panx1
OXPHOS
AMP>ATP
AMPK
Pro-survival genes